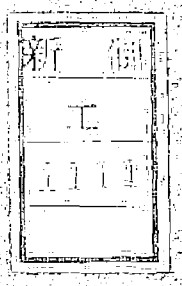

Theoretical Study on the Excited States and Electron Transfer Reactions in Photosynthetic Reaction Center

Jun-ya Hasegawa

1998

Theoretical Study on the Excited States and Electron Transfer Reactions in Photosynthetic Reaction Center

Jun-ya Hasegawa

1998

Preface

New discoveries on the determination of structures and on the machineries of proteins *in vivo* have often been highly exciting and surprising events, since the elucidated facts were sometimes quite far away from our imaginations. Such pleasurable betrayals by the nature provide us sources of curiosity and motivations of the studies. In the area of photosynthetic systems, many great discoveries have been accomplished in the last decade. Molecular structures of bacterial photosynthetic reaction centers were elucidated by Deisenhofer et al. in 1984. In their study, the chromophores in the reaction center were shown to have a symmetric alignment in the protein. Further studies revealed the highly efficient property of electron transfers in the system, which transduce the solar energy into the driving forces of the biochemical reactions in the photosynthesis. Recently, McDermott et al. determined the structure of a bacterial antenna protein which absorbs the solar energy and transfers it to the reaction center. Twenty seven chromophores were found to align quite symmetrically in a circle and their energy transfer ability achieves nearly 100 % yield. Our curiosities have been continuously stimulated by these mysteries in the nature. Why such beautiful structures are required in these systems? Why are the reactions so efficient? What can we learn from the nature?

In the present, methods of modern quantum chemistry have been developed extensively and have achieved the chemical accuracy in molecular ground and excited states. Recent years, to expand the applicability in large systems is one of the topics in quantum chemistry. The applicability is said to be one of the necessary conditions in order to be an useful theory. SAC/SAC-CI method proposed by Nakatsuji in 1978 is one of the accurate theories describing electron correlations in the ground and excited states. The method gives reliable results for various chemical processes. In part I, the SAC/SAC-CI method is applied to the ground, excited, and ionized states of biologically

important porphyrin compounds, moderately large systems, which had been thought to be unmanageable for modern accurate theories in a few years ago. The computation program applicable to larger systems has developed and attempts are made to free base porphin, Mg porphin, oxyheme, chlorin, bacteriochlorin, pheophytin *a*, and chlorophyll *a*. The aims of the studies are to make sure the accuracy of the method in such larger systems, to investigate the electronic structures, to make reliable assignments for the excitation spectra, and to understand effects on the excited states by metal coordinations and substituents

The photosynthetic reaction center of *Rhodopseudomonas viridis* is one of the systems which have stimulated strongly our scientific interests. The system transduces the solar energy to driving forces of chemical reactions without any loss of the yield. Although the reaction center has a pseudo-C_2 symmetric structure in which two electron transfer passways (L- and M-branches) are composed by chromophores, only L-branch is selectively utilized for the electron transfer. These issues have been studied extensively in the last decade. However the assignment of the absorption spectrum and the reasons of the high-efficiency and the unidirectionality have not been established yet. In Part II, these problems are attempted to investigate from a quantum chemical view point by using the SAC/SAC-CI method. The SAC/SAC-CI method is applied to the excited states and electron transfers in the reaction center. The theoretical excitation spectrum is compared with the absorption spectrum and the SAC-CI wave functions are utilized to calculate electronic factors in the rate constants so as to analyze the dynamics of the electron transfer reactions.

In Part III, applications of the SAC-CI method to an inner-valence ionization spectrum and an excitation spectrum of a metal complex are shown. The accurate descriptions of the inner-valence ionized states require to include higher order excitation operators, since the states are characterized as multi-electron processes. A serious problem is that the number of the operators

increases rapidly with the excitation level. However, the effective operators should be limited and should be selected by any selection procedure. A combined use of exponential generation algorithm proposed by Nakatsuji in 1987 and a perturbation technique is applied to the selection of linked operators for higher-excitations in the SAC-CI wave functions. The effectiveness is shown in the calculation on the inner-valence ionization spectrum of ethylene.

Acknowledgments

The present thesis is a summary of the studies carried out at the Faculty of Engineering of Kyoto University from 1992 to 1997. The author would like to express his sincere gratitude to Professor Hiroshi Nakatsuji for his continuous guidance, valuable comments, and philosophy of study.

The author would also like to express his acknowledgment to Dr. M. Hada, Dr. H. Nakai, Dr. M. Ehara, and Dr. Z. Hu for their discussions and warm encouragement during the course of the study.

The author appreciates Dr. Y. Tokita, Mr. K. Toyota, Mr. K. Ohkawa, Mr. Y. Ozeki, Mr. H. Ueda, and Mr. M. Nonoguchi for their collaborations which were indispensable for my thesis.

The author is indebted to the colleagues in Professor Nakatsuji's laboratory for their encouragements and enjoyable conversation which enrichened his studying life at the university.

Numerical calculations in the studies were performed on the NEC SX-3 computer at the Institute for Molecular Science and the work stations in the Nakatsuji Laboratory.

These studies were supported in part by a Grant-in-aid for Scientific Research from the Japanese Ministry of Education, Science and Culture and by the New Energy and Industrial Technology Development Organization. The author acknowledges the Research Fellowships from the Japan Society for the Promotion of Science for Young Scientists.

Finally, the author wishes to express his sincere gratitude to his family for their support and for all their patience.

Kyoto in January 1998

Jun-ya Hasegawa

Contents

		Page
Preface		**i**
Acknowledgments		**iv**
Contents		**v**
Part I	**Ground and Excited States of Porphyrins Studied by the SAC (symmetry adapted cluster) /SAC-CI (configuration interaction) Theory**	**1**
Chapter 1	Excited and ionized states of free base porphin	3
Chapter 2	Excited states of Mg porphin	33
Chapter 3	Ground and excited states of oxyheme	50
Chapter 4	Excitation spectra of chlorin, bacteriochlorin, pheophytin *a*, and chlorophyll *a*	69
Part II	**SAC-CI study on the excitation spectrum and the electron transfer reactions in the photosynthetic reaction center of *Rhodopseudomonas viridis***	**95**
Chapter 5	Excitation spectrum of the photosynthetic reaction center	97
Chapter 6	Mechanism and unidirectionality of the electron transfer reaction in the photosynthetic reaction center	130
Part III	**Theoretical study on the excitation and ionization spectra**	**163**
Chapter 7	Theoretical study on the ionized states of ethylene by the SAC-CI (general-*R*) method	165
Chapter 8	SAC-CI study on the electronic spectrum of $TcO4^-$	182
List of publications		**203**

Part I

Ground and Excited States of Porphyrins Studied by the SAC (symmetry adapted cluster) / SAC-CI (configuration interaction) Theory

Chapter 1

Excited and ionized states of free base porphin

ABSTRACT

The SAC(symmetry adapted cluster)/SAC-CI method is applied to the calculations of the ground, excited, and ionized states of the free base porphin. The electronic spectrum of porphin is well reproduced and new assignments for the B (Soret), N, L and M bands are proposed. The present result shows that the four orbital model is strongly perturbed for the B and N bands by the excitations from the lower $4b_{1u}$ MO and that the σ electron correlations are important for the description of the excited states. The absorption peaks in the ionization spectrum are assigned and the reorganization effect is found to be large especially for the n and σ electron ionizations.

I. INTRODUCTION

Porphyrins play a key role in some biological reactions like photosynthesis and oxygen absorption.[1] To clarify the electronic mechanisms of these reactions, the electronic structures of porphyrins have been actively investigated.[2-19] The excited and ionized states of porphyrins observed in the VUV spectra[20] and the photoelectron spectra[21] are also investigated by the semi-empirical[2-8] and ab initio[9-13] methods. Among them, the CASPT2 study by Roos et al.[13] would be the best calculation so far made.

In the electronic spectrum of free base porphin, shown in the upper side of Fig. 1, the peaks are named as Q, B (Soret), N, L and M bands from low-energy peaks. The polarization studies[22,23] showed that the two peaks of the Q band are polarized perpendicular to each other, and the same is true for the B and N bands.

Previous theoretical studies[7-13] showed that the lower energy peak is polarized parallel to the inner H-H axis (Q_x) and the other one perpendicular (Q_y). Similar polarizations were also assumed for the B band: The lower and higher energy regions of the peak have the same polarizations as the Q_x and Q_y peaks, respectively.[12,13] However, some ambiguity still remains in these studies, since in the past, porphin was a large molecule for accurate theories of quantum chemistry.

We study here the ground, excited, and ionized states of porphin, based on the SAC (symmetry adapted cluster) theory for the ground state[24] and the SAC-CI theory for the excited, ionized and electron attached states.[25] We use here the accelerated version[26] of the SAC85 program.[27] The SAC/SAC-CI method has been shown to be quite accurate and useful for studying molecular spectroscopy and (catalytic) surface reactions.[28] It has been applied successfully, for example, to five-membered ring compounds,[29] benzene,[30] pyridine,[31] naphthalene,[32] many metal complexes like tetra-oxo

complexes[33-36] and halogen complexes,[37-39] and the models of surface reactions like Pd_nH_2 (n=1~3),[40] Ag_4O_2,[41] etc. A review was published in Ref. 28. Recently, some accelerations of the program were done for the integral evaluation and diagonalization parts.[26] Preliminary results of the present calculations were presented at the Workshop held in Braunlage in the summer of 1994.[42]

II. COMPUTATIONAL DETAILS

Free base porphin $C_{20}N_4H_{14}$ is assumed to have D_{2h} symmetry with D_{4h} skeleton. The atomic coordinate is taken from Sekino and Kobayashi.[7]

The basis set is of double-ζ quality for the valence 2p orbitals. We used Huzinaga's (63/5)/[2s2p] set[43] for carbon and nitrogen and (4)/[1s] set[44] for hydrogen. The total number of contracted GTO's is 206. The Hartree-Fock SCF orbitals, calculated by the HONDO program,[45] consists of 81 occupied and 125 unoccupied MO's.

In the SAC/SAC-CI calculations, the higher 42 occupied orbitals and the lower 114 unoccupied orbitals are included in the active space. The total number of active orbitals is 156. The active space includes all the π-type orbitals, 13 occupied π- and 35 unoccupied π*-orbitals, and a large number of σ orbitals are included. The frozen cores consist of 1s AO's and some lower combinations of 2s AO's of carbon and nitrogen and their antibonding counterparts at the top of the unoccupied space. From the previous calculations on benzene etc.,[5,12,13,30] the reorganization of the σ-electron space due to the π-π* excitation is important especially for the V states.

All single excitations and the selected double excitations are included in the linked term. The selection scheme in the SAC-CI calculation is modified slightly from the original one[46] by adding the SE-CI coefficient C_i^a of the

reference configuration Ψ_i^a to the second-order perturbation energy expression as

$$\frac{\left| C_i^a \left\langle \Psi_i^a \middle| H \middle| \Psi_{jk}^{bc} \right\rangle \right|^2}{\left\langle \Psi_i^a \middle| H \middle| \Psi_i^a \right\rangle - \left\langle \Psi_{jk}^{bc} \middle| H \middle| \Psi_{jk}^{bc} \right\rangle}.$$

In this scheme, the weight of the reference configuration is reflected in the selection scheme.

For the ground state, the energy thresholds of 1×10^{-5} and 2×10^{-5} hartree are used for the π-π^* and the other excitations, respectively. For the singlet excited states, two calculations with different sets of energy thresholds are carried out. In calculation A, the energy threshold is 1×10^{-6} hartree. In calculation B, doubly excited configurations having coefficients larger than 0.05 in calculation A are added to the reference configurations for the selection and the energy threshold for the π–π^* excitations is improved to 5×10^{-7} hartree. For the ionized states, the thresholds, 1×10^{-5} and 2×10^{-5} hartree are used for the ionizations from the π and the other orbitals, respectively. The numbers of the reference states and of the resultant linked configurations are summarized in Table I. The unlinked terms of the SAC and SAC-CI calculations represent the higher-order effects and the transferable correlations, respectively. They are included by the standard procedure.[28,46] Table II shows the timing data of the SAC/SAC-CI calculations of porphin.

III. RESULTS AND DISCUSSIONS

A. GROUND STATE

The energies and the natures of some higher occupied and lower unoccupied MOs are shown in Table III. The π-type orbitals gather in the

HOMO, LUMO regions. In particular, the HOMO(2au), next-HOMO(5b1u), the LUMO(4b2g), next-LUMO(4b3g), called "four orbitals", are well separated from the other orbitals, implying the validity of the four orbital model of Gouterman.[1] Two lone pair orbitals on the nitrogens, $7b_{2u}$ and $8a_g$ MOs, lie in the deeper side of the occupied π orbitals. The σ-type orbitals are below of most occupied π orbitals.

In Fig. 2, the orbital shapes of the four orbitals and the lower occupied 4b1u and 7b2u (lone pair) MOs are shown. These orbitals are π-type except for the 7b2u MO. The 5b1u (n-HOMO) and 2au (HOMO) MOs have 20-membered π-conjugation with 8 nodes and the 4b3g (n-LUMO) and 4b2g (LUMO) MOs have 18-membered π-conjugation with 10 nodes. The energy separations within these two pairs of MOs depend on whether the π-conjugation involves the nitrogen atoms, since the lower D2h symmetry exists only around these atoms.

The 4b1u MO will be shown important later for it strongly perturbs the four orbital model, and the 7b2u nitrogen lone pair MO gives the lowest n-π^* excitation. The MO shapes of Fig. 2 are useful when we investigate the substituent effects on the UV and ionization spectra.

The SAC correlation energy for the ground state is 10.0 eV. This is a reasonable value for our valence 2p double-ζ basis, since it is comparable with the correlation energy of 12.6 eV obtained by the MRSDCI calculation using split valence basis.[12] However, it is small in comparison with those obtained by the CASPT2[13] and MP2[14] calculations because of the smallness of the active space and the basis set used.

In the eigenvector for the ground state, the Hartree-Fock configuration is dominant. Though the four orbitals lie close to each other, the coefficients of the excited configurations involving these orbitals are less than 0.05. Then the single reference theory can describe the ground state of the free base porphin with a sufficient accuracy.

B. EXCITED STATES

Ab initio calculations of the excited states of porphin have appeared in recent years.[10-13] Fig. 3 shows the results together with the present ones (calculation B). The dotted lines show the assignments of the experimental peaks by each method. Only the lower four levels were calculated in the previous calculations.

Nagashima et al.[10] performed MRSDπCI using the minimal basis set. The results were not satisfactory because of the crudeness of the basis set and the limitation of the active space within π-orbitals. Foresman et al.[11] reported CIS calculations using 6-31G+ basis. Though the energies for the Q band were much improved, those for the Soret band were not improved: Higher excited configurations are necessarily included for an improvement. Yamamoto et al. carried out MRSDσπCI[12] using split valence basis and much improved the previous π-CI results[10]. The peaks Q_x and Q_y for the Q band and the B band were calculated in good agreement with the experiment, though the polarizations of the two peaks corresponding to the B band may contradict with the experimental result.[22,23] The CASPT2 result reported by Roos et al.[13] showed a good agreement with experiment, though it tends to underestimate the excitation energy.

Our present result is also shown in Fig. 3. Different from the previous ab initio calculations, our SAC-CI calculation gives the excitation energies for all the states observed in the VUV spectrum. Our method is general and effective so that we can calculate all the excited states lying in the observed energy range. In Fig. 1, the SAC-CI theoretical spectrum is compared with the experimental one in a vapor phase measured by Edwards and his co-workers.[20] Table IV summarizes the details of the SAC-CI results not only for the optically allowed states, but also for the optically forbidden singlet

states. The optically allowed eight π-π^* and one n-π^* excited states and the dipole-forbidden six π-π^* and three n-π^* states are calculated in the present SAC-CI study. Main configurations, natures, excitation energies and oscillator strengths are given together with the experimental and other ab initio theoretical results.

Referring to Figs. 1 and 3, we see that the present SAC-CI results reproduce well the experimental spectrum in both excitation energy and oscillator strength. The average discrepancy from the observed peaks are 0.13 and 0.14 eV by the present calculations A and B, respectively. We discuss each band subsequently below.

The Q band is composed of the two weak peaks Q_x and Q_y at 1.98 and 2.42 eV, respectively, and Q_y has a larger intensity than Q_x. By the SAC-CI calculations, Q_x and Q_y are assigned to the 1^1B_{3u} and 1^1B_{2u} states calculated at 1.8 and 2.2 ~ 2.3 eV, respectively. No other excited states including forbidden states are found in this area. The error in the excitation energy is within 0.2 eV. The present calculations reproduce the energy separation between Q_x and Q_y and the order of the oscillator strength in the experimental spectrum. Since the 1^1B_{3u} and 1^1B_{2u} states polarize in x and y directions, respectively, the present result is consistent with the experiment. The main configurations shown in Table IV are composed of the excitations within "4-orbitals": two configurations mix strongly and cause a quasi-degenerate nature of these states.

A strong absorption band that consists of a sharp peak and a shoulder in the higher energy side is observed in the 310 ~ 400 nm region of the spectrum. The sharp peak and the shoulder are called B (Soret) and N bands, respectively. The 18 membered cyclic polyene model[47,48] of porphin explained that the B band consists of the two degenerate states. In some previous theoretical studies including the ab initio ones[10-13] and the semi-empirical ones,[7,8] the B band was assigned to the two nearly degenerate

2^1B_{3u} and 2^1B_{2u} states, following the Gouterman's four orbital model, and the N band to another electronic state.

The present SAC/SAC-CI results indicate different assignment. The excitation energies of the 2^1B_{3u} and 2^1B_{2u} states are calculated to be 3.59 and 3.79 eV, respectively, in the calculation A and 3.56 and 3.75 eV, respectively, in the calculation B and no other peaks are calculated in the 3 ~ 4 eV region. Then, we assign the 2^1B_{3u} and 2^1B_{2u} states to the B and N bands, respectively. In other words, the N band which is the shoulder of the B band in the experimental spectrum shown in Fig. 1 is actually B_y and the B band is B_x. The excitation energies for these states are overestimated by 0.26 and 0.14 eV, respectively, in the calculation A and 0.23 and 0.10 eV in the calculation B. The energy splitting between the B and N bands, which is 0.32 eV, is calculated to be 0.20 eV. If the conventional assignment is adopted in our present result, no assignment is possible for the N band. Namely, the present proposal for the B and N bands are based not only on the calculated excitation energies for the $2B_{2u}$ and $2B_{3u}$ states, but also on the comparison of the present results, as a whole, with the peaks in the experimental spectrum.

The polarization studies for the free base tetraphenylporphin[22,23] showed that the sharp B band and the shoulder are polarized perpendicular to each other and that the B band and its shoulder have the same polarization as the Q_x and Q_y peaks, respectively. This is consistent with our assignment.

The symmetry lowering from D_{4h} metal porphyrins to its D_{2h} free base ones often cause a spectral broadening on the B band.[20] This is consistent with the present assignment, since the 2^1B_{2u} and 2^1B_{3u} states of the present molecule (D_{2h}) become degenerated in the D_{4h} symmetry. In the followings, we use the traditional notations B and N, though they are actually B_x and B_y, respectively, for the free base porphin.

The main configurations of the 2^1B_{3u} and 2^1B_{2u} states include not only the excitations within the 4-orbitals, but also the excitations from the lower $4b_{1u}$ orbital (see Table III and Fig. 2). As shown in Table IV, the two transitions from the $4b_{1u}$ MO to the $4b_{2g}$ and $4b_{3g}$ MOs strongly mix into the configurations within the 4 orbital model in the calculated 2^1B_{3u} and 2^1B_{2u} states, respectively. Furthermore, the extent of mixing is quite different between the 2^1B_{3u} and 2^1B_{2u} states, so that these states are no longer degenerate. The natures of the B (2^1B_{3u}) and N (2^1B_{2u}) bands are different in this point from that of the Q band. In the CASPT2F calculation, the $4b_{1u}$ MO was not included in the active space of CASSCF, though as shown here it strongly perturbs the picture of the four orbital model of the B band.

Referring to Fig. 1 and Table IV, we see that the calculated intensity is larger for the 2^1B_{2u} (N) states than for the 2^1B_{3u} (B) states. This may contradict with the observed spectrum shown in Fig. 1. However, we may interpret the observed spectrum as follows. The N band is a broad band, the B band is sharp, and the B band lies on the right-hand side top of the broad N band, so that the N band looks like a shoulder of the B band.

The effects of the σ electron-correlation were found to be important for the description of the π-π^* excitations of the π conjugated systems. This is now a well-known fact verified by the SAC-CI,[28-32] CASPT2,[13,49-52] and other calculations[53-56] in particular for larger π-electron molecules. In Table V, the number of the configurations whose CI coefficients are larger than 0.01 is shown for several states. The σ-σ^* excitations mix with the π-π^* excitations especially in the 2^1B_{3u} (B) and 2^1B_{2u} (N) states. The difference of these states from the Q band is clear also from this point.

For the L and M bands, no ab initio calculations have been reported except for the semi-empirical treatments.[7,8] The L bands at 4.25 and 4.67 eV are assigned to the 3^1B_{3u} and 3^1B_{2u} states, respectively, since these two states have relatively large intensities (for the 1^1B_{1u} state, see later). The

errors of the SAC/SAC-CI excitation energies from the experiment are within 0.2 eV. Since the intensity of the 3^1B_{3u} state is larger than that of the 3^1B_{2u} state, the shape of the L band is unsymmetric with higher intensity in the lower energy side. The main configurations of the 3^1B_{3u} and 3^1B_{2u} states are the transitions from the $4b_{1u}$ MO to the $4b_{2g}$ and $4b_{3g}$ MOs, respectively. These are the mixing configurations to the four orbital model in the B and N states. The σ-σ^* effect is relatively large in the 3^1B_{3u} states as shown in Table V.

It is interesting to note that we have obtained several n-π^* type transitions for the porphin as shown in Table IV. Among these, the optically allowed one is the 1^1B_{1u} state calculated at 4.51 eV, but the calculated intensity is very small and is similar to those of the Qx and Qy peaks. In the experimental spectrum shown in Fig. 1, this peak may be concealed by the L band. Since the $7b_{2u}$ MO is the lone pair orbital on nitrogen, it will be blocked by forming metal porphyrins, so that this peak will disappear. We have obtained several other n-π^* states, 1^1B_{2g} state at 4.05 eV, 1^1A_u state at 4.18 eV and 1^1B_{3g} state at 4.37 eV, though they are all optically forbidden at the D_{2h} symmetry. In the semi-empirical calculation of Baker and Zerner[8], a n-π^* excitation was calculated at 4.91 eV with the oscillator strength of 0.019.

In the absorption band lying in the energy region 4.0 ~ 4.7 eV, which is called L band in the spectrum shown in Fig. 1, it became clear that at least three optically allowed transitions exist, 3^1B_{3u}, 1^1B_{1u} (n-π^*), and 3^1B_{2u} states, and their polarization are all different, x, z, and y directions, respectively, though the intensity of the 1^1B_{1u} (n-π^*) state is small. Therefore, a detailed polarization study for the peaks in this energy region is very interesting and waited. We note that for free base tetraphenylporphin, three peaks, L, 1, and 2 were reported in the energy region of the L band of the free base porphin.[20]

The M band at around 5.5 eV in the experimental spectrum is composed of the two π-π^* transitions due to the 4^1B_{2u} and 4^1B_{3u} states. They are the transitions from the $3b_{1u}$ MO to the $4b_{3g}$ and $4b_{2g}$ MOs, respectively. In comparison with the L band, the starting MO is lower but the ending MOs are the same. Note that the order of the polarizations is different: x and y in the increasing energy for the L band and y and x for the M band. Experimental examination of such polarization property is also interesting.

In the present SAC-CI calculations, two different thresholds are used in the perturbation selection procedure for examining the accuracy of the present result. In the calculation B, the better thresholds are used for the π–π^* excitations and some doubly excited configurations, which might be important in the excited states, are used as reference configurations in the perturbation selection step. The calculation B is therefore more accurate than the calculation A. Comparing two sets of the results shown in Table IV, we find the two calculations to be quite similar: no special differences are observed between the calculations A and B. The calculation B gives about 0.03 eV lower energy than the calculation A. This result indicates that the principal correlations necessary for describing the excited states of porphin are already included in the calculation A, and that the present result should be already approximation invariant.

C. IONIZED STATES

The photoelectron spectrum of the free base porphin in a vapor phase was observed by Dupuis et al.[21] and is shown in Fig. 4. It is very characteristic that the first ionization potential of the free base porphin is as low as 6.9 eV. This low IP is believed to have some relation with the photosynthesis.

The SAC-CI ionization spectrum is compared with the Dupuis' experimental spectrum in Fig. 4. The dotted lines denote the correspondence between the SAC-CI result and the Koopmans result. The reorganization effect is larger as the IP level is deeper. The observed spectrum can be assigned by the SAC-CI spectrum. Some of the lower ionized states calculated by the SAC-CI method are summarized in Table VI. For the first and second ionizations, both the Koopmans and SAC-CI IP's underestimate the observed values. The peaks at 6.9 and 7.2 eV are assigned to the ionizations from HOMO ($5b_{1u}$) and next HOMO ($2a_u$), respectively. Since our present basis set is 2p double-ζ quality and does not include polarization functions, the ionization potentials due to the HOMO and the next HOMO are not properly reproduced.

In the region deeper than 8 eV, the Koopmans method is not appropriate for the assignment. From the SAC-CI result shown in Fig. 4, the absorption band in 8.0 ~ 9.5 eV is found to be composed of the eight ionized states (six π ionized states and two σ ionized states). Two ionizations from the $2b_{3g}$ and $1a_u$ MOs are assigned to the peaks in the region 9.5 ~ 11.0 eV. The observed broad peak in 11 ~ 16.0 eV region involves the ionizations from the σ-type MOs. We also found many shake-up ionization peaks in this region. However, since the present SAC-CI calculations include only singles and doubles in the linked term, it is difficult to reproduce the shake-up ionizations with enough accuracy. The SAC-CI (general-R) method[57] can give more accurate descriptions of the shake-up processes.

In Table VI, Δ shows the difference between the Koopmans IP and the SAC-CI IP. It represents the reorganization and electron correlation effects. We see that the Δ values are grouped into four. The Δ values for the IP's from HOMO and next HOMO are about 0.4 eV, those for the π-type MOs are 1.1 ~ 1.4 eV, those for the σ-type MOs are about 2 eV, and those for the n-type MOs are 2.6 eV. This clearly shows the relative importance of the

reorganization and correlation effects in each type of the ionized states. Similar tendency was also found previously for the π-conjugated molecules like benzene[30] and pyridine[31].

As shown in Fig. 4, the Koopmans ionization spectrum is much improved by using the SAC-CI method, since the electron correlation and the reorganization effects are important.

Almlöf performed in 1974 the ΔSCF calculations for the π- and n- type ionization potentials of the free base porphin.[15] Table VI also shows his result. The difference between the ΔSCF IP and the orbital energy corresponds to the orbital reorganization energy after ionization. This reorganization energy is 0.3 ~ 0.6 eV for the π-type MOs and 0.9 ~ 1.5 eV for the n-type orbitals. In comparison with the present Δ values discussed above, these Almlöf's values are much smaller. This is because the present Δ values include not only the orbital reorganization, but also the electron correlation effects. It is interesting to note that for the first two IP's (1^2B_{1u} and 1^2A_u), the present difference value is so close to that of Almlöf.

Table VI gives the information on the main configurations. In most states the Koopmans configuration is the main configuration, but for the 1^2B_{2g} and 2^2B_{2g} states, the ionizations from the $3b_{2g}$ and $2b_{2g}$ MOs mix strongly.

IV. CONCLUSION

The SAC/SAC-CI method is applied to the calculations of the ground, excited and ionized states of the free base porphin. The theoretical result for the excitation energy and the oscillator strength reproduce well the experimental spectrum. New assignments for the B, N, L and M bands are proposed.

The B and N bands in the experimental spectrum shown in Fig. 1 are assigned to the 2^1B_{3u} and 2^1B_{2u} states, respectively, so that they are actually

B_x and B_y states, respectively. This assignment does not contradict with the polarization experiments, the spectral intensity, and the spectral differences between the D_{2h} and D_{4h} porphyrins. Further examinations of this proposal are now in progress. The assignments of the Q_x and Q_y peaks are the same as the previous ones.

Though the Gouterman's four orbital model holds well for the Q band, it breaks down for the B (and N) bands because the excitations from the lower $4b_{1u}$ orbital mix strongly to these bands. Further, the mixing is different for the B and N bands.

Since the SAC-CI method is general and effective, we need not to restrict our subject to the lower four levels. The L band lying in the 4.2 ~ 4.7 eV region is assigned to be composed of the 3^1B_{3u}, 1^1B_{1u} and 3^1B_{2u} states. Their polarizations are x, z, and y, respectively and the intensity of the n-π^* transition due to the 1^1B_{1u} state should be very small. The M band is assigned to the 4^1B_{2u} and 4^1B_{3u} states whose transitions have the polarizations in y and x directions, respectively.

We have also calculated several symmetry forbidden states as shown in Table IV. They involve π-π^* and n-π^* transitions.

The mixing of the σ-σ^* excitations to the π-π^* excitations is shown important particularly in the 2^1B_{3u} (B), 2^1B_{2u} (N) and 3^1B_{3u} (L) states.

The average discrepancies of the present SAC-CI results from the experimental peaks are 0.13 and 0.14 eV for the calculations A and B, respectively. Two calculations differ only about 0.01 eV, showing that the present result is already approximation invariant within the present basis set and the framework of the theory.

The SAC-CI ionization spectrum compares reasonably well with the Dupuis' photoelectron spectrum. The reorganization and electron correlation effects are large for the ionizations from the n and σ orbitals. The first two ionization potentials are calculated at 6.09 and 6.35 eV, which are smaller

than the experimental values, 6.9 and 7.2 eV. This is probably due to the lack of the flexibility in the valence region and the polarization function in our basis set.

REFERENCES

[1] M.Gouterman, *The porphyrins*, edited by D.Dolphin, (Academic, NewYork, 1977), Vol. 3.

[2] C.Weiss, H.Kobayashi, and M.Gouterman, J. Mol. Spectrosc. **16**, 415 (1965).

[3] M.Sundbom, Acta Chim. Scand. **22**, 1317 (1968).

[4] A.J.McHugh, M.Gouterman, and C.Weiss, Theoret. Chim. Acta. **24**, 346 (1972).

[5] H.Sekino and H.Kobayashi, J. Chem. Phys. **86**, 5045 (1987)

[6] W.D.Edwards, B.Weiner, and M.C.Zerner. J. Am. Chem. Soc. **108**, 2196 (1986).

[7] H.Sekino and H.Kobayashi, J. Chem. Phys. **75**, 3477 (1981).

[8] J.D.Baker and M.C.Zerner, Chem. Phys. Lett. **175**, 192 (1990).

[9] J.D.Petke, G.M.Maggiora, L.L.Shipman, and R.E.Christoffersen, J. Mol. Spectrosc. **71**, 64 (1978).

[10] U.Nagashima, T.Takada, and K.Ohno, J. Chem. Phys. **85**, 4524. (1986)

[11] J.B.Foresman, M.Head-Gordon, J.A.Pople, and M. J. Frisch, J. Phys. Chem. **96**, 135 (1992).

[12] Y.Yamamoto, T.Noro, and K.Ohno, Int. J. Quantum Chem. **42**, 1563 (1992).

[13] M.Merchán, E.Ortí, and B.O.Roos, Chem. Phys. Lett. **226**, 27 (1994).

[14] J.Almlöf, T. H. Fischer, P. G. Gassman, A. Ghosh, and M. Häser, J. Phys. Chem. **97**, 1993, (10964).

[15] J.Almlöf, Int. J. Quantum Chem. **3**, 915 (1974).

[16] S.F.Suntum, D.A.Case, and M.Karplus, J. Chem. Phys. **79**, 7881 (1983).

[17] M.Merchán, E.Ortí, and B.O.Roos, Chem. Phys. Lett. **221**, 136 (1994).

[18] S.Yamamoto, and H.Kashiwagi, Chem. Phys. Lett. **205**, 306 (1993).

[19] S.Yamamoto, J.Teraoka, and H.Kashiwagi, J. Chem. Phys. **88**, 303 (1988).

[20] L.Edwards and D.H.Dolphin, J. Mol. Spectrosc. **38**, 16 (1971).

[21] P.Dupuis, R.Roberge, and C.Sandorfy, Chem. Phys. Lett. **75**, 434 (1980).

[22] J.W.Weigl, J. Mol. Spectrosc. **1**, 133 (1953).

[23] B.G.Anex and R.S.Umans, J. Am. Chem. Soc. **86**, 5026 (1964).

[24] H.Nakatsuji, K.Hirao, J. Chem. Phys. **68**, 2035 (1978).

[25] H.Nakatsuji, Chem. Phys. Lett. **59**, 362 (1978); **67**, 329, 334 (1979)

[26] H.Nakatsuji, M.Hada, H.Nakai, and J.Hasegawa, the accelerated version of SAC85, to be published.

[27] H.Nakatsuji, Program System for SAC and SAC-CI calculations, Program.Library No.146(Y4/SAC), Data Processing Center of Kyoto University,1985; Program Library SAC85, No.1396, Computer Center of the Institute for Molecular Science,Okazaki, 1981.

[28] H.Nakatsuji, Acta. Chim. Hung. **129**, 719 (1992).

[29] H.Nakatsuji, O.Kitao, and T.Yonezawa, J. Chem. Phys.**83**, 723 (1985).

[30] O.Kitao and H.Nakatsuji, J. Chem. Phys. **87**, 1169 (1987).

[31] O.Kitao and H.Nakatsuji, J. Chem. Phys. **88**, 4913 (1988).

[32] H.Nakatsuji, M.Komori, and O.Kitao Chem. Phys. Lett. **142**, 446 (1987).

[33] H.Nakatsuji and S.Saito, J. Chem. Phys. **93**, 1865 (1990).

[34] H.Nakatsuji and S.Saito, Intern. J. Quantum Chem. **39**, 93 (1991).

[35] H.Nakai, Y.Ohmori, and H.Nakatsuji, J. Chem. Phys. **95**, 8287 (1991).

[36] S. Jitsuhiro, H.Nakai, M.Hada, and H.Nakatsuji, J. Chem. Phys.,**101** ,1029 (1994) .

[37] H.Nakatsuji, M.Ehara, M.H.Palmer, and M.F.Guest, J. Chem. Phys. **87**, 2561 (1992).

[38] K.Yasuda and H.Nakatsuji, J. Chem. Phys. **99**, 1945 (1993).

[39] H.Nakatsuji and M.Ehara, J. Chem. Phys. **101**, 7658 (1994).

[40] H.Nakatsuji, M.Hada, and T.Yonezawa, J. Am. Chem. Soc. **109**, 1902 (1987).

[41] H.Nakatsuji and H.Nakai, J. Chem. Phys. **98**, 2423 (1992).

[42] H.Nakatsuji, International workshop on electronic structure methods for truly large systems: moving the frontiers in quantum chemistry, Braunlage, Germany, August 1-7, 1994.

[43] S.Huzinaga, J.Andzelm, M.Klobukowski, E.Radzio-Andzelm, Y.Sakai, and H.Tatewaki, Gaussian basis set for Molecular Calculations (Elsevier, New York, 1984).

[44] S.Huzinaga, J.Chem.Phys. **42**, 1293 (1965).

[45] M.Dupuis and A.Farazdel, MOTECC-91 (Center for Scientific and Engineering Computations, IBM Corporation, 1991).

[46] H.Nakatsuji, Chem. Phys. **75**, 425 (1983).

[47] H.Kuhn, J. Chem. Phys. **17**, 1198 (1949).

[48] W.T.Simpson, J. Chem. Phys. **17**, 1218 (1949).

[49] B.O.Roos, M.Fülscher, P. Malmqvist, M. Merchán and L.Serrano-Andés, *Theoretical Studies of the Electronic Spectra of Organic Molecules*, p78.

[50] B. O. Roos, K. Andersson, and M. P. Fülscher, Chem. Phys. Lett. **192**, 5 (1992).

[51] L. Serrano-Andrés, M. Merchán, I. Nebot-Gil, B. O. Roos, and M. P. Fülscher, J. Am. Chem. Soc. **115**, 6184 (1993).

[52] M. P. Fülscher, K. Andersson, and B. O. Roos, J. Phys. Chem. **96**, 9204 (1992).

[53] R. J. Cave, and E. R. Davidson, J. Phys. Chem. **91**, 4481 (1987).

[54] J. M. O. Matos, B. O. Roos, and P. Malmqvist, J. Chem. Phys. **86**, 1458 (1987).

[55] M. H. Palmer, and I. C. Walker, Chem. Phys. **133**, 113 (1989).

[56] Y. Yamamoto, T. Noro, and K. Ohno, Intern. J. Quantum Chem. **51**, 27 (1994).

[57] H.Nakatsuji, Chem. Phys. Lett. **177**, 331 (1991).

TABLE I. Dimensions of the SAC/SAC-CI calculations for the singlet and ionized states.

state	singlet state						ionized state		
		Calc. A		Calc. B					
	before selection	N(1)[a]	after selection	N(1)[a]	N(2)[a]	after selection	before selection	N(1)[a]	after selection
SAC									
Ag	1362631	1	10879						
SAC-CI									
Ag	1362631	3	42176	3	9	46199	25560	8	6939
B1g	1360246	3	51051	3	12	54848	25523	7	5985
B2g	1308922	1	20723	1	2	21230	22979	3	3082
B3g	1308922	1	20882	1	2	21441	22979	3	2809
Au	1308888	1	20145	1	2	20688	22962	2	1755
B1u	1308958	1	20280	1	2	20855	22993	5	4215
B2u	1360282	4	49836	4	11	53515	25543	7	6301
B3u	1360282	4	45905	4	9	49391	25543	7	6478

[a] N(n) denotes the number of the n electron excited configurations used as the reference configurations in the configuration selection scheme.

TABLE II. Timing data for the SAC/SAC-CI calculations of porphin.[a]

Step	Timing
SCF	17 min.
Integral transformation	93 min.
SAC (for ground state)	84 min.
SAC-CI (per state)	
Singlet excited state	80 min.
Ionized state	2 min.

[a] Computations are performed by the NEC SX-3 computer at the Computer Center of the Institute for Molecular Science.

TABLE III. HF orbital energy and orbital nature of porphin.

MO	orbital energy (eV)	character
Higher occupied orbitals		
$7a_g$	-14.661	σ
$6b_{2u}$	-14.646	σ
$7b_{3u}$	-14.480	σ
$7b_{1g}$	-14.355	σ
$1a_u$	-12.216	π
$7b_{2u}$	-11.415	n
$8a_g$	-11.263	n
$3b_{1u}$	-10.679	π
$2b_{2g}$	-10.632	π
$2b_{3g}$	-10.590	π
$3b_{2g}$	-10.321	π
$4b_{1u}$	-9.327	π
$3b_{3g}$	-9.122	π
$5b_{1u}$	-6.686	π
$2a_u$	-6.521	π
Lower unoccupied orbitals		
$4b_{2g}$	-0.069	π
$4b_{3g}$	0.141	π
$3a_u$	2.842	π
$6b_{1u}$	5.064	π
$5b_{2g}$	5.698	π
$5b_{3g}$	5.702	π
$4a_u$	6.177	π
$8b_{3u}$	6.852	σ
$8b_{2u}$	7.437	σ
$8b_{1g}$	8.046	σ

TABLE IV. Excited states of free base porphin calculated by the SAC-CI method.

state[a]	SAC-CI (B)					SAC-CI (A)		expt.[b]		other ab initio theoretical excitation energy (eV)			
	main configuration (C > 0.3)	nature	excitation energy (eV)	polari-zation	oscillator strength (eV)	excitation energy (eV)	polari-zation	excitation energy (eV)		MRSDπCI[c]	CIS[d]	MRSDσπCI[e]	CASPT2F[f]
$1B_{3u}$	0.73 ($5b_{1u} \rightarrow 4b_{2g}$)-0.61 ($2a_u \rightarrow 4b_{3g}$)	π–π*	1.75	x	1.13×10^{-3}	1.80	x	1.98	Q_x	2.27	2.53	1.97	1.70
$1B_{2u}$	-0.70 ($2a_u \rightarrow 4b_{2g}$)-0.66 ($5b_{1u} \rightarrow 4b_{3g}$)	π–π*	2.23	y	5.66×10^{-3}	2.25	y	2.42	Q_y	3.42	2.66	2.40	2.26
$1B_{1g}$	0.93 ($3b_{3g} \rightarrow 4b_{2g}$)	π–π*	3.55		0.0	3.59							
$2B_{3u}$	-0.64 ($2a_u \rightarrow 4b_{3g}$)+0.52 ($4b_{1u} \rightarrow 4b_{2g}$)	π–π*	3.56	x	1.03	3.59	x	3.33	B	4.72	4.6	3.41	2.91
	-0.43 ($5b_{1u} \rightarrow 4b_{2g}$)									5.29	4.8	3.24	3.04
$2B_{2u}$	0.66 ($5b_{1u} \rightarrow 4b_{3g}$)-0.63 ($2a_u \rightarrow 4b_{2g}$)	π–π*	3.75	y	1.73	3.79	y	3.65	N				
	-0.25 ($4b_{1u} \rightarrow 4b_{3g}$)												
$1B_{2g}$	0.94 ($8a_g \rightarrow 4b_{2g}$)	n–π*	4.05		0.0	4.06							
$1A_u$	-0.93 ($7b_{2u} \rightarrow 4b_{2g}$)	n–π*	4.18		0.0	4.18							
$3B_{3u}$	0.76 ($4b_{1u} \rightarrow 4b_{2g}$)+0.33 ($2a_u \rightarrow 4b_{3g}$)	π–π*	4.24	x	0.976	4.28	x	4.25	L				
	-0.40 ($5b_{1u} \rightarrow 4b_{2g}$)												
$2A_g$	0.88 ($3b_{3g} \rightarrow 4b_{3g}$)-0.32 ($2a_u \rightarrow 3a_u$)	π–π*	4.25		0.0	4.29							
$1B_{3g}$	0.94 ($8a_g \rightarrow 4b_{3g}$)	π–π*	4.37		0.0	4.38							
$1B_{1u}$	0.93 ($7b_{2u} \rightarrow 4b_{3g}$)	n–π*	4.51	z	5.30×10^{-3}	4.54	z		L				
$3B_{2u}$	0.89 ($4b_{1u} \rightarrow 4b_{3g}$)	π–π*	4.52	y	0.350	4.55	y	4.67	L				
$2B_{1g}$	0.91 ($2a_u \rightarrow 6b_{1u}$)	n–π*	4.62		0.0	4.63							
$3A_g$	-0.86 ($2a_u \rightarrow 3a_u$)-0.35 ($3b_{3g} \rightarrow 4b_{3g}$)	π–π*	4.74		0.0	4.78							
$3B_{1g}$	0.66 ($2b_{3g} \rightarrow 4b_{2g}$)+0.65 ($3b_{2g} \rightarrow 4b_{3g}$)	π–π*	5.13		0.0	5.17							
$4A_g$	0.86 ($3b_{2g} \rightarrow 4b_{2g}$)-0.31 ($2b_{3g} \rightarrow 4b_{3g}$)	π–π*	5.28		0.0	5.32							
$4B_{2u}$	0.90 ($3b_{1u} \rightarrow 4b_{3g}$)	π–π*	5.31	y	0.280	5.34	y		M				
$4B_{3u}$	-0.93 ($3b_{1u} \rightarrow 4b_{2g}$)	π–π*	5.45	x	0.351	5.48	x	5.50	M				

[a] Bold face letter is for the optically allowed state. [b] Ref 20. [c] Ref 10. [d] Ref 11. [e] Ref 12. [f] Ref 13.

TABLE V. The number of configurations that have CI coefficients larger than 0.01.

state		$1B_{2u}$	$2B_{2u}$	$3B_{2u}$	$4B_{2u}$	$1B_{3u}$	$2B_{3u}$	$3B_{3u}$	$4B_{3u}$
	$\pi-\pi^*$	15	22	15	20	18	19	15	18
nature	$\sigma-\pi^*$	0	0	0	0	0	0	0	0
	$\sigma-\sigma^*$	0	8	1	1	0	4	3	0

TABLE VI. Ionized states of free base porphin.

state	main configuration (C > 0.3)		exptl.[a] (eV)	present (eV)			Almlöf[b] (eV)		
				SAC-CI IP	Koopmans IP	Δ[c]	ΔSCF IP	orbital energy	orbital reorganization energy
1^2B_{1u}	-0.97 ($5b_{1u}$)	:π	6.9	6.09	6.52	0.43	8.00	8.42	0.42
1^2A_u	0.98 ($2a_u$)	:π	7.2sh	6.35	6.69	0.34	8.39	8.78	0.39
1^2B_{3g}	-0.97 ($3b_{3g}$)	:π	8.4	7.98	9.12	1.14	10.41	11.02	0.61
2^2B_{1u}	0.97 ($4b_{1u}$)	:π		8.21	9.33	1.12	11.08	11.41	0.33
1^2A_g	-0.96 ($8a_g$)	:n	8.8sh	8.65	11.26	2.61	11.82	12.76	0.94
1^2B_{2u}	-0.96 ($7b_{2u}$)	:n		8.79	11.42	2.63	11.24	12.76	1.52
1^2B_{2g}	-0.69 ($3b_{2g}$) -0.68 ($2b_{2g}$)	:π	9.11	9.10	10.32	1.22	12.16	12.74	0.58
3^2B_{1u}	0.96 ($3b_{1u}$)	:π		9.34	10.68	1.34	12.44	12.75	0.31
2^2B_{2g}	0.69 ($2b_{2g}$) -0.68 ($3b_{2g}$)	:π		9.42	10.70	1.28	12.35	12.58	0.28
2^2B_{3g}	-0.97 ($2b_{3g}$)	:π		9.54	10.63	1.09	12.62	12.89	0.27
2^2A_u	-0.97 ($1a_u$)	:π		10.85	12.22	1.37			
1^2B_{1g}	-0.97 ($7b_{1g}$)	:σ		12.40	14.36	1.96			
1^2B_{3u}	0.95 ($7b_{3u}$)	:σ		12.43	14.48	2.05			
2^2B_{1g}	-0.94 ($6b_{1g}$)	:σ		12.67	14.63	1.96			

[a] Ref. 21. [b] Ref 15. [c] Δ is the difference between the Koopmans IP and the SAC-CI IP.

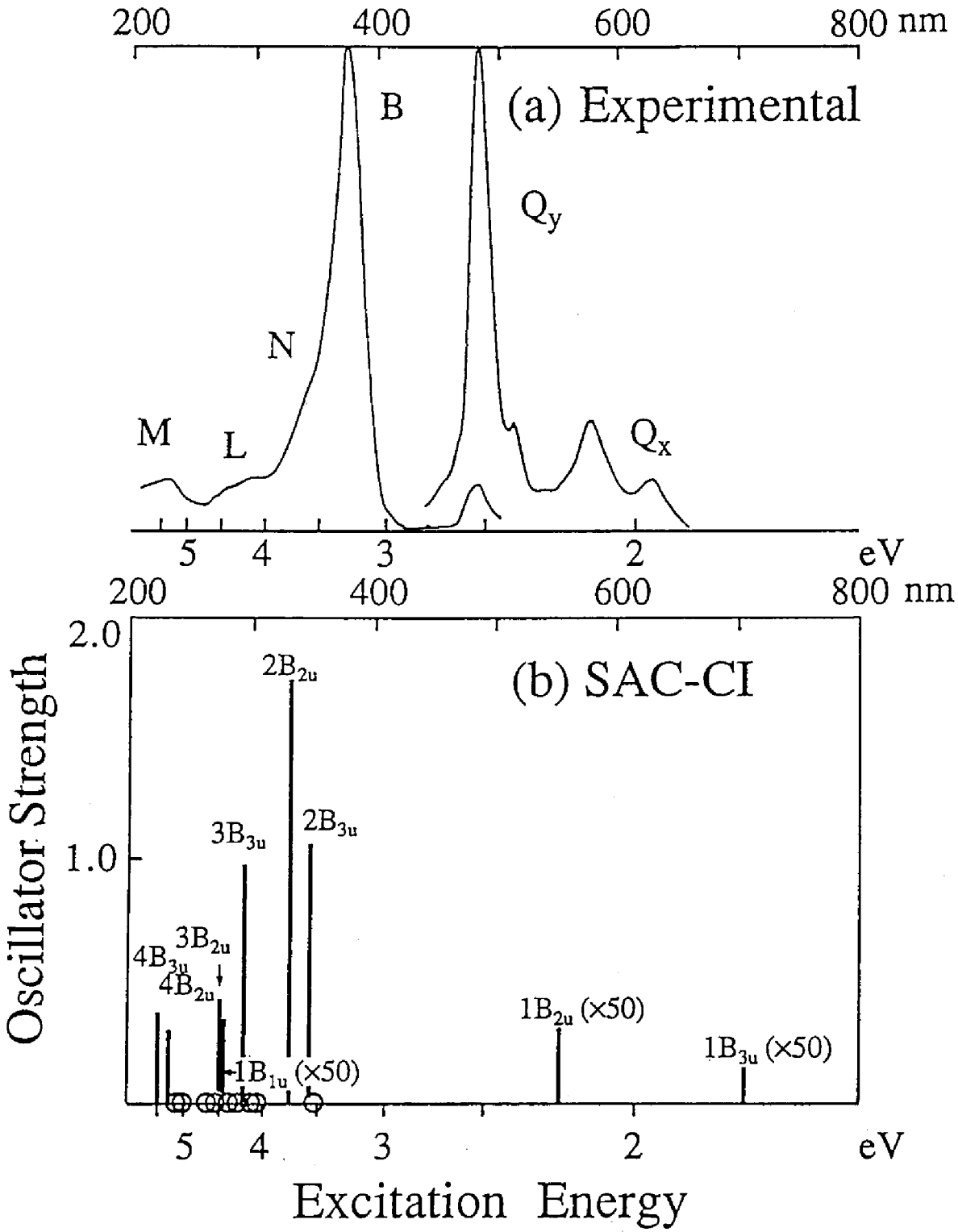

FIG. 1. Electronic spectrum of free base porphin. (a) Gas-phase experimental spectrum due to Edwards et al. (Ref. 20) and (b) SAC-CI theoretical spectrum. The optically forbidden states are indicated by open circles.

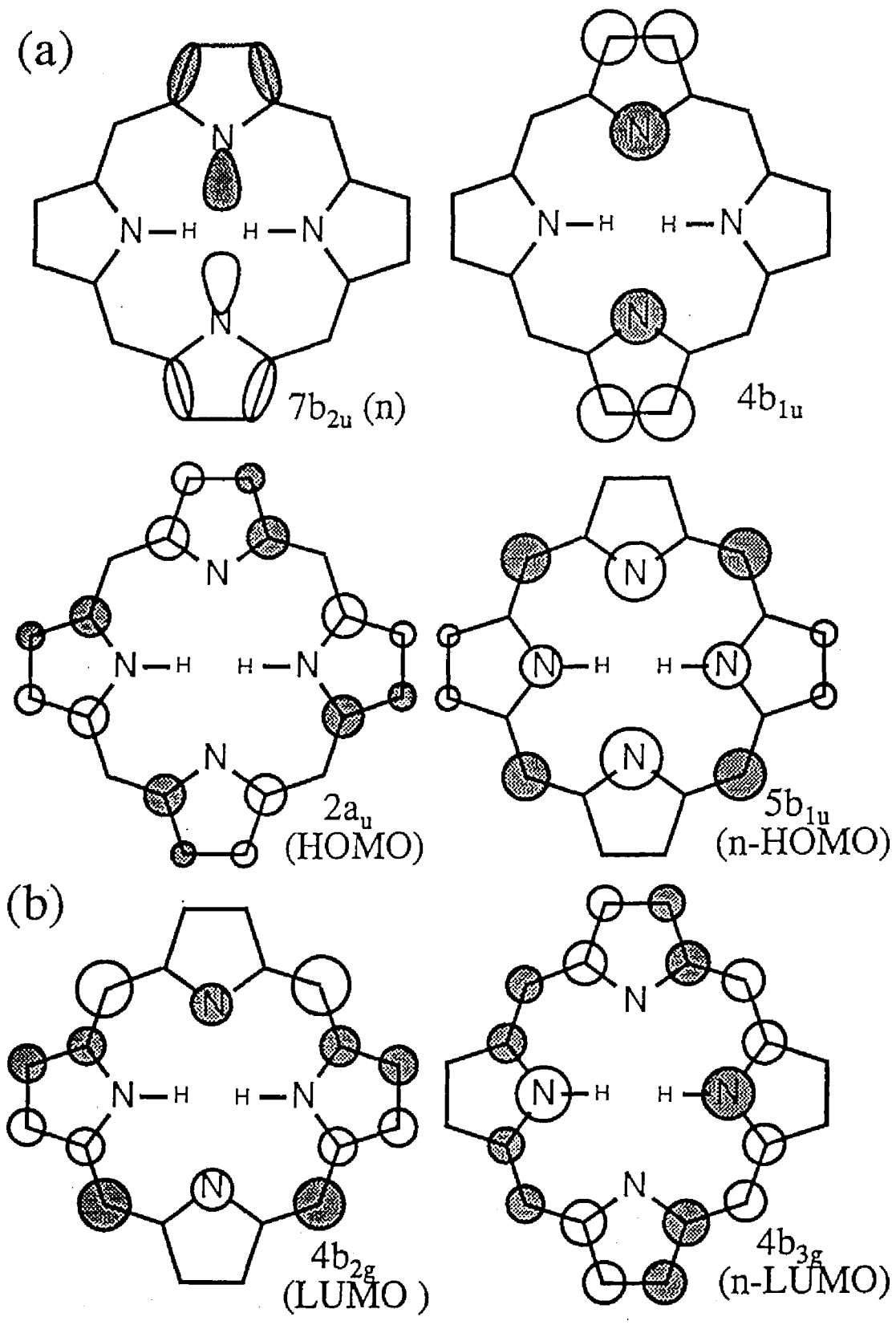

FIG. 2. Illustration of the orbitals for (a) the occupied MOs (7b2u, 4b1u, 5b1u and 2au) and (b) the unoccupied MOs (4b2g and 4b3g) .

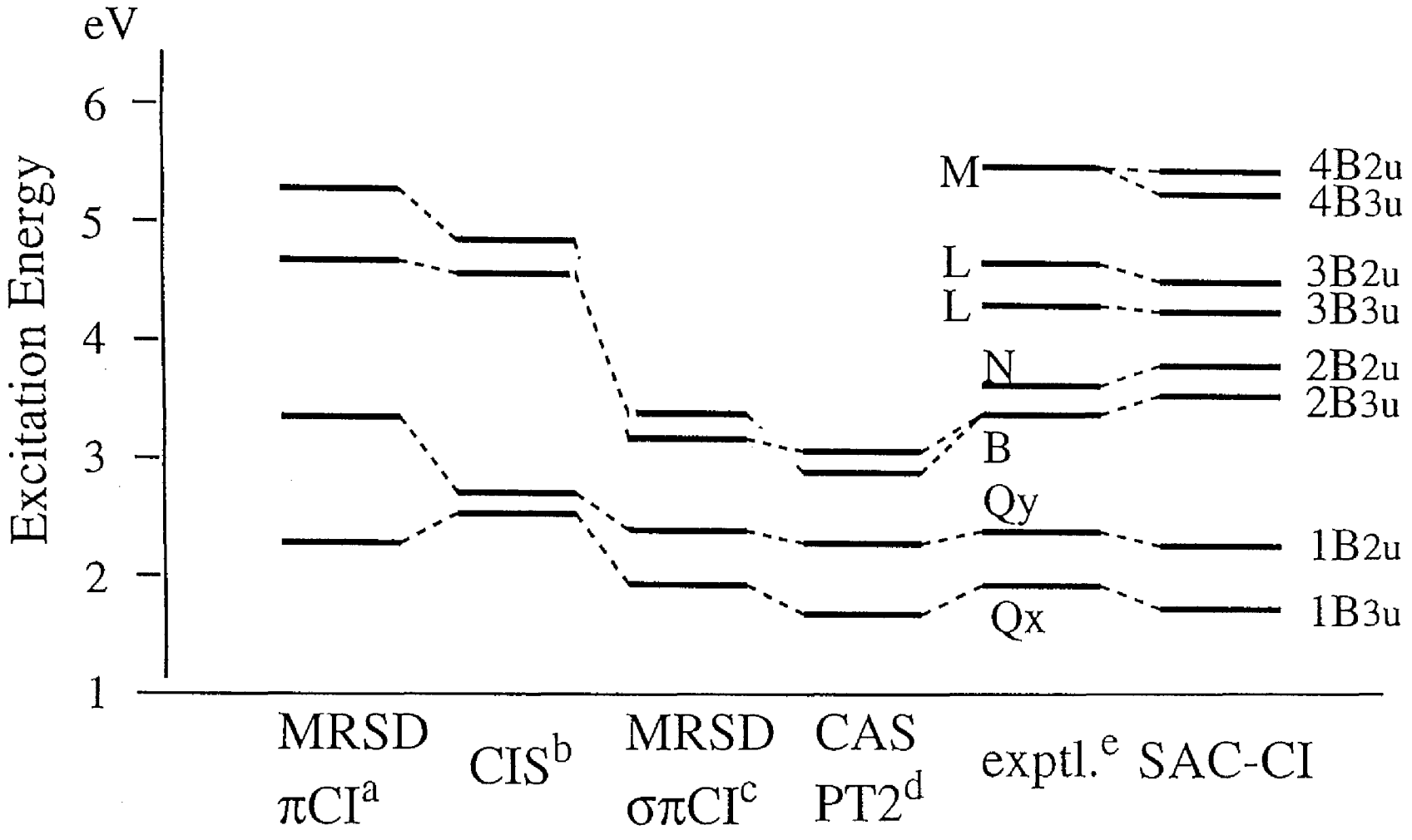

FIG. 3. Ab initio theoretical electronic spectra for free base porphin. The dotted lines show the assignment of the experimental peaks by each method. (a) Reference 10. (b) Reference 11. (c) Reference 12. (d) Reference 13. (e) Reference 20.

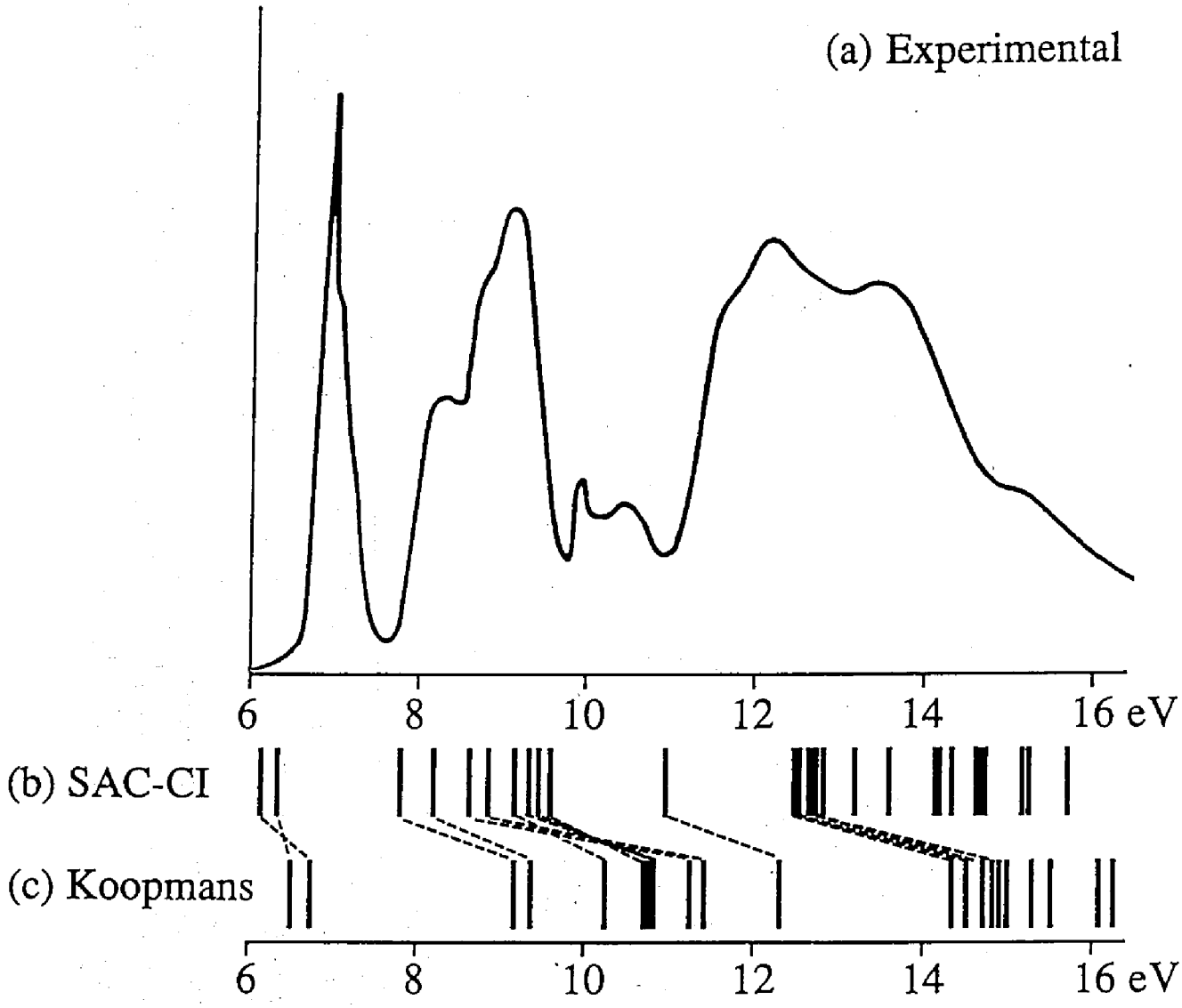

FIG. 4. Ionization spectrum of free base porphin. (a) Photoelectron spectrum (Ref. 21). (b) SAC-CI and (c) Koopmans ionization potentials. The dotted lines show the correspondences between the Koopmans IP's and the SAC-CI ones.

Chapter 2

Excited states of Mg porphin

Abstract

The SAC(symmetry adapted cluster)/SAC-CI method is applied to the ground and excited states of magnesium porphin (MgP). The π interaction between the Mg atom and the porphin ring is small and therefore the essential difference between MgP and free base porphin (FBP) lies in symmetry; the former is D_{4h} and the latter D_{2h}. The degenerate excited states in MgP split into two in FBP. The SAC-CI results for the excitation energy and the oscillator strength compare reasonably well with the experimental spectra for Mg etioporphyrin (MgEtio) and Mg tetraphenylporphin (MgTPP) and the natures of the excited states are clarified. Gouterman's four-orbital model holds well for the Q band, but the excitations from the $2a_{2u}$ MO below the four orbitals mix in the B band, as was found previously for FBP. The natures of the N bands are different between MgP and FBP.

1. Introduction

Photosynthesis is one of the most important biological reactions. In the X-ray crystallographical structure of the reaction center of *Rhodopseudomonus (Rps.) viridis* [1], Mg porphyrin takes a central part as a special pair and its important role in the photosynthesis is more and more revealed by many studies. It is said that the excitations of the special pair initiates the charge separation in the photosynthesis, so that it is significant to study the electronic structures of the ground and excited states of Mg porphyrins.

Gouterman proposed that the lower excited states of porphyrins are well understood by the four-orbital model [2]. Many calculations on the excited states of porphyrins were reported using semi-empirical methods [2-5] and ab initio methods [2,6-13]. For free-base porphin (FBP), accurate and reliable calculations for the ground and excited states were reported by Roos et al. with the CASPT2 method [10] and by Nakatsuji et al. with the SAC-CI method [11]. They revealed some important aspects of the electronic structures of FBP. More recently, we have also studied the ground and low-lying excited states of oxyheme [12] and tetrazaporphin [13] by the SAC-CI method.

We study here the ground and excited states of Mg-porphin (MgP) using the SAC[14]/SAC-CI[15] method [16,17]. We use here the modified version [18] of the SAC85 program [19]. We have to note that the EOM-CC method [20,21] published from Bartlett's group is essentially the same as our SAC-CI method published much earlier. The SAC-CI theory is a wide and essentially exact concept [15,16] and includes not only excitations but also ionizations and electron attachments and, therefore, the SAC-CI method also involves the IP-EOMCC [22] and EA-EOMCC [23] method: such ideas have been published many years ago [16] and used for many years in various applications [17,24-

26]. Our SAC-CI program can deal with the ground and excited states having spin multiplicities from singlet to septet [27].

2. Computational details

MgP, $MgC_{20}N_4H_{12}$ has D_{4h} symmetry and is considered as the complex of the Mg^{2+} ion coordinated at the center of the dianion porphin ring. For the nuclear coordinates of the porphin skeleton, those of the FBP by Sekino and Kobayashi [3] are adopted and the Mg atom is located at the inversion center of the D_{4h} symmetry.

The basis set is of double-ζ quality for the valence 2p orbitals of carbon and nitrogen. We used (63/5)/[63/41] set of Huzinaga [28] for carbon and nitrogen, and Huzinaga's (4)/[4] set [29] for hydrogen. For Mg atom, we used two different basis sets. In calculation (A) we used Huzinaga's (533/5)/[53111/41] set [28] plus two p-type polarization functions (α= 0.045, 0.143), and in calculation (B) we used (533/5)/[53111/311] set plus the same p-type functions and the d-type polarization functions (α= 1.01). The total number of the contracted GTO's is 221 for calculation (A) and 230 for calculation (B). The Hartree-Fock (HF) - Self Consistent Field (SCF) orbitals were calculated by the HONDO program [30]: the number of the occupied MOs is 86.

The electron correlations in the ground and excited states are taken into account by the SAC/SAC-CI method. In calculation (A), the higher 42 occupied orbitals and the lower 124 virtual orbitals, and in calculation (B), the higher 53 occupied orbitals and the lower 132 virtual orbitals are included in the active space: in calculation (B), only the inner core MOs are frozen. The total number of the active orbitals is 166 in calculation (A) and 185 in calculation (B). The active space includes all π-type orbitals and a large number of σ-orbitals. All

the single excitations and the selected double excitations are included in the linked term. The energy threshold in the configuration selection step is different for the π–π^* excitations and for the other ones. For the former, the energy thresholds, 1.0×10^{-5} and 5.0×10^{-7} a.u. are used for the ground and excited states, respectively, and for the latter, 2.0×10^{-5} and 1.0×10^{-6} a.u., respectively, are used [11,31]. Table 1 shows the dimensions of the linked terms before and after the selection.

3. Ground state electronic structure

The orbital energy and the nature of some higher occupied and lower unoccupied MOs are shown in Table 2. The π-type orbitals gather in the HOMO, LUMO regions. In particular, the HOMO, next-HOMO, and the LUMO which is degenerate are well separated from the other orbitals, implying the validity of the four-orbital model of Gouterman [2]. These four orbitals and some lower orbitals which play an important role in the present study are illustrated in Fig. 1. All of these orbitals are well localized on the porphin ring. Four occupied lone-pair (n) orbitals on the nitrogens lie below the most of the π MOs and the σ-type orbitals are below of these orbitals.

The Mg 3s orbital mixes in the lower three n orbitals, representing the coordination bonds between the Mg atom and the porphin ring. They lie in a rather lower side of the occupied MOs as shown in Table 2. In the unoccupied manifold, some MOs have the Mg component but they lie higher than the LUMO belonging to the four orbitals. Actually, the energy levels and the characters of the MOs of the Mg porphin are quite similar to those of FBP. The HOMO-LUMO energy gaps are also quite similar: 6.45 eV in FBP and 6.53 (calc A) or 6.52 (calc B) eV in MgP.

These facts indicate that the π–interaction between the Mg atom and the porphin ring is small, implying a similarity in the nature of the excited states between FBP and MgP. However, a large difference that exists between them is the symmetry. Some orbitals and excited states are degenerate in MgP, but not in FBP. This causes a large difference in the excitation spectrum, as shown below.

The correlation energy for the ground state is calculated to be 9.67 (calc B) or 8.70 (calc A) eV by the SAC method. In the eigenvector for the ground state, the Hartree-Fock configuration is dominant. For example, the coefficients of the excited configurations involving the four orbitals are less than 0.05. Thus, the single reference theory can describe the ground state of MgP with a sufficient accuracy.

4. Excited states

The SAC-CI theoretical spectrum for MgP is compared in Fig. 2 with the experimental spectrum for Mg etioporphin (MgEtio) measured in the vapor phase by Edwards et al. [32]. Table 3 summarizes the SAC-CI results for the optically allowed states. The main configurations, characters, excitation energies and oscillator strengths are shown.

We have observed in the above section that the π–interaction between the Mg atom and the porphin ring is small in the MgP and that the Mg orbitals do not lie in the HOMO-LUMO region nor mix with the four orbitals. This means that the nature of the lower excited states should be similar between FBP and MgP. However, a large difference lies in symmetry; the former is D_{2h} but the latter D_{4h}. Therefore, the degenerate excitations in MgP should split into two in FBP. A comparison between the spectra of FBP and MgP should thus be quite

useful for the assignment of the observed peaks. However, a point of difficulty is that there is no observed spectrum for MgP, though we have that for FBP. In Fig. 3 and Table 3, we compare the SAC-CI levels of the excited states of FBP and MgP with the experimentally observed levels for FBP, free base TPP (tetraphenylporphin), MgEtio, and MgTPP [32]. The dotted lines in Fig. 3 connect the states having similar nature. In Fig. 2, the experimental spectrum is actually for MgEtio.

The Q band is composed of a weak peak observed at about 2.1 eV. By the SAC-CI calculations, the Q band is assigned to the degenerate 1^1E_u state calculated at 2.1 eV in calculation (A) and 2.0 eV in calculation (B). The intensity is small in accordance with the weakness of the observed peak. The main configuration of the 1^1E_u state is composed of the excitations within the four orbitals and the weight of the two main configurations, $1a_{1u} \rightarrow 4e_g$ and $3a_{2u} \rightarrow 4e_g$ are almost the same, causing quite a small intensity of the Q band [13]. This nature is essentially the same as that of FBP [11], though it splits into Q_x and Q_y peaks in FBP.

A strong sharp absorption peak is observed around 400 nm in the experimental spectrum. It is called the B (Soret) band. The B band is assigned to the degenerate 2^1E_u state calculated at 3.78 eV in calculation (A) and 3.63 eV in calculation (B). The peak in the experimental spectrum lie in the 3.0~3.5 eV region for MgEtio (see Fig. 2) and MgTPP. The main configuration of the 2^1E_u state includes not only the excitations within the four orbitals but also the excitation from the lower $2a_{2u}$ MO. This was also seen previously for FBP [11]. In FBP the mixing of the excitations from the $4b_{1u}$ MO, corresponding to the $2a_{2u}$ MO in this case, was large; the weight was 27 % in the 2^1B_{3u} state. For MgP, the weight is smaller and only about 7%. Thus, the four-orbital model applies better to MgP than to FBP.

The N band is a weak peak observed in the 3.8~4.0 eV region for MgEtio and MgTPP. This band is assigned to the 3^1E_u state calculated at 4.4 eV in calculation (A) and 4.2 eV in calculation (B). The main configuration, $2b_{2u} \rightarrow 4e_g$ does not belong to the excitations within the four orbitals. The nature of this state is different from that of FBP. The N band of MgP corresponds to the L band of FBP, and the N band of FBP corresponds to one element of the degenerate B band of MgP, as clearly seen from Fig. 3. This difference in the electronic structure of the N band between FBP and MgP is supported by the difference in the intensity. In the observed spectra, the intensity of the N band is quite small for MgTPP and MgEtio in comparison with that of the B band, but for FBP and free base TPP, the intensity of the N band is comparable with that of the B band [32]. Our theoretical results agree with this observation. The calculated intensity of the N band of FBP is comparable with that of the B band since it originates from the same degenerate electronic state [11], but the calculated intensity of the N band of the MgP is quite small in comparison with that of the B band. Furthermore, comparing the experimental energy levels of MgTPP directly with those of TPP as shown in Fig. 3, we notice that the N band of MgTPP is closer to the L band of TPP than to its N band.

The experimental spectra for MgEtio and MgTPP show considerably strong absorptions, called the M band, in the 5.8~6.2 eV region. This band may be assigned to the 4^1E_u state calculated at 5.1 eV in calculation (A) and 4.9 eV in calculation (B). The main configuration of this state is again out of the four-orbital model.

The 1^1A_{2u} state obtained in this calculation has only a very week intensity and we can not see the band which corresponds to it in the experimental spectrum of MgEtio. However, in the experimental spectrum of MgTPP, we can see a weak "1" band in the corresponding energy region [32], so that the 1^1A_{2u} state might correspond to it. The calculated excitation energy of the

1^1A_{2u} state is 4.8 eV by calculation (B) and lies between the 3^1E_u and 4^1E_u state. This ordering is seen in the experimental spectrum of MgTPP. The result of calculation (A) does not reproduce this ordering. In the case of FBP, the 1^1B_{1u} state corresponds to this 1^1A_{1u} state of MgP. The 1^1B_{1u} state of FBP is due to the excitation from the lone pair orbital of nitrogen to the LUMO or next LUMO, while the 1^1A_{1u} state of MgP is due to the excitation from the next HOMO to the Mg 3s orbital. In calculation (B), we have given a wider freedom to the Mg basis set than in calculation (A), so that the stability of about 0.6 eV for the 1^1A_{2u} state of MgP is reasonable.

References

[1] J.Deisenhofer, O.Epp, K.Miki, R.Huber and H.Michel, J. Mol. Biol. 180 (1984), 385.

[2] M.Gouterman, The porphyrins, edited by D.Dolphin, Vol. 3 (Academic, New York, 1977).

[3] H.Sekino and H.Kobayashi, J. Chem. Phys. 75 (1981) 3477; 86 (1987) 5045.

[4] J.D.Baker and M.C.Zerner, Chem. Phys. Letters 175 (1990) 192.

[5] M.A. Thompson and M.C. Zerner, J. Am. Chem. Soc. 113 (1991) 8210.

[6] J.D.Petke, G.M.Maggiora, L.L.Shipman and R.E.Christoffersen, J. Mol. Spectr. 71 (1978) 64.

[7] J.D.Petke and G.M.Maggiora, J. Chem. Phys. 84 (1986) 1640.

[8] U.Nagashima, T.Takada and K.Ohno, J. Chem. Phys. 85 (1986) 4524.

[9] Y.Yamamoto, T.Noro and K.Ohno, Intern. J. Quantum Chem. 42 (1992) 1563.

[10] M.Merchán, E.Ortí and B.O.Roos, Chem. Phys. Letters 226 (1994) 27.

[11] H.Nakatsuji, J.Hasegawa and M. Hada, J. Chem. Phys. in press.

[12] H.Nakatsuji, J.Hasegawa, H.Ueda and M.Hada, submitted to Chem. Phys. Letters.

[13] K.Toyota, J.Hasegawa and H.Nakatsuji, submitted to Chem. Phys. Letters.

[14] H.Nakatsuji, and K.Hirao, J.Chem.Phys. 68 (1978) 2035.

[15] H.Nakatsuji, Chem. Phys. Letters 59 (1978) 362.

[16] H.Nakatsuji, Chem. Phys. Letters 67 (1979) 329, 334.

[17] H.Nakatsuji, Acta. Chim. Hung. 129 (1992) 719

[18] H.Nakatsuji, M.Hada, J.Hasegawa and H.Nakai, the modified version of SAC85, to be published.

[19] H.Nakatsuji, Program System for SAC and SAC-CI calculations program. Library No.146 (Y4/SAC), Data Processing Center of Kyoto University, 1985;

Program Library SAC85, No.1396, Computer Center of the Institute for Molecular Science, 1986.

[20] J.Geertsen, M.Rittby and R.J.Bartlett, Chem. Phys. Letters 164 (1989) 57.

[21] S.R.Gwaltney and R.J.Bartlett, Chem. Phys. Letters 241 (1995) 26.

[22] J.F.Stanton and J.Gauss, J. Chem. Phys. 101 (1994) 8938.

[23] M.Nooijen and R.J.Bartlett, J. Chem. Phys. 102 (1995) 3629.

[24] H.Nakatsuji and K.Hirao, Intern. J. Quantum Chem. 20 (1981) 1301.

[25] H.Hakatsuji, K.Ohta, and T.Yonezawa, J. Phys. Chem. 89 (1983) 3068.

[26] H.Hakatsuji, Intern. J. Quantum. Chem. S17 (1983) 241.

[27] H.Hakatsuji and M.Ehara, J. Chem. Phys. 98 (1993) 7179.

[28] S.Huzinaga, J.Andzelm, M.Klobukowski, E.Radzio-Andzelm, Y.Sakai, H. Tatewaki, Gaussian basis set for Molecular Calculations (Elsevier, New York, 1984).

[29] S.Huzinaga, J.Chem.Phys. 42 (1965) 1293.

[30] M.Dupuis and A.Farazdel, MOTECC-91 (Center for Scientific and Engineering Computations, IBM Corporation, 191).

[31] H. Nakatsuji, Chem. Phys. 75 (1983) 425.

[32] L.Edwards and D.H.Dolphin, J. Mol. Spectr. 35 (1970) 90; 38 (1971) 16.

Table 1
Dimensions of the linked terms in the SAC/SAC-CI calculations of the singlet states of MgP

state	Calc. A			Calc. B		
	before selection	N [a]	after selection	before selection	N [a]	after selection
SAC						
^1A_g	1738599	1	10827	3185815	1	11755
SAC-CI						
$^1B_{1u}$ ($^1A_{1u}$)	1655788	1	12172	2935912	1	13152
$^1B_{2u}$ (^1E_u)	1735955	4	51654	3182250	4	60539
$^1B_{3u}$ (^1E_u)	1735955	4	51654	3182250	4	60539

[a] N is the number of states used in the configuration selection step.

Table 2
HF orbital energy and orbital character of MgP in calculation B

MO	orbital energy (eV)	character	Mg-component [a]
Higher occupied orbitals			
$4b_{1g}$	-14.897	σ	
$9e_u$	-14.628	σ	
$1b_{2u}$	-14.609	π	
$4a_{2g}$	-14.407	σ	
$6a_{1g}$	-14.401	n	3s
$5b_{2g}$	-14.380	σ	
$10e_u$	-12.791	n	
$1b_{1u}$	-12.058	π	
$5b_{1g}$	-11.807	n	
$2e_g$	-10.295	π	
$2a_{2u}$	-9.989	π	
$3e_g$	-9.622	π	
$2b_{2u}$	-9.501	π	
$3a_{2u}$ (next-HOMO)	-6.651	π	
$1a_{1u}$ (HOMO)	-6.368	π	
Lower unoccupied orbitals			
$4e_g$ (LUMO)	0.153	π	
$7a_{1g}$	2.824	σ	3s
$2b_{1u}$	2.932	π	
$4a_{2u}$	3.405	π	pol. p_z
$11e_u$	5.169	σ	pol. p_x, p_y
$3b_{2u}$	5.319	π	
$5e_g$	5.721	π	d_{xz}, d_{yz}
$2a_{1u}$	6.311	π	
$2b_{1u}$	6.892	π	
$8a_{1g}$	7.370	σ	3s

[a] Mg AOs included.

Table 3
Ground and excited states of MgP

state	SAC-CI (B)				SAC-CI (A)		Exptl. [a]			
	main configuration (C>0.3)	character	excitation energy (eV)	oscillator strength	excitation energy (eV)	oscillator strength	excitation energy(eV) MgEtio	MgTPP	intensity	
X^1A_{1g}	1.00(HF [b])		0.00 [c]	—	0.00 [d]	—				
1^1E_u	0.68($1a_{1u}\rightarrow 4e_g$) -0.67($3a_{2u}\rightarrow 4e_g$)	π–π*	2.01	1.52×10^{-3}	2.14	5.65×10^{-3}	2.14	2.07	Q	w
2^1E_u	-0.67($1a_{1u}\rightarrow 4e_g$) -0.61($3a_{2u}\rightarrow 4e_g$) -0.27($2a_{2u}\rightarrow 4e_g$)	π–π*	3.63	1.99	3.78	2.14	3.18	3.04	B	s
3^1E_u	-0.90($2b_{2u}\rightarrow 4e_g$)	π–π*	4.15	0.069	4.38	0.0723	3.82	3.96	N	m
1^1A_{2u}	0.96($3a_{2u}\rightarrow 7a_{1g}$)	π–Mg(3s)	4.75	4.46×10^{-3}	5.38	6.93×10^{-3}	4.7	5.16	L	w
4^1E_u	-0.88($2a_{2u}\rightarrow 4e_g$)	π–π*	4.89	0.590	5.12	0.566	5.23	6.20	M	ms

[a] Ref. [32].
[b] Hartree Fock configuration.
[c] Correlation energy for the ground state is 9.67 eV.
[d] Correlation energy for the ground state is 8.70 eV.

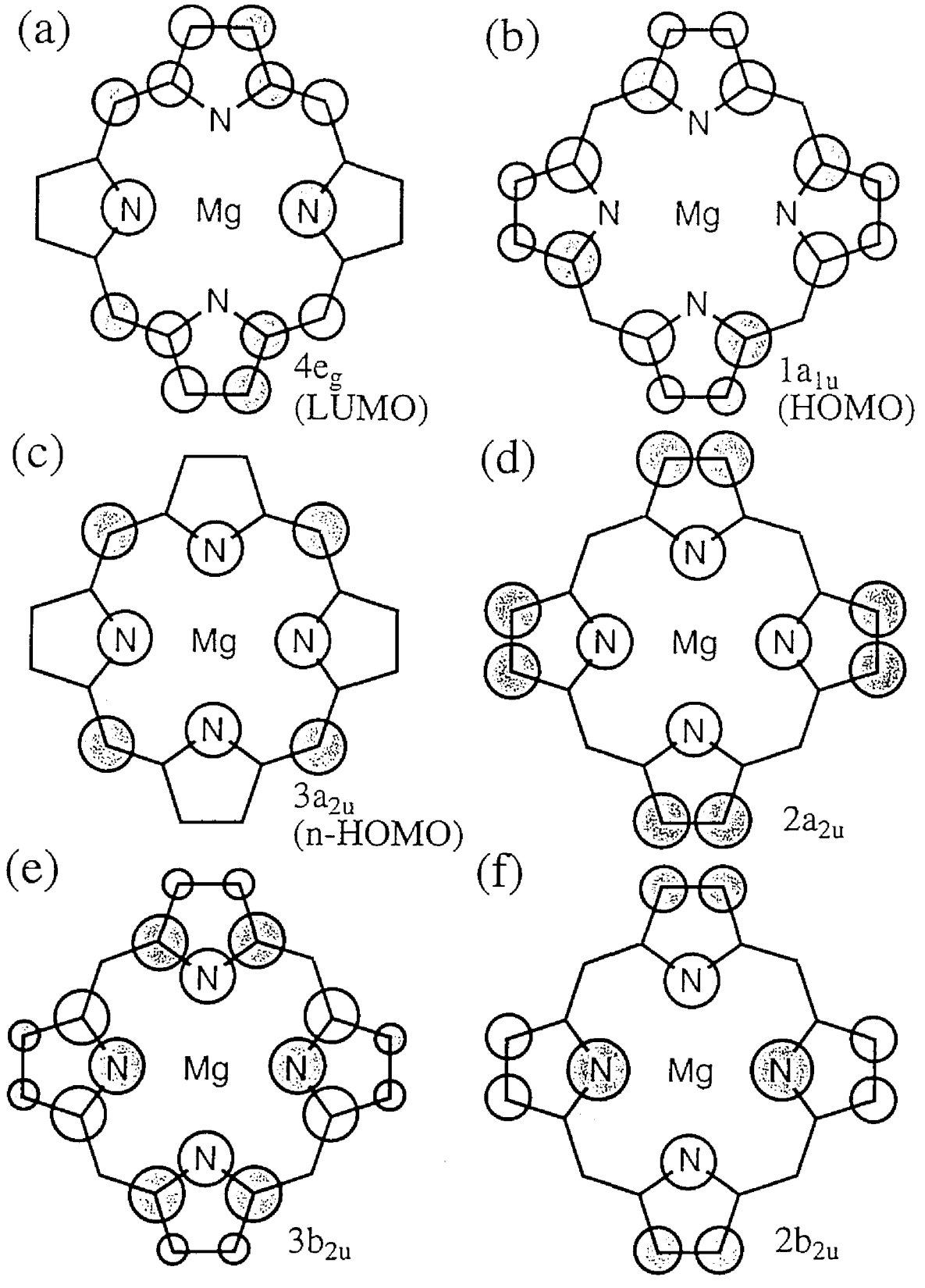

Fig. 1. Some molecular orbitals of MgP. (a) $4e_g$ (LUMO), (b) $1a_{1u}$ (HOMO), (c) $3a_{2u}$ (n-HOMO), (d) $2a_{2u}$, (e) $3b_{2u}$, (f) $2b_{2u}$.

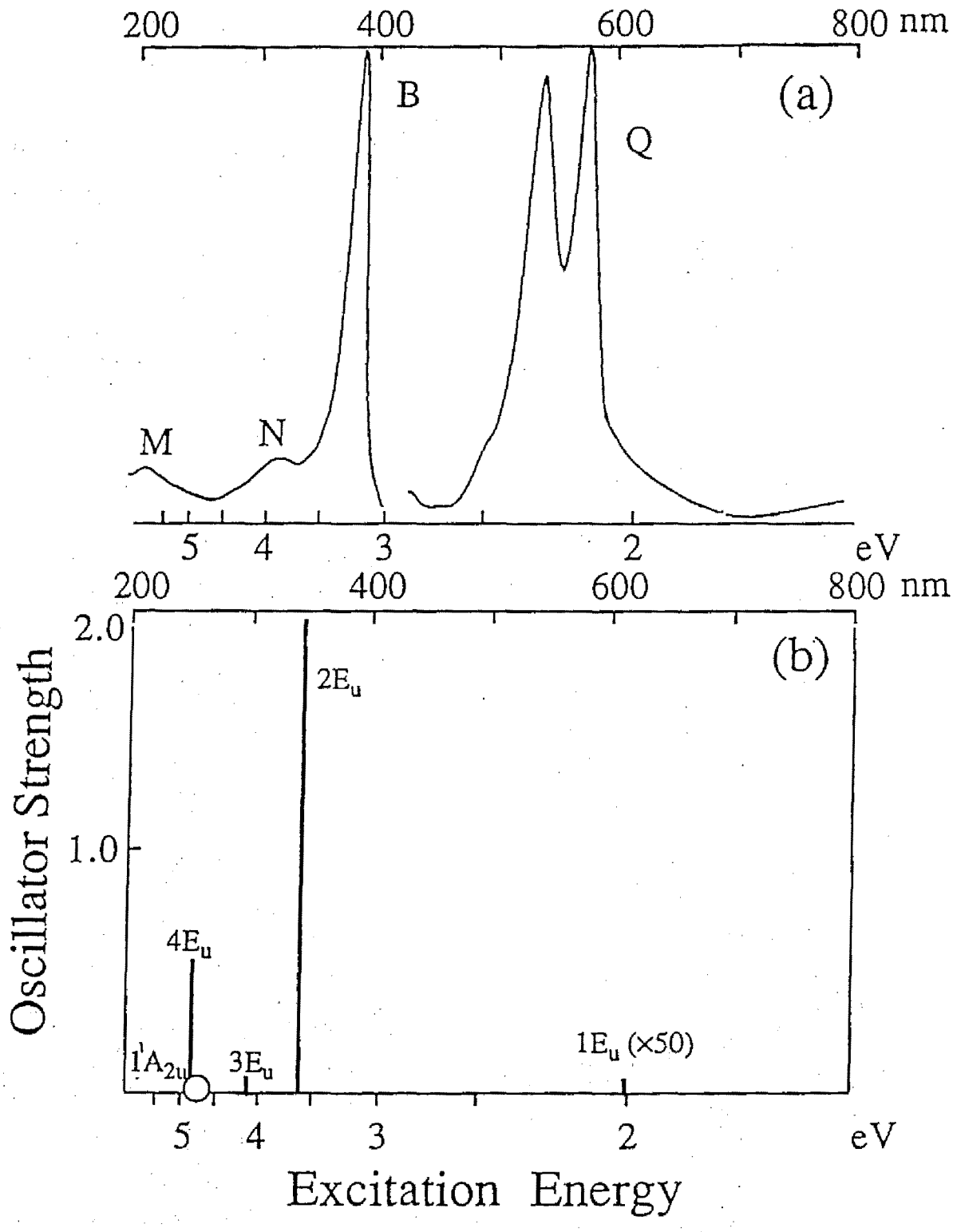

Fig. 2. (a) Vapor-phase experimental electronic spectrum of MgEtio [32] and (b) SAC-CI theoretical spectrum of MgP, where an open circle denotes the 1^1A_{2u} state.

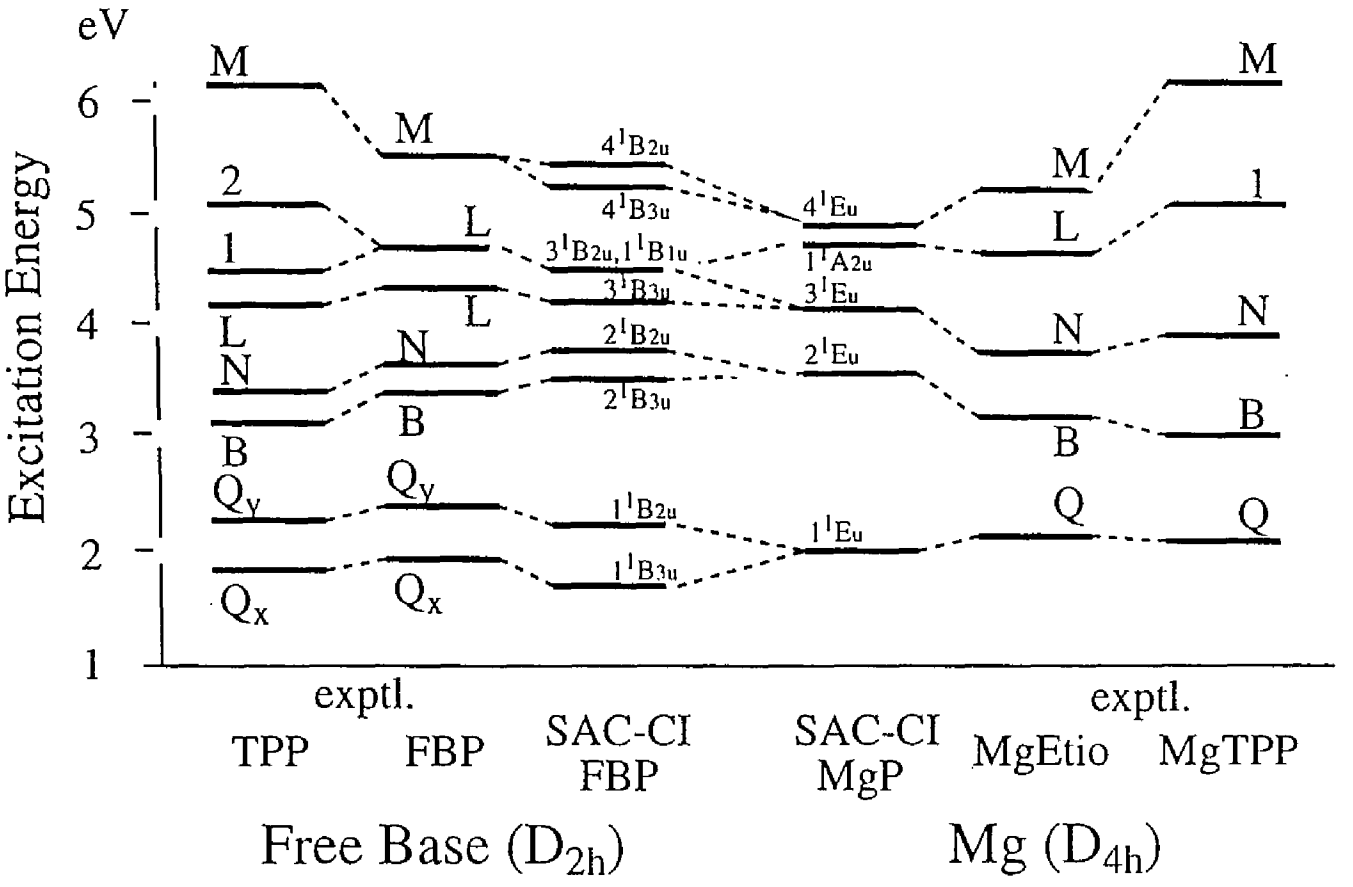

Fig. 3. Energy levels of the excited states of FBP and MgP calculated by the SAC-CI method compared with the experimentally observed energy levels for FBP, TPP, MgEtio, and MgTPP [32].

Chapter 3

Ground and excited states of oxyheme

Abstract

The SAC(symmetry adapted cluster)/SAC-CI(configuration interaction) method is applied to the ground and low-lying excited states of oxyheme ($FeC_{23}N_6O_2H_{16}$). The ground state ($^1A'$) is suitably represented by the Pauling model, Fe(II) (S=0) + O_2 ($^1\Delta_g$). The SAC-CI result reproduces well the lower excitation spectrum of oxyhemoglobin. The lowest peak observed at 1.34 eV is assigned to the $^1\Delta_g \rightarrow {}^1\Sigma_g^+$ excitation of the O_2 ligand. Many transitions originating from the iron d orbitals are calculated, however their intensities are very small. The lowest triplet state ($1^3A''$), which is due to the $^1\Delta_g \rightarrow {}^3\Sigma_g^-$ transition around the O_2 ligand, is calculated at 0.47 eV above the ground state, but its level is sensitive to the electron correlations included. In the geometry of the deoxy form, this $1^3A''$ state becomes more stable than the closed-shell singlet state ($^1A'$), indicating a geometrical control of oxygen affinity of heme.

1. Introduction

Hemoglobin and myoglobin play an important role in mammalian life through the transport and storage of oxygen. Fe-porphyrin complex, called heme, constitutes their reaction center and binds oxygen reversibly [1]. Oxyheme which has oxygen O_2 at the sixth site and imidazole at the fifth site as a residue of histidine in protein is diamagnetic [2] , while deoxyheme is in a high-spin state [3].

The nature of the Fe-O_2 bond in oxyheme has been studied both experimentally and theoretically and some review articles were published [1,3,4]. X-ray crystal structure analysis revealed an end-on oxygen binding structure [5]. Several models were proposed for the ground-state electronic structure of oxyheme. The Fe(II) (S=0) - O_2 (S=0) valence bond (VB) model by Pauling [6] is σ-donation from singlet oxygen ($^1\Delta_g$) and π back donation from the Fe d orbital. The Fe(II) (S=1) - O_2 (S=1) VB model by Goddard et al. and others [7,8] is based on the spin coupling between the two unpaired electrons on oxygen and on Fe(II). The Fe(III)-O_2^- model by Weiss [9] involves one-electron transfer from Fe to O_2, so that O_2 is regarded as superoxide.

Electron correlations are important for the description of the ground state of oxyheme [10,11]. Previous CI [12] and CASSCF [10] calculations gave different electronic structures for the ground states. For the triplet state, the previous CI calculation [12] failed to reproduce the energy ordering between the singlet ground state and the lowest triplet state. This indicates that a more elaborate study is necessary for the lower states of oxyheme.

The SAC(symmetry adapted cluster) [13]/SAC-CI(configuration interaction) [14] method [15] is suitable for calculating electron correlations in the ground and excited states of even relatively large systems like oxyheme. The theory is designed to be efficient and accurate and the calculational algorithms are rather

flexible and not so restrictive to the computing system [15]. This method has successfully reproduced the electronic spectra of a wide variety of molecules [15], from water, formaldehyde, and ethylene to benzene, pyridine, metal complexes, and catalytic systems, and up to free base porphin (FBP) [16]. Note that the EOM-CC method by Bartlett et al. [17] belong to the SAC-CI method [18] published more than a decade ago than theirs. The differences they claimed [17] are quite a minor variation of the calculational method of the SAC-CI theory, which is formally exact. In this study, the ground and some low-lying singlet and triplet excited states of oxyheme are calculated by the SAC/SAC-CI method and the electronic structures and the spectrum of these states are discussed.

2. Computational details

The geometry of oxyheme is taken from the X-ray crystallographic data [19] for oxyhemoglobin of sperm whale with some small modifications. The porphyrin skeleton is fixed to D_{4h} symmetry and the entire molecular symmetry to C_s symmetry. The imidazole plane, one of the N_{Por}-Fe-N_{Por} axes, and the O-O axis are put on the mirror plane as shown in Fig. 1. The C-H distances in the porphyrin ring and in imidazole are taken from refs. 20 and 21, respectively. The atomic coordinates are shown in Table 1.

Natural deoxyheme has a five-coordinated geometry in which Fe sits out of the porphyrin plane by 0.6 Å [22]. We also carry out the calculation of oxyheme in the geometry of the deoxy form, in which the porphyrin ring is moved towards oxygen by 0.6 Å along the O-Fe-N_{Im} axis and all others are fixed at the oxyheme geometry.

The basis set for the porphyrin ring is of 2p double zeta quality, which is the same as our previous calculations for FBP [16]. For the Fe atom, we use Huzinaga's (5333/53/5)/[53321/53/41] set [23] plus p-type polarization function (α=0.082) and for oxygen (63/5)/[63/41] set [23] plus p-type anion basis (α=0.059) [23]. The basis set for imidazole is minimal; for C and N, (63/5)/[63/5] set [23] and for H, (4)/[4] set [24].

Hartree-Fock(HF) molecular orbitals (MOs) are used as the reference orbitals in the SAC/SAC-CI calculations. For the active space, higher 47 occupied MOs and lower 109 unoccupied MOs are used, and all the single excitations and the selected double excitations within this active space constitute the linked operators and their products the unlinked operators. The perturbative configuration selection procedure [16,25] is carried out for the main reference configurations, with the energy threshold 1×10^{-5} a.u. for the ground state and 1×10^{-6} and 2×10^{-6} a.u. for the singlet and triplet excited states, respectively. The resultant dimensions for the SAC/SAC-CI calculations are shown in Table 2. The program HONDO [26] and the accelerated version [27] of the SAC85 [28] program are used for the HF and SAC/SAC-CI calculations.

3. Ground state electronic structure

First we analyze the HF orbitals for the ground state. We use the following notations; "π_u" and "π_g" denote the π-type bonding and antibonding orbitals localized on oxygen. The superscripts "o" and "p" as in "π_u^o" and "π_g^p" denote that the orbitals are on and perpendicular to the mirror plane, respectively. In Table 3, the orbital energies and characters are shown. The so called "four orbitals", 26a', 21a", 23a", and 27a' of the porphyrin ring are located around

the HOMO-LUMO region, but the LUMO of oxyheme is the antibonding MO between the Fe d_{yz} and O_2 π_g^p orbitals and in 23a" MO (next LUMO), the oxygen π_g^p orbital mixes. The interaction between Fe and O_2 is classified into σ and π types. 17a' MO is localized on O_2 but has the nature of the σ donation from O_2 π_g^o to Fe d_{z^2}. 3a", 14a", and 22a" MOs represent Fe-O_2 π interaction which have 3-center 4-electron bond character, however 14a" MO is delocalized over the entire molecule and the 22a" MO (LUMO) is localized on the O_2 π_g^p orbital. The LUMO energy level is low, which is characteristic to oxyheme and affects its excited states, as shown below.

In Table 4, the ground state and some low-lying singlet and triplet states of oxyheme calculated by the SAC/SAC-CI method are summarized. In previous SCF [29] and SCF-CI [12] studies, some open-shell singlet and triplet states were calculated to be more stable than the closed-shell state. In CASSCF calculations [10], the closed-shell state was the ground state and the open-shell singlet state was by 0.7 eV above the ground state. In our SECI calculation, the open-shell triplet and singlet states (O_2 $\pi_g^o \rightarrow O_2$ π_g^p - Fe d_{yz}) lie, respectively, 0.86 eV below and 0.33 eV above the closed-shell state. The energy ordering is much changed by the SAC/SAC-CI treatment: the closed-shell state is the ground state and the open-shell triplet and singlet states lie by 0.47 and 1.54 eV above the ground state, respectively, as seen in Table 4. This result is consistent with the antiferromagnetic nature of oxyheme.

In the ground state, the configuration mixing lowers the state energy quite effectively, indicating a crucial role of electron correlation. The main configuration is the HF configuration, which mixes with several double excitations, e.g. from Fe-O_2 bonding to antibonding MOs.

The electronic structure of the Fe-O_2 bond in oxyheme is characterized by

$$\text{Fe(II)}\ (S=0) + O_2\ (^1\Delta_g)\ (S=0) \qquad (1)$$

based on the electron population analysis and from the nature of the HF MOs. In Table 5, the Mulliken population analysis is given for the lowest five states shown in Table 4. In the ground state, the electron population of the Fe atom is roughly $(d_{xy})^2(d_{xz})^2(d_{yz})^2$, and that for the the O_2 ligand is $(\pi_u^o)^2(\pi_u^p)^2(\pi_g^o)^2$. In this point, our present result is different from Goddard's in which the population is $(d_{xy})^2(d_{xz})^2(d_{yz})^1(d_{z^2})^1(\pi_u^o)^2(\pi_u^p)^2(\pi_g^o)^1(\pi_g^p)^1$ from their GVB-CI calculation [8]. A reason is that they used a seriously approximate model which ignored the porphin ring itself and imidazole. The net charge of the Fe atom in the ground state is almost +2 and that of the O_2 molecule is almost neutral, negating the superoxide structure of O_2 in the Weiss model. This result supports the Pauling model as most appropriate for the ground state of oxyheme among the models proposed, though the amount of the π back donation from Fe d_{yz} to O_2 π_g^p is small as shown in Table 5.

Harcourt [30] indicated that the electronic structure (1) based on the MO calculation may include the VB component corresponding to the Goddard model [7,8]. We examined therefore the present result using the Harcourt method and found that the component corresponding to the Goddard model little contributes to the present ground state of oxyheme. This is supported by a large difference in the electron distribution between the present result and the Goddard one [8].

4. Low-lying excited states

The nature of some low-lying singlet and triplet excited states are shown in Tables 4 and 5. The ordering is $1^3A''$, $1^1A''$, $2^3A''$, and $1^3A'$ which lie by 0.47, 1.54, 1.95, and 1.97 eV, respectively, above the ground state. The electronic structures of these states are represented as

$1^3A''$; Fe(II) (S=0) + O_2 ($^3\Sigma_g^-$) (S=1) (2)

$1^1A''$; Fe(II) (S=0) + O_2 ($^1\Sigma_g^+$) (S=0) (3)

$2^3A''$, $1^3A'$; Fe(II) (S=1) + O_2 ($^1\Delta_g$) (S=0) (4).

Note that the energy ordering of the free O_2 molecule is $^3\Sigma_g^-$ (0.0eV) < $^1\Delta_g$ (0.98eV) < $^1\Sigma_g^+$ (1.64eV) [31]. The $1^1A''$ and $1^3A''$ states arise by one electron excitation from the O2 π_g^o MO to the O_2 π_g^p-d_{yz} MO (LUMO) and the $2^3A''$ ($1^3A'$) state from Fe d_{yz} (d_{xz}) to d_{z^2}. Table 5 clearly shows the changes in the electron population by these transitions.

The excitations, $X^1A' \rightarrow 1^3A''$ and $X^1A' \rightarrow 1^1A''$, correspond to the reorganizations of the electronic structure of oxygen, namely, $^1\Delta_g \rightarrow {}^3\Sigma_g^-$ and $^1\Delta_g \rightarrow {}^1\Sigma_g^+$, respectively. We note that the $1^3A''$ state has a very small excitation energy of 0.47 eV, since the LUMO energy level is very low and since the excitation is actually the relaxation of the O_2 electronic structure to its ground state, i.e., $^3\Sigma_g^-$. Therefore, the $1^3A''$ state should be stabilized to a larger extent than the closed shell state as the Fe - O_2 distance is separated. These results suggest that the $1^3A''$ state has a possibility to participate in the O_2 capture and release process of heme.

In Fig. 2, the absorption spectrum of oxyhemoglobin [32] and the SAC-CI theoretical spectrum are compared in the region of below 3 eV. The calculated spectrum well reproduces the experimental one. The first peak at about 1.34 eV is assigned to the $1^1A''$ state which is characterized as the $^1\Delta_g \rightarrow {}^1\Sigma_g^+$ excitation within O_2 ligand, as described above. This assignment is confirmed by comparing the absorption spectrum of the horse oxyhemoglobin with that of the carboxyhemoglobin [32]: the peak at 1.34 eV exists in the former but not in the latter. The second and third absorptions, called the Q band, are assigned to the $2^1A'$ and $3^1A''$ states, respectively. These Q bands look similar to those of FBP, but a difference is that the five orbitals, instead of the four orbitals, are involved in the excitations. In addition to the so-called four orbitals, the LUMO

which is localized in the Fe-O_2 region also participates in the Q bands as seen from Table 4.

At the energies 2.82, 2.83, and 3.13 eV, there exist 3 excited states originating from the Fe d-orbitals, which are roughly characterized as the ligand field d-d excitations within the Fe atom. The intensities are therefore quite small. The excitations calculated at 2.75, 3.02, and 3.08 eV are the electron transfer transitions from Fe d-orbital to oxygen. These excited states have the electronic structure represented by the Weiss model [9].

In a previous study [33], some very weak peaks were observed at the lower energy side of the 1.34 eV peak. We may qualitatively assign these peaks to the triplet states, however, more decisive assignment is difficult at the present stage of the calculation.

5. Ground and excited states in the deoxy form

Next we calculate the low-lying singlet and triplet states of oxyheme in a deformed geometry, i.e., in the "deoxy form". The aim is to examine the effect of the deformation on the relative stability of the low-lying singlet and triplet states. An X-ray crystal structure analysis [22] showed that in deoxyheme the porphyrin ring moves towards the sixth sites by 0.6 Å along the Fe-N_{Im} axis. The results of the SAC-CI calculation for this geometry are shown in Table 4.

In the deoxy form, the closed-shell state become unstable, lying over the triplet $1^3A''$ state by 0.15 eV. This indicates that if some geometrical change is induced to oxyheme through a conformational change of the heme protein, the O_2 affinity of heme is lowered, facilitating the Fe - O_2 bond breaking process. Though the $1^3A''$ state in the present deoxy form is 3.95 eV (90kcal/mol) higher than the X^1A' state of the oxy form, the activation energy should be

much smaller than this value, since we did not consider any geometric relaxation effect in this calculation. The $X^1A' \rightarrow 1^3A''$ transition would occur at the geometry between the oxy and the deoxy form. More detailed study on this process is in progress.

References

[1] W. D. Scheidt and C. A. Reed, Chem. Rev. 81 (1981) 543; Y. Nishida, Inorganic Biological Chemistry (Shokado, Tokyo, 1994) p. 26-58.

[2] L. Pauling and C. D. Coryell, Proc. Natl. Acad. Sci. US. 22 (1936) 210.

[3] M. Montenteau and C. A. Reed, Chem. Rev. 94 (1994) 659.

[4] I. Bytheway and M. B. Hall, Chem. Rev. 94 (1994) 639.

[5] J. P. Collman, R. R. Gage, C. A. Reed, W. T. Robinson, and G. A. Rodley, Proc. Natl. Acad. Sci. U.S.A. 71 (1974) 1326.

[6] L. Pauling, Stanford Med. Bull. 6 (1948) 215; L. Pauling, Nature 203 (1964) 182.

[7] D. S. Maclure, Radiation Res. Suppl. 1 (1960) 218; R. D. Harcount, Lecture note in chemistry, Vol 30. Qualitative valence bond descriptions of electron-rich molecules (Splinger, Berlin, 1982) p. 205; B. D. Olafson and W. A. Goddard III, Proc. Natl. Acad. Sci. US 74 (1977) 1315.

[8] W. A. Goddard III and B. D. Olafson, Proc. Natl. Acad. Sci. US 72 (1975) 2335.

[9] J. J. Weiss, Nature 202 (1964) 83.

[10] S. Yamamoto and H. Kashiwagi, Chem. Phys. Letters 161 (1989) 85; S. Yamamoto and H. Kashiwagi, Chem. Phys. Letters 206 (1993) 306.

[11] J. E. Newton and M. B. Hall, Inorg. Chem. 23 (1984) 4627.

[12] M. -M. Rohmer, Mathematical and Physical Sciences, Vol. 176 (Reidel, Holland, 1986) p. 377.

[13] H. Nakatsuji and K. Hirao, J. Chem. Phys. 68 (1978) 2035.

[14] H. Nakatsuji, Chem. Phys. Letters 59 (1978) 362; Chem. Phys. Letters 67 (1979) 329, 334.

[15] H. Nakatsuji, Acta. Chim. Hung. 129 (1992) 719.

[16] H. Nakatsuji, J. Hasegawa, and M. Hada, J. Chem. Phys. in press.

[17] J. Geertsen, M. Ritby, and R. J. Bartlett, Chem. Phys. Letters 164 (1989) 57; S. R. Gwaltney and R. J. Bartlett, Chem. Phys. Letters 241 (1995) 26.

[18] H. Nakatsuji and M. Ehara, J. Chem. Phys. 101 (1994) 7658.

[19] S. E. V. Phillips, J. Mol. Biol. 142 (1980) 531; S. E. V. Phillips, Nature 273 (1978) 247.

[20] H. Sekino and H. Kobayashi, J. Chem. Phys. 86 (1987) 5045.

[21] J. E. D. Bene and I. Cohen, J. Am. Chem. Soc. 100 (1978) 5285.

[22] G. Fermi, J. Mol. Biol. 97 (1975) 237.

[23] S. Huzinaga, J. Andzelm, M. Klobukowski, E. Radzio-Andzelm, E. Sakai, and H. Tatewaki, Gaussian basis set for molecular calculations, (Elsevier, New York, 1984)

[24] S. Huzinaga, J. Chem. Phys. 42 (1965) 1293.

[25] H. Nakatsuji, Chem. Phys. 75 (1983) 425.

[26] M. Dupuis, A. Farazdel, MOTECC-91, (Center for Scientific and Engineering Computations, IBM Corporation, 1991).

[27] H. Nakatsuji, M. Hada, H. Nakai, and J. Hasegawa, the accelerated version of SAC85, to be published.

[28] H. Nakatsuji, Program System for SAC and SAC-CI Calculations, (Program Library No.146 (Y4/SAC), Data Processing Center of Kyoto University, 1985); Program Library SAC85 No.1396, (Computer Center of the Institute for Molecular Science, 1981).

[29] T. Nozawa, M. Hatano, U. Nagashima, S. Obara, and H. Kashiwagi, Bull. Chem. Soc. Jpn. 56 (1983) 1721.

[30] R. D. Harcourt, Chem. Phys. Letters 167 (1990) 374.

[31] K. P. Huber and G. Herzberg, Molecular spectra and molecular structure, Vol III, (Van Nostrand Reinhold Co., New York, 1979).

[32] M. W. Makinen and W. A. Eaton, Ann. N.Y. Acad. Sci. 206 (1973) 210.

[33] W. A. Eaton, L. K. Hanson, P. J. Stephans, J. C. Sutherland, and J. B. R. Dunn, J. Am. Chem. Soc. 100 (1978) 4991.

Table 1
Atomic coordinates of oxyheme (Å)

segment	atom[a]	x	y	z	segment	atom[a]	x	y	z
porphin	N1	1.9537	0.0	0.0	imidazole	N1	0.0	0.0	-2.0654
	C2	4.1889	0.6915	0.0		C2	-1.2095	0.0	-2.7916
	C3	2.8060	1.1297	0.0		N3	-0.8706	0.0	-4.2036
	C4	2.4702	2.4702	0.0		C4	0.5376	0.0	-4.2391
	H5	5.0604	1.3294	0.0		C5	1.0562	0.0	-2.9478
	H6	3.2339	3.2339	0.0		H6	-2.2826	0.0	-2.6693
oxygen[b]	O1	0.0	0.0	1.8267		H7	-1.5281	0.0	-5.0604
	O2	1.0979	0.0	2.3507		H8	1.0035	0.0	-5.2134
iron	Fe	0.0	0.0	0.0		H9	2.0637	0.0	-2.5587

[a] The numberings of the atoms in each segments are given in Fig. 1.

[b] The lengths of Fe-O1, O1-O2, Fe-N_{Por}, and Fe-N_{Im} are 1.83, 1.21, 1.95, and 2.07 Å, respectively. The Fe-O1-O2 angle is 115.5°.

Table 2
Dimensions of the SAC/SAC-CI calculations for the singlet and triplet states of oxyheme

state	singlet state			triplet state		
	before selection	N[a]	after selection	before selection	N[a]	after selection
Oxy form						
SAC(ground state)						
A'	6567495	1	14799			
SAC-CI(excited state)						
A'	6567495	11	103107	9743589	3	41924
A"	6562755	11	112160	9744303	3	42928
Deoxy form						
SAC(ground state)						
A'	6568552	1	13649			
SAC-CI(excited state)						
A'	6568552	3	50683	9744796	3	50068
A"	6561728	3	49357	9743096	3	55044

[a] N denotes the number of the reference states in the configuration selection procedure.

Table 3
Orbital energies and characters of some HF orbitals of oxyheme

Orbital	Orbital energy (eV)	Nature [a]
Occupied orbitals		
2a"	-18.456	$O_2\ \pi_u^p$ + por σ
3a"	-18.073	$O_2\ \pi_u^p$ + Fe d_{yz}
:		
15a'	-14.079	$O_2\ \pi_g^o$ + por π
:		
17a'	-13.499	$O_2\ \pi_g^o$ + Fe d_{z^2}
18a'	-13.286	$O_2\ \pi_g^o$ + Fe d_{xz}
13a"	-12.720	Fe d_{xz} + $O_2\ \pi_g^o$ +Fe p_z + Im σ +Fe s +por σ
19a'	-12.405	Fe d_{xz}
:		
14a"	-12.157	O(2)[b] p_y – Fe d_{yz} + por σ + Fe p_y
:		
16a"	-11.813	Fe d_{xy}
17a"	-11.555	Fe d_{yz} – Im π
:		
23a'	-9.418	por π
:		
25a'	-8.825	Fe d_{xz} – por π
20a"	-8.754	Fe d_{yz} – por π
26a'	-6.544	por π (n-HOMO; 4-orbitals)
21a"	-6.035	por π (HOMO; 4-orbitals)
Unoccupied orbitals		
22a"	0.139	$O_2\ \pi_g^p$ – Fe d_{yz} (LUMO)
23a"	0.420	por π – $O_2\ \pi_g^p$ (n-LUMO; 4-orbitals)
27a'	0.428	por π (4-orbitals)
:		
38a'	9.914	Fe d_{z^2} – por σ
39a'	10.062	Fe $d_{x^2-y^2}$ – por σ
:		
42a'	10.740	Fe $d_{x^2-y^2}$ – por σ
43a'	10.798	Fe d_{z^2} – Fe p_x – por σ – Im σ – O(1)[b] p_x
:		
46a'	11.420	Fe d_{z^2} – $O_2\ \pi_g^o$ – Im σ – por σ
47a'	12.035	Fe $d_{x^2-y^2}$ – por σ

[a] The plus (+) and minus (–) signs denotes the bonding and antibonding interaction, respectively.
[b] O(1) and O(2) atoms are illustrated in Fig. 1.

Table 4
Ground and excited states of oxyheme in the two different geometries

state	oxy form						deoxy form
	SAC/SAC-CI				Exptl.		SAC/SAC-CI
	excitation energy (eV)	main configuration	nature	oscillator strength (direction)	excitation energy (eV)	oscillator strength[a]	excitation energy (eV)
ground state							
X^1A'	0.0	1.00(HF) -0.15(3a"→22a",3a"→22a") +0.11(3a"→22a",2a"→22a")					0.0[c]
excited state							
$1^3A"$	0.47	0.66(17a'→22a") +0.42(18a'→22a") -0.37(15a'→22a")	$O_2(\pi_g^o)\rightarrow O_2(\pi_g^P)$				-0.15[d]
$1^1A"$	1.54	0.63(17a'→22a") +0.40(18a'→22a") -0.34(15a'→22a")	$O_2(\pi_g^o)\rightarrow O_2(\pi_g^P)$	8.2×10^{-5} (y)	1.29[a], 1.34[b]	2.6×10^{-3}	0.67
$2^3A"$	1.95	0.33(17a"→38a') -0.31(13a"→38a')	$Fe(d_{yz})\rightarrow Fe(d_z^2)$				1.55
$1^3A'$	1.97	0.53(19a'→43a') +0.52(19a'→38a')	$Fe(d_{xz})\rightarrow Fe(d_z^2)$				
$2^1A'(Q_x)$	2.38	0.65(21a"→23a") +0.63(26a'→27a') -0.32(21a"→22a")	$por(\pi)\rightarrow por(\pi)$	0.017 (x,z)	2.22[a]	0.12 (Q_0)	
$2^1A"$	2.44	-0.62(26a'→22a") -0.55(21a"→27a') +0.47(26a'→23a")	$por(\pi)\rightarrow O_2(\pi_g^P),por(\pi)$	2.9×10^{-4} (y)			
$3^1A"(Q_y)$	2.64	0.69(26a'→22a") +0.50(26a'→23a") -0.39(21a"→27a')	$por(\pi)\rightarrow O_2(\pi_g^P),por(\pi)$	0.0073 (y)			
$3^1A'$	2.71	0.88(21a"→22a") +0.34(21a"→23a")	$por(\pi)\rightarrow O_2(\pi_g^P)$	8.7×10^{-5} (x,z)			
$4^1A"$	2.75	-0.59(25a'→22a") -0.58(19a'→22a")	$Fe(d_{xz})\rightarrow O_2(\pi_g^P)$	3.0×10^{-5} (y)			
$5^1A"$	2.82	-0.31(17a"→38a')	$Fe(d_{yz})\rightarrow Fe(d_z^2)$	9.0×10^{-5} (y)			
$4^1A'$	2.83	0.51(19a'→43a') +0.48(19a'→38a') +0.31(19a'→46a')	$Fe(d_{xz})\rightarrow Fe(d_z^2)$	0.0015 (x,z)			
$5^1A'$	3.02	-0.68(20a"→22a") +0.32(17a"→22a")	$Fe(d_{yz})\rightarrow O_2(\pi_g^P)$	0.022 (x,z)			
$6^1A'$	3.08	0.88(16a"→22a")	$Fe(d_{xy})\rightarrow O_2(\pi_g^P)$	0.0010 (x,z)			
$6^1A"$	3.13	-0.56(16a"→42a') +0.51(16a"→39a') -0.40(16a"→47a')	$Fe(d_{xy})\rightarrow Fe(d_{x^2-y^2})$	5.0×10^{-7} (y)			

[a] Solution spectrum for horse oxyhemoglobin[33].
[b] Solution spectrum for horse oxyhemoglobin[32].
[c] The lowest singlet state of the deoxy form is higher by 4.11 eV than the ground state of the oxy form.
[d] Calculated lowest state of the deoxy form.

Table 5
Mulliken population analysis for the ground and excited states of oxyheme

	X^1A'(SAC)	$1^3A''$	$1^1A''$	$2^3A''$	$1^3A'$
Fe (net charge)	1.9069	1.9068	1.9144	1.9601	1.9629
d_{x^2}	0.2061	0.1970	0.1998	0.2399	0.4699
d_{y^2}	0.2118	0.2019	0.2050	0.4658	0.2454
d_{z^2}	0.1576	0.1370	0.1400	0.7510	0.7497
d_{xy}	1.9837	1.9878	1.9876	1.9911	1.9912
d_{xz}	1.9761	1.9772	1.9654	1.9813	1.0344
d_{yz}	1.9267	1.9603	1.9579	1.0020	1.9368
O1[a](net charge)	0.0506	0.0158	0.0161	0.0326	0.0416
p_x	1.2443	1.1425	1.1449	1.2465	1.2420
p_y	1.0818	1.5167	1.5051	1.0815	1.0744
p_z	1.7165	1.4267	1.4117	1.7342	1.7290
O2[a](net charge)	-0.0134	0.0233	-0.0053	0.0095	-0.0070
p_x	1.2479	1.1319	1.1310	1.2489	1.2440
p_y	0.9884	1.5102	1.5221	0.9617	0.9850
p_z	1.8376	1.3951	1.4128	1.8401	1.8382
Por[b] (net charge)	-1.7698	-1.7728	-1.7521	-1.7982	-1.7933
Im[c] (net charge)	-0.1742	-0.1731	-0.1731	-0.2038	-0.2042

[a] The numberings of atoms are given in Fig. 1.
[b] Porphyrin ring.
[c] Imidazole.

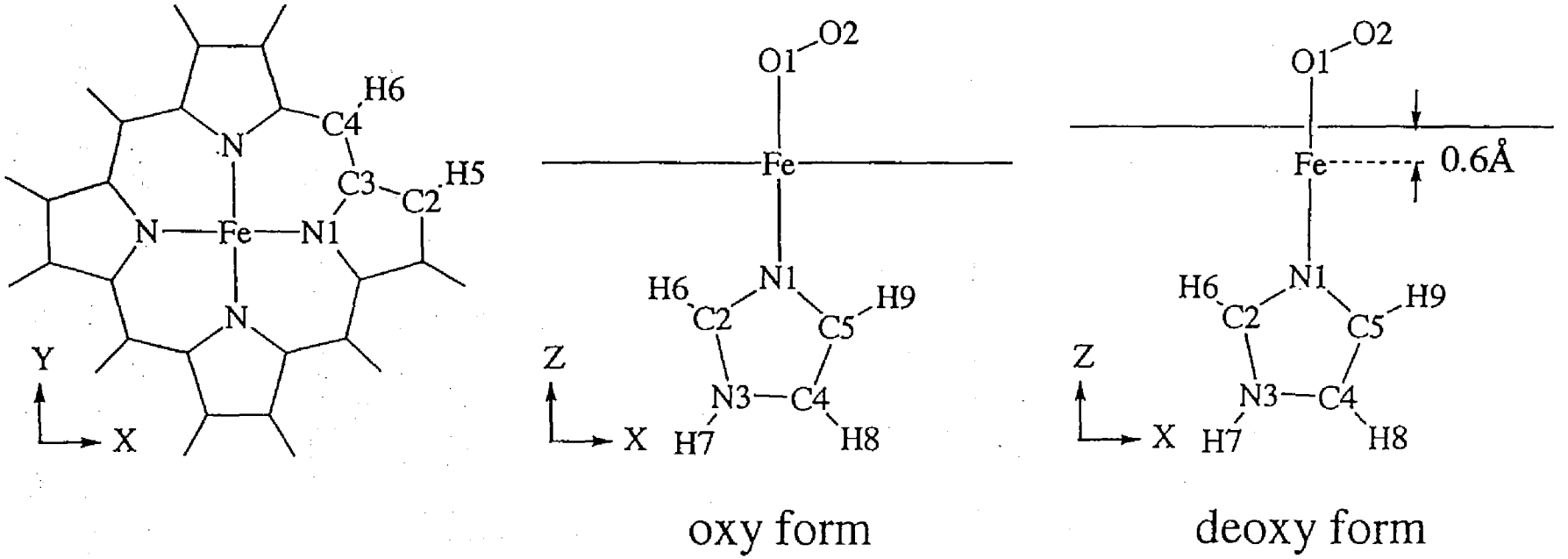

Fig. 1. Geometries of oxyheme in the oxy and deoxy forms. The numbering of the atoms corresponds to those shown in Table 1.

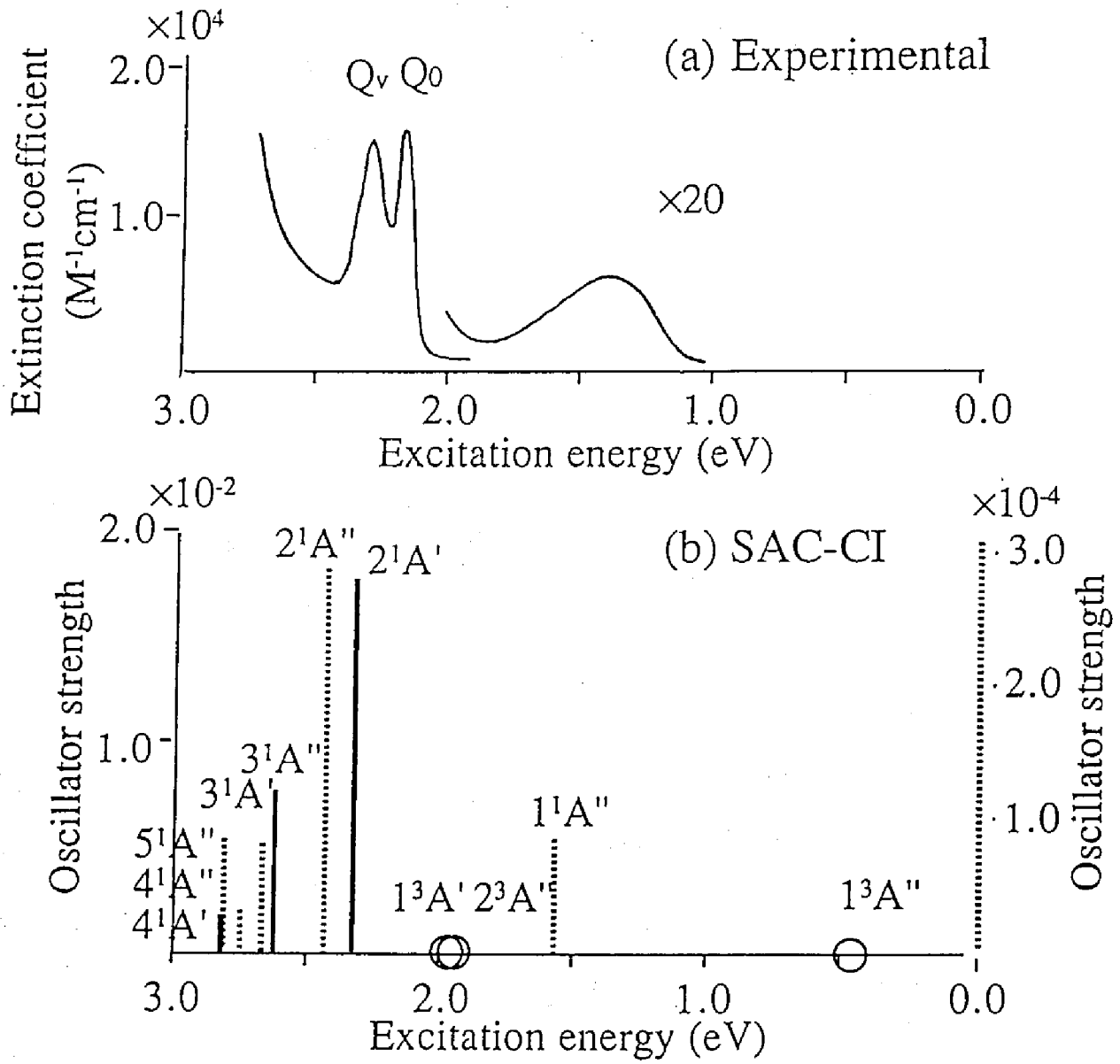

Fig. 2. Electronic spectrum of oxyheme. (a) Experimental spectrum of horsehemoglobin [32]. (b) SAC-CI theoretical spectrum. Open circles denote triplet excited states. Left and right vertical axes correspond to the spectral intensities drawn by the real and dotted lines, respectively.

Chapter 4

Excitation spectra of chlorin, bacteriochlorin, pheophytin *a*, and chlorophyll *a*

Abstract

Excited states of Free Base Chlorin (FBC), Free Base Bacteriochlorin (FBBC), Pheophytin *a* (Pheo *a*), and Chlorophyll *a* (Chlo *a*), which are derivatives of free base porphin (FBP), were calculated by the SAC (Symmetry Adapted Cluster)/SAC-CI (Configuration Interaction) method. The results reproduced well the experimentally determined excitation energies. The reduction of the outer double bonds in the porphin ring in the order of FBP, FBC, and FBBC causes a breakdown of the symmetry and a narrowing of the HOMO - LUMO gap, which result in a red shift of the Q_X band and an increase of its intensity. In the change from Pheo *a* to Chlo *a*, the Mg-coordination reduces the quasidegeneracy in the Q_X state and then increases the spectral intensity. The disappearance of the Q_Y humps from the absorption spectrum of Pheo *a*, compared with that of Chlo *a*, is due to the red shift of the Q_Y state.

Introduction

Many biological systems contain porphyrins, chlorins, and bacteriochlorins.[1,2] These compounds often take an important part in the biochemical reactions, such as light absorption, electron transfer,[1] and oxygen transport and storage.[2] Due to their scientific importance, they have been the subject of a wide variety of studies. In particular, the electronic structures of the ground and excited states of these compounds are an active field of interest[3-9]. Semi-empirical INDO/S calculations[4,5] have been applied to elucidate the energetics of electron transfer in the photosynthetic reaction center. Using the ab initio method, some large-scale SCF calculations for the ground[6,7] and anionized states[7] have been reported. As for the excited states, although pioneering CI calculations[8] have been reported for chlorophyllide *a* and pheophorbide *a*, there have been few calculations using a reliable ab initio method.

Porphyrin, chlorin, and bacteriochlorin have different π-electron conjugations. The number of reduced double bonds in the pyrrole rings is zero, one, and two in porphyrins, chlorins, and bacteriochlorins, respectively. These reductions causes a considerable change in the excited states of these compounds, as seen in their absorption spectra.[9,10] The simplest macrocycles without any substituents, i.e., free base porphin (FBP), free base chlorin (FBC), and free base bacteriochlorin (FBBC), are shown in Fig. 1. From FBP to FBC, the absorption intensity of the first excited state, Q_x, increases.[9] From FBC to FBBC, the Q_x absorption shows a red shift and increases further in its intensity, while the intense B (Soret) band shows a blue shift.[10]

Another characteristic of these macrocycles lies in their various substituents. Chlorophylls and bacteriochlorophylls have many substituents; e.g., an additional ring V, a long hydrocarbon chain (phytyl group), etc. Simplified models of chlorophyll *a* (Chlo *a*) and pheophytin *a*

(Pheo *a*) are shown in Fig. 1 and they have only an additional ring V and the substituents which may affect the π-conjugations of the chlorin ring. Another characteristic is metal coordination. Previous X-ray studies have revealed the entire structures of the photosynthetic reaction centers of some bacteria.[1,11] They contain both Mg-coordinated bacteriochlorophylls and free base bacteriopheophytins. Spectroscopically, Mg-coordination increases the absorption coefficient of the Q_X band.[12] This effect is interesting, since in a previous study on porphin and Mg-porphin,[13] the Mg-coordination affected only the symmetric degeneracy of the absorption, and not the intensity of the Q_X band.

In this study, we examine the above features of the excited states of these macrocycles by the SAC[14]/SAC-CI[15] method.[16] The SAC/SAC-CI method has already established as an efficient and reliable method for studying electron correlations in the ground and excited states of a variety of molecules and molecular systems[16] including porphyrins.[13,17-20] We study the excited-state electronic structures of FBP, FBC, and FBBC with regard to the differences in the π-conjugation. We then study the effects of the substituents and the Mg-coordination on the excited states of Pheo *a* and Chlo *a* in comparison with FBC. Conclusion of the study is given in the last section.

Computational Details

An optimized geometry[21] is used for FBC. For FBBC, the same porphin skeleton as in FBP[17] is used, except for the reduced pyrrole ring, for which the geometry used in a previous calculation[9] was taken. FBC and FBBC are assumed to have C_{2v} and D_{2h} symmetries, respectively. For Pheo *a*, X-ray data[22] are used, but for simplicity, some substituents are replaced by protons, except for the substituents which can conjugate

with the π-orbitals of the chlorin ring. For Chlo *a*, the Mg atom is coordinated to the central nitrogen atoms in Pheo *a*. These computational models are shown in Fig. 1.

The basis sets used in this series of molecules are the same. Huzinaga's (63/5)/[2s2p] set[23] is used for C, N and O atoms, and (4)/[1s] set[24] is used for H. For Mg, we used Huzinaga's (533/5)/[5s/3p] set[23] plus two p-type polarization functions (ζ=0.045 and 0.143) and a d-type polarization function (ζ=1.01), which are the same as those used previously.[13]

In the SAC/SAC-CI calculations, only the inner-core orbitals are excluded from the active space. All single excitations and selected double excitations are included in the linked term. The energy threshold for the perturbation selection[17,25] is 1×10^{-5} hartree for the ground state and for the excited state, 5×10^{-7} and 1×10^{-6} hartree for $\pi-\pi^*$ and other excitations, respectively. The results of the selections of the linked terms are shown in Table 1. The number of the reference states are generally 4 so that the accuracy of the present calculations is not very good for the B states. The correlation energies calculated for the ground states of these compounds are also shown.

The Hartree-Fock SCF calculations are performed using the HONDO (ver. 8) program[26] and the SAC/SAC-CI calculations by the SAC85 program[27] modified for large-scale calculations.[28]

Excited States of FBP, FBC, and FBBC

FBP, FBC, and FBBC have π-conjugate systems which are different in the number of the reduced pyrrole rings, as shown in Fig. 1. The HF orbital energies of the HOMO, next-HOMO, LUMO, and next-LUMO of FBP, FBC and FBBC are shown in Fig. 2. Orbitals having similar characters are connected by dotted lines. As changing from FBP, FBC, to FBBC, the near degeneracies between the HOMO and next-HOMO, and

between the LUMO and next-LUMO, which are called the "four orbitals",[3] are removed considerably. It is already established that the "four orbitals" play crucial roles in the valence excited states of porphyrin compounds.[3,13,17-20] Fig. 2 shows that in FBP, FBC, and FBBC, the reduction of the pyrrole rings considerably affects the energy levels of the HOMO, LUMO, and next-LUMO. The molecular orbital shapes of these "four orbitals" are shown in Fig. 3. The next HOMOs of FBP, FBC, and FBBC have no amplitudes on the reduced pyrrole positions, so that their energy levels are scarcely changed, while the HOMOs have some coefficients so that the reduction destabilizes the MOs due to the shortening of the π-conjugation. Exactly the same argument is also valid for the LUMO and next-LUMO of these compounds.

The excited states of FBP, FBC, and FBBC as calculated by the SAC/SAC-CI method and the experimentally determined excitation energies are shown in Table 2. For FBBC, however, we could not find the experimental data, so that those of the bacteriochlorin derivative, bacteriopheophorbide (BPheo),[10] are cited. The excitation energies calculated for FBP, FBC, and FBBC show good agreement with the experimental values, with an average discrepancy of 0.19 eV. The low-energy shift of the Q_X band from FBC to FBBC and the increase in the intensity of the Q_X band from FBP to FBBC are faithfully reproduced.

The first bands at 1.98 and 1.6 eV in FBC[9] and BPheo[10] are assigned to the *x*-polarized $1B_1$ and $1B_{3u}$ states, respectively, by comparison of the experimental values and the theoretical results. In FBC and FBBC, these Q_X states represent HOMO $\rightarrow$ LUMO excitation which is strongly coupled with next-HOMO $\rightarrow$ next-LUMO excitation. In FBP, the electronic structure of the Q_X state is characterized as quasidegenerate excited configurations. However, this quasidegeneracy is relaxed in FBC and FBBC, as shown in Table 2. The ratios of the weights of the two

excitations are 1:0.70, 1:0.50, and 1:0.27 in FBP, FBC, and FBBC, respectively.

In FBC and FBBC, destabilization of the HOMO and next-LUMO levels produces red shifts and relaxation of the quasidegeneracy in the Q_X states. Table 3 shows the energies and the orbital energy gaps for the main configurations of the Q_x bands. In FBP, the energies of the $5b_{1u} \rightarrow 4b_{2g}$ and $2a_u \rightarrow 4b_{3g}$ excited configurations are similar: 4.15 and 4.22 eV, respectively. However, in FBC and FBBC, destabilization of the HOMO and next-LUMO levels makes the orbital energy gap ($\Delta\varepsilon$ in Table 3) between the HOMO and LUMO small and that between the next-HOMO and next-LUMO large. The energies of the HOMO $\rightarrow$ LUMO configurations are stabilized and those of the next-HOMO $\rightarrow$ next-LUMO configurations are destabilized in FBC and FBBC as shown in Table 3. Since a greater energy difference leads to a weaker coupling of the two configurations, the Q_X state takes a greater HOMO $\rightarrow$ LUMO character and a smaller excitation energy. The main factor of these energy shifts of the configurations is the change of the orbital energy gaps, $\Delta\varepsilon$, as shown in Table 3. The coulomb and exchange integrals which appear in the diagonal term have little contribution to these energy change.

The relaxation of the quasidegeneracy leads to an increase in the intensity of the Q_X bands in FBC and FBBC. In FBP, the two main configurations are almost degenerate and the transition moments of each configuration cancel each other. The contributions of the $5b_{1u} \rightarrow 4b_{2g}$ and $2a_u \rightarrow 4b_{3g}$ excited configurations to the transition moment (product of the SAC-CI coefficient and the transition dipole moment for each configuration) are -3.18 and 2.85, respectively, which offset each other. This causes the small intensity of the FBP Q_X band.[19,34] However, the quasidegeneracy in FBP is relaxed in FBC and FBBC. The difference in the SAC-CI coefficients causes incomplete cancellation of the transition

moment and an increase in the intensity of the Q_X band in FBC and FBBC. Weiss[34] identified this incomplete cancellation mechanism using a qualitative model. The present results support this mechanism.

Further, the change in the configuration-transition dipole moment due to the HOMO → LUMO excitation ifself, $<0|r|HOMO \rightarrow LUMO>$ (r=x,y,z), is also a cause of the increase in the transition dipole of the Q_X states in FBBC. The configuration-transition dipole moment is shown in Table 3. The value of the element in FBBC, $<0|x|3a_u \rightarrow 4b_{3g}>$, (5.60) is larger than that in FBP, $<0|x|5b_{1u} \rightarrow 4b_{2g}>$, (4.61) or FBC, $<0|x|6a_2 \rightarrow 9b_2>$ (4.60). To better understand which atoms have a large contribution, a population analysis for the transition dipole moment in the HOMO → LUMO configuration for FBC and FBBC and in the HOMO → next-LUMO configuration for FBP were calculated as in a Mulliken population analysis as explained in the Appendix. Fig. 4 shows the results of the analysis for the atoms whose contributions are greater than 0.01. The sum of the atomic transition moments of the pyrrole rings having N-H bonds increases considerably in FBBC. This finding is related to the π-conjugation narrowing caused by the reduction of the pyrrole rings in FBBC.

The second bands at 2.29 and 2.3 eV in FBC[9] and BPheo[10] are assigned to the y-polarized $2A_1$ and $1B_{2u}$ states calculated at 2.39 and 2.42 eV, respectively. This assignment agrees with the conventional one,[9,31] and the ordering of the polarization directions of the Q bands is the same as in FBP. The Q_Y bands of FBC and FBBC are characterized as the next-HOMO → LUMO excitation, which is strongly coupled with the HOMO → next-LUMO excitation. The effects of the reduction on the excitation energy and the configuration mixing of the Q_Y bands are small, as shown in Table 2, since the energy gaps between next-HOMO and

LUMO and between HOMO and next-LUMO are affected very little, as seen in Fig. 2, by the reduction from FBP to FBC and to FBBC.

As for the B band in FBC, the strong peak at 3.18 eV in the absorption spectrum[9] is assigned to the *x*-polarized $2B_1$ state calculated at 3.59 eV. Our SAC-CI SD-R calculation tends to overestimate the excitation energy of the B-band.[16] This state is characterized as next-HOMO → next-LUMO excitation, which is strongly coupled to HOMO → LUMO excitation. The broad shoulder[9] in a blue side is assigned to the *y*-polarized $3A_1$ state calculated at 3.74 eV, which is characterized as HOMO → next-LUMO excitation coupled to next-HOMO → LUMO excitation. The order of polarization is supported by experimental results[35]. Previous MRSDπCI calculations by Nagashima et. al.[9] gave the same assignment. As for FBBC, the calculation indicates that the $2B_{2u}$ (B_y) and $2B_{3u}$ (B_x) states are at 4.11 and 4.24 eV, respectively, which may overestimate the experimental values. Their characters are HOMO → next-LUMO excitation and next-HOMO → next-LUMO excitation, respectively. The B states of FBBC shift to higher energy region than those of FBP and FBC. Since we can not find experimental data for the B band of FBBC, direct comparison with experiments is impossible. However, the same blue shifts were observed in the absorption spectra of their derivatives, bacteriopheophorbide and pheophorbide.[10]

In FBBC, the ordering of the B_x and B_y states are reversed due to the high energy shift of the B_x state in FBBC. With respect to the orbital energy difference, the B_x state is higher than the B_y state in FBP, FBC and FBBC, as seen from Fig. 2. However, after SAC-CI treatment, the B_x state is more stable than the B_y state in FBP and FBC. This is very general as seen in our previous studies on porphyrins.[16,19] In FBBC, since the energy difference between the two configurations is very large, the coupling between the two main configurations is weakened and then the

B_x state lies on the blue side of the B_y state. Experimental examination of the order of the polarizations of the peaks involved in the B band is very interesting.

Excited States of Pheo *a* and Chlo *a*

In the photosynthetic reaction center of plants, chlorophyll and pheophytin play important roles in the electron transfer. Chlorophyll is a substituted and Mg-coordinated chlorin and pheophytin[10] is a free-base form of chlorophyll. The absorption spectrum of pheophytin is almost the same as that of FBC with regard to the excitation energy,[10,30] although the vinyl group and ring V seem to affect the π-electron system of the chlorin ring through π-conjugation, since in X-ray coordinates the molecular plane of these substituents is parallel to that of the chlorin ring.[22] On the other hand, with Mg-coordination, the absorption spectrum of chlorophyll[10,32] is much different from that of pheophytin.[32] First, the intensity of the first excited state increases. Second, the double humps in the 500-nm region of pheophytin spectrum are not found in chlorophyll one. This coordination effect is very interesting, since for FBP, the Mg-coordination only affects the symmetric degeneracy in the absorption spectrum.[13]

Substitutions and Mg-coordination affect orbital energy. The HF orbital energy levels of the "four orbitals" for Pheo *a* and Chlo *a* are also shown in Fig. 2. In comparing FBC and Pheo *a*, the substitution stabilizes the HOMO (79th MO) and the LUMO (80th MO). Actually, small orbital mixing of the substituent orbitals (the vinyl group and oxygen in ring V) is observed in HOMO and LUMO of Pheo *a*. In comparing Pheo *a* and Chlo *a*, the Mg-coordination slightly destabilizes the orbital energy of HOMO (78th MO) and next-LUMO (80th MO) by 0.1 and 0.2 eV, respectively, while those of LUMO and next-HOMO are almost

unchanged. Little, if any, orbital mixing between Mg and the "four orbitals" is seen in Chlo *a*.

The calculated excited states of Pheo *a* and Chlo *a* are shown in Table 2. As for the Q band, the SAC-CI results reproduce well the experimental peak positions and the increase in the intensity of the first excited state in Chlo *a*. As for the B band, the present results overestimate the experimental excitation energies.

The first bands of Pheo *a* and Chlo *a*, which are the Q_x bands both at 1.87 eV,[32,33] are assigned to the *x*-polarized 2A excited state calculated both at 1.81 eV. In comparison with the Q_x band of FBC observed at 1.98 eV and calculated at 1.68 eV, the substituents and the Mg-coordination do not have a large effect on the excitation energy of the Q_x state. However, as shown in Table 3, the energies of the configurations which comprise the Q_x states of these compounds are different. For Pheo *a*, the two main configurations shift equally to a higher energy region by about 0.2 eV, compared to FBC. For Chlo *a*, the HOMO $\rightarrow$ LUMO excitation is stabilized by 0.19 eV and the next-HOMO $\rightarrow$ next-LUMO excitation is destabilized by 0.18 eV, compared to Pheo *a*. For Pheo *a*, the ratio of the weights of the two configurations is the same as in FBC, due to the parallel energy shifts of the two main configurations. However, in Chlo *a*, the weight of the HOMO $\rightarrow$ LUMO excitation increases and that of the next-HOMO $\rightarrow$ next-LUMO excitation decreases. The configuration interactions give a different mixing of the configurations but accidentally similar excitation energies.

The difference in the configuration mixing leads to different properties of the Q_x states of Pheo *a* and Chlo *a*; i.e. the transition moment. In comparing FBC and Pheo *a*, the spectral intensities of the Q_x bands are similarly small, since in each molecule, the contributions to the transition moments due to the two main configurations cancel each other

owing to the similarity of the SAC-CI coefficient.[19] On the other hand, Chlo *a* shows different configuration-mixing, as mentioned above, so that the cancellation is rather incomplete leading to a greater intensity of Chlo *a* than that of FBC and Pheo *a*.

For FBP, FBC and FBBC, the incomplete cancellation is caused by the coefficients and the transition moments of the configurations, as examined in section 3. For FBC, Pheo *a*, and Chlo *a*, the transition moments of the configurations are similar, as shown in Table 3, due to a small mixing with the substituents and Mg. Therefore, the incomplete cancellation in Pheo *a* and Chlo *a* is mainly due to the breakdown of the quasidegeneracy.

In our previous study on Mg porphin (MgP),[13] Mg-coordination was shown to have little effect on the intensity of the Q band. In the Q state of MgP, the two main configurations were almost degenerate. Due to the Mg-coordination in FBP, the weight of the most important configuration, $5b_{1u} \rightarrow 4b_{2g}$, decreased due to a destabilization of the $4b_{2g}$ orbital, while that of the next most important configuration, $2a_u \rightarrow 4b_{3g}$, increased due to a destabilization of the $2a_u$ orbital, which leads to a more degenerate situation. Therefore, the cancellation of the transition moments between these two excitations were almost complete in MgP. However, in Chlo *a*, a destabilization of the HOMO (77th MO) contributes to an increase in the weight of the most important HOMO $\rightarrow$ LUMO excitation and a destabilization of the next LUMO (79th MO) contributes to the decrease in the weight of the next most important $76 \rightarrow 79$ excitation. This causes a reduction in the quasidegeneracy of the two main configurations and give a net transition moment due to an incomplete cancellation of the two contributions.

The second bands measured at 2.3 eV for Pheo *a*[10,30,32] and at 2.1 eV for Chlo *a*[32,33] were assigned to the *y*-polarized 3A excited states

calculated at 2.33 and 2.17 eV, respectively. The disappearance of the humps at 480~550 nm in the Pheo *a* spectrum[10,30,32] is explained by the red shift of the 3A state in Chlo *a*. The main configurations of the 3A states of Pheo *a* and Chlo *a* consist of the next-HOMO → LUMO excitation strongly coupled to the HOMO → next-LUMO excitation.

As for the B band, the SAC-CI calculations reproduce the experimental absorption of Pheo *a* with a discrepancy of 0.28 eV, but overestimate that of Chlo *a* by 0.6 eV. As for Pheo *a*, the strong peak and the shoulder of the B band are assigned to the *x*-polarized 4A state and the *y*-polarized 5A state, calculated at 3.37 and 3.52 eV, respectively. These states are characterized as next-HOMO → next-LUMO excitation and HOMO → LUMO excitation, respectively. The ordering of the polarizations of the B band of Pheo *a* is the same as that of FBC. In a previous fluorescence polarization study in meso-pyromethyl pheophorbide, the ordering of the polarization was considered to be lower *y*-polarization and higher *x*-polarization, and the substituents were thought to change the order of the polarizations.[36] However, a more recent fluorescence polarization study on pheophorbide *a* by Goedheer[33] showed a different result in that the lower and higher sides of the B band are *x*- and *y*- polarizations, respectively. Our SAC-CI results support Goedheer's results. In our study, the substituents did not change the order of the polarizations.

The peak of the B band of Chlo *a* is observed at 2.90 eV in ether.[35] The SAC-CI calculation gives an excitation energy of 3.48 eV (y-polarizations). The counterpart of the B state is calculated at 3.65 eV (x-polarizations. This ordering is different to that of Pheo *a* and FBC, but corresponds to the experimental results.[32,33,36-38] The Mg-coordination reverses the order of the polarization in the B band of Chlo *a* from that of Pheo *a*.

In the SECI calculations of FBC and Pheo *a*, the polarizations of the B states were *y*- and *x*-polarization in the order of increasing energy, in contrast to the results of the SAC-CI calculation. In FBC and Pheo *a*, the *x*-polarized B states which are dominated by next-HOMO → next-LUMO excitation are stabilized by strong mixing with low-energy HOMO → LUMO excitation. By the SAC-CI treatment, the weights of the HOMO → LUMO excitations in the B_x states are further increased in FBC and Pheo *a* . This causes the x-polarized B states to be more stable than the *y*-polarized B states. However, in Chlo *a*, the SAC-CI treatment increases the weight of the next-HOMO → next-LUMO excitation in the *x*-polarized B states. These results show the importance of the electron correlations for the descriptions of the B states.

Conclusion

The excited states of biochemically important compounds FBC, FBBC, Pheo *a*, and Chlo *a* were calculated by the SAC/SAC-CI method. The results of calculations well reproduced the absorption spectra of these compounds. This together with the previous results for porphyrins[13,17-20] shows that the SAC/SAC-CI method, which gives accurate results for small molecules,[16] is also applicable to relatively large biochemical compounds. These results encourage us to apply the SAC-CI method to the energetics of biochemical reactions, including different electronic excited states.

The effects of the reduction in the pyrrole rings of the porphyrins are studied for the absorption spectra of FBP, FBC, and FBBC. Such reduction destabilized the HOMO and next-LUMO levels due to a shortning in the π-conjugation of these compounds. Since the HOMO - LUMO gap decreases, the Q_x states shift to a lower energy region and their quasidegenerate characters are relaxed, causing an incomplete

cancellation in the transition dipole moment which leads to an increase in the intensity of the Q_X band of FBBC relative to that of FBP. Further an increase in the configuration-transition dipole moment itself is also a reason of the increase of the transition intensity.

The effects of the substitutions and the Mg-coordination were analyzed. The substitutions do not affect the HOMO - LUMO gap of Pheo *a*. On the other hand, in Chlo *a*, the Mg-coordination reduced the HOMO-LUMO gap causing a breakdown of the quasidegenerate character of the Q_X state. This leads to an increase of the intensity of the Q_X band of Chlo *a* due to a smaller cancellation of the transition moment than in Pheo *a*.

Appendix

Molecular orbitals φ_i are described in LCAO approximation as,

$$\varphi_i = \sum_r C_{ir}\chi_r, \tag{1}$$

where χ_r is an atomic orbital and C_{ir} a MO coefficient. The transition dipole matrix element for a single excitation is written as,

$$\begin{aligned}\langle \Phi_{HF}|Q|\Phi_{i\to a}\rangle &= \sqrt{2}\langle \varphi_i|Q|\varphi_a\rangle \\ &= \sqrt{2}\sum_{r,s} C_{ri}C_{sa}\langle \chi_r|Q|\chi_s\rangle,\end{aligned} \tag{2}$$

where i and a show occupied and unoccupied orbitals, respectively, and Φ_{HF} denotes the HF configuration. Q is a dipole operator (Q=x, y, or z). Eq. 2 can be divided into the contribution of each atom:

$$\langle \Phi_{HF}|Q|\Phi_{i\to a}\rangle = \sum_A \langle Q\rangle_A, \tag{3}$$

where the atomic contribution to the transition dipole element is written as

$$\langle Q\rangle_A = \sqrt{2}\sum_{r\in Atom\,A}\sum_s C_{ri}C_{sa}\langle \chi_r|Q|\chi_s\rangle, \tag{4}$$

like the Mulliken population analysis.

References

(1) Michel-Beyerle, M. E. ; In *Antennas and Reaction Centers of Photosynthetic Bacteria* ; Springer-Verlag, Berlin, 1985.

(2) Scheidt, W. D.; Reed, C. A.; *Chem. Rev.* **1981**, *81*, 543.

(3) Gouterman, M. In *The Porphyrin*:; Dolphin, D., Ed.; Academic Press: New York, 1978; Vol III.

(4) Thompson, M. A.; Zerner, M. C. *J. Am. Chem. Soc.* **1991**, *113*, 8210.

(5) Scherer, P. O. J.; Scharnagl, C.; Fischer, S. F. *Chem. Phys* **1995**, *197*, 333.

(6) Zhang, L. Y. ; Friesner, R. A. *J. Phys Chem.* **1995**, *99*, 16479.

(7) Sakuma, T; Kashiwagi, T; Takada, H; Nakamura, H, *Int. J. Quantum Chem.* **1997**, *61*, 137.

(8) Christoffersen, R. E. *Int. J. Quantum Chem.* **1979**, *16*, 573.

(9) Nagashima, U.; Takada, T.; Ohno, K. *J. Chem. Phys.* **1986**, *85*, 4524.

(10) Scheer, H.; Inhoffen, H. H. In *The Porphyrin*: Dolphin, D., Ed.; Academic Press: New York, 1978; Vol II; pp 45-90.

(11) Desienhofer, J.; Epp, O; Miki, K.; Huber, R.; Michel, H. *J. Mol. Biol.* **1984**, *180*, 385.

(12) Weiss, C. *J. Mol. Spectrosc.* **1972**, *44*, 37.

(13) Hasegawa, J.; Hada, M.; Nonoguchi, M.; Nakatsuji, H. *Chem. Phys. Lett.* **1996**, *250*, 159.

(14) Nakatsuji, H.; Hirao, K. *J. Chem. Phys.* **1978**, *68*, 2035.

(15) Nakatsuji, H. *Chem. Phys. Lett.* **1978**, *59*, 362; **1979**, *67*, 329, 334.

(16) Nakatsuji, H; In *Computational Chemistry*: Leszczynski J., Ed.; World Scientific: 1997; Vol II; pp 62-124. Nakatsuji, H.; Acta. Chim. Hung. **1992**, *129*, 719.

(17) Nakatsuji, H.; Hasegawa, J.; Hada, M. *J. Chem. Phys.* **1996**, *104*, 2321.

(18) Nakatsuji, H.; Hasegawa, J.; Ueda, H.; Hada, M. *Chem. Phys. Lett.* **1996**, *250*, 379.

(19) Toyota, K.; Hasegawa, J.; Nakatsuji, H. *Chem. Phys. Lett.* **1996**, *250*, 437.

(20) Nakatsuji, H.; Tokita, Y.; Hasegawa, J.; Hada, M. *Chem. Phys. Lett.* **1996**, *256*, 220; Tokita Y.; Nakatsuji, H. *J. Phys. Chem. B* **1997**, *101*, 3281.

(21) Almlöf, J.; Fisher, T. H.; Gassman, P. G.; Ghosh, A.; Häser, M. *J. Phys. Chem.* **1993**, *97*, 10964.

(22) Fisher, M. S.; Temleton, D. H.; Zalkin, A.; Calvin, M. *J. Am. Chem. Soc.* **1982**, *104*, 3613.

(23) Huzinaga, S.; Andzelm, J.; Klobukowski, M.; Radzio-Andzelm, E.; Sakai, Y.; Tatewaki, H. In *Gaussian Basis Set for Molecular Calculations*; Elsevier: New York, 1984.

(24) Huzinaga, S. *J. Chem. Phys.* **1965**, *42*, 1293.

(25) Nakatsuji, H. *Chem. Phys.* **1983**, *75*, 425.

(26) Dupuis, M.; Farazdel, A. *MOTECC-91*; Center for Scientific and Engineering Computations, IBM Corporation, 1991.

(27) Nakatsuji, H. *Program System for SAC and SAC-CI Calculations*, Program Library No. 146 (Y4/SAC), Data Processing Center of Kyoto University, 1985. Program Library SAC85, No. 1396, Computer Center of the Institute for Molecular Science, Okazaki, 1981.

(28) Nakatsuji, H.; Hada, M.; Ehara, M.; Hasegawa, J; Nakajima, T.; Nakai, H.; Kitao, O.; Toyota, K. *SAC/SAC-CI Program System (SAC-CI96) for Calculating Ground, Excited, Ionized, and Electron Attached States and Singlet to Septet Spin Multiplicities.*

(29) Edwards, L; Dolphin, D. H. *J. Mol. Spectrosc.* **1971**, *38*, 16.

(30) Eisner, U.; Linstead, R. P.; *J. Chem. Soc.* **1955**, 3742.

(31) Seely, G. R. *J. Chem. Phys.* **1957**, *27*, 125.

(32) Houssier, C.; Sauer, K. *J. Am. Chem. Soc.* **1970**, *92*, 779.

(33) Goedheer, J. C. In *The Chlorophylls*: Vernon, L.; Seely. G. R., Eds.; Academic Press: New York, 1966.

(34) Weiss, C. In *The Porphyrin*: Dolphin, D., Ed.; Academic Press: New York, 1978; Vol III.

(35) Sevchenko, A. N.; Solov'ev, K. N.; Mashenkov, V. A.; Shkirman, S. F. Losev, A. P. *Sov. Phys.-Dokl.* **1966**, *10*, 778.

(36) Bär, F.; Lang, H.; Schnabel, E.; Kurn, H. *Z. Electrochimie* **1961**, *65*, 346.

(37) Gouterman, M.; Stryer, L. *J. Chem. Phys.* **1962**, *37*, 2260.

(38) Houssier, C.; Sauer, K. *Biochim. Biophys. Acta* **1969**, *172*, 492.

TABLE 1: Dimensions of the SAC/SAC-CI calculations for FBC, FBBC, Pheo *a*, and Chlo *a*

State	Before Selection	Reference State	After Selection[a]
FBC			
Ground state(SAC)			
A_1	7009800	1	22810
Excited states(SAC-CI)			
A_1	7009800	4	70206
B_1	7006134	4	78721
FBBC			
Ground state(SAC)			
A_{1g}	3661607	1	28190
Excited states(SAC-CI)			
A_{1g}	3661607	1	26672
B_{2u}	3657853	4	64167
B_{3u}	3657832	4	71162
Pheo *a*			
Ground state(SAC)			
A	76935809	1	23621
Excited states(SAC-CI)			
A	76935809	4	60692
Chlo *a*			
Ground state(SAC)			
A	91848680	1	24971
Excited states(SAC-CI)			
A	91848680	4	71422

[a] Correlation energies for the ground states of FBC, FBBC, Pheo *a*, and Chlo *a* are -0.38933, -0.48829, -0.24554, and -0.31067 hartree, respectively.

TABLE 2: Excited states of FBP, FBC, FBBC, Pheo *a*, and Chlo *a* calculated by the SAC/SAC-CI method

State	SAC-CI: Main configuration (C ≥ 10.21)	Nature	SAC-CI: Excitation energy (eV)	SAC-CI: Oscillator strength		Exptl.: Excitation energy (eV)	
FBP[a]							
$1B_{3u}$	$0.73(5b_{1u}\rightarrow4b_{2g})+0.61(2a_u\rightarrow4b_{3g})$	π-π*	1.75	1.13×10^{-3}	; x	1.98[b],2.02[c]	; Q_x
$1B_{2u}$	$-0.70(2a_u\rightarrow4b_{2g})-0.66(5b_{1u}\rightarrow4b_{3g})$	π-π*	2.23	5.66×10^{-3}	; y	2.42[b],2.39[c]	; Q_y
$2B_{3u}$	$-0.64(2a_u\rightarrow4b_{3g})+0.52(4b_{1u}\rightarrow4b_{2g})-0.43(5b_{1u}\rightarrow4b_{2g})$	π-π*	3.59	1.03	; x	3.33[b],3.15[c]	; B
$2B_{2u}$	$0.66(5b_{1u}\rightarrow4b_{3g})-0.63(2a_u\rightarrow4b_{2g})-0.25(4b_{1u}\rightarrow4b_{3g})$	π-π*	3.79	1.73	; y	3.65[b]	; N
FBC							
$1B_1$	$-0.78(6a_2\rightarrow9b_2)-0.55(8b_2\rightarrow7a_2)$	π-π*	1.68	6.24×10^{-2}	; x	1.98[c],1.94[d]	; Q_x
$2A_1$	$-0.75(8b_2\rightarrow9b_2)+0.58(6a_2\rightarrow7a_2)$	π-π*	2.39	8.02×10^{-3}	; y	2.29[c],2.29[d]	; Q_y
$2B_1$	$-0.75(8b_2\rightarrow7a_2)+0.53(6a_2\rightarrow9b_2)-0.22(7b_2\rightarrow7a_2)$	π-π*	3.58	1.28	; x	3.18[c],3.19[d]	; B
$3A_1$	$0.72(6a_2\rightarrow7a_2)+0.56(8b_2\rightarrow9b_2)+0.22(7b_2\rightarrow9b_2)$	π-π*	3.74	1.68	; y		
FBBC							
$1B_{3u}$	$0.85(3a_u\rightarrow4b_{3g})+0.44(5b_{1u}\rightarrow5b_{2g})$	π-π*	1.47	1.88×10^{-1}	; x	(1.6)[e]	; Q_x
$1B_{2u}$	$0.77(5b_{1u}\rightarrow4b_{3g})-0.54(3a_u\rightarrow5b_{2g})$	π-π*	2.42	2.57×10^{-2}	; y	(2.3)[e]	; Q_y
$2B_{2u}$	$-0.77(3a_u\rightarrow5b_{2g})-0.54(5b_{1u}\rightarrow4b_{3g})-0.20(4b_{1u}\rightarrow4b_{3g})$	π-π*	4.11	1.86	; y	(3.1[shoulder])[e]	; B
$2B_{3u}$	$-0.84(5b_{1u}\rightarrow5b_{2g})+0.44(3a_u\rightarrow4b_{3g})$	π-π*	4.24	2.11	; x	(3.4)[e]	; B
Pheo *a*							
2A	$-0.74(79\rightarrow80)-0.51(78\rightarrow81)-0.23(79\rightarrow81)$	π-π*	1.81	7.22×10^{-2}	; x	1.9[f],1.86[g],1.87[d]	; Q_x
3A	$-0.74(78\rightarrow80)+0.52(79\rightarrow81)-0.28(79\rightarrow80)$	π-π*	2.33	4.57×10^{-2}	; y	2.3[f],2.33[g],2.30[d]	; Q_y
4A	$-0.73(78\rightarrow81)+0.51(79\rightarrow80)$	π-π*	3.37	1.20	; x	3.1[f],3.04[g]	; B
5A	$-0.72(79\rightarrow81)-0.50(78\rightarrow80)+0.24(78\rightarrow81)$ $+0.22(77\rightarrow80)$	π-π*	3.52	1.03	; y	3.2[f]	; B
Chlo *a*							
2A	$0.81(77\rightarrow78)-0.37(76\rightarrow79)-0.25(76\rightarrow78)$ $+0.21(77\rightarrow79)$	π-π*	1.81	0.179	; x	1.87[h],1.88[g]	; Q_x
3A	$-0.77(76\rightarrow78)+0.44(77\rightarrow79)-0.31(77\rightarrow78)$	π-π*	2.17	8.26×10^{-2}	; y	2.14[h],2.16[g]	; Q_y
4A	$+0.78(77\rightarrow79)+0.42(76\rightarrow78)+0.26(74\rightarrow78)$	π-π*	3.48	1.01	; y	2.88[h],2.90[g]	; B
5A	$-0.84(76\rightarrow79)+0.35(77\rightarrow78)$	π-π*	3.65	1.38	; x		

[a] Reference 17
[b] In Gas phase. Reference 29
[c] In benzene. Reference 9
[d] In benzene. Reference 30
[e] Data for bacteriopheophorbide and not for FBBC. Reference 10
[f] Reference 10
[g] In ether. Reference 32
[h] In ether. Reference 33

TABLE 3: The energies (in eV) and moments (in a.u.) of the main configurations of the Q_X band for FBP, FBC, FBBC, Pheo *a* and Chlo *a*.

Molecule	FBP		FBC		FBBC	
Excitation	$5b_{1u}\rightarrow4b_{2g}$	$2a_u\rightarrow4b_{3g}$	$6a_2\rightarrow9b_2$	$8b_2\rightarrow7a_2$	$3a_u\rightarrow4b_{3g}$	$5b_{1u}\rightarrow5b_{2g}$
Weight	0.53	0.37	0.61	0.30	0.72	0.19
$<0\|x\|i\rightarrow a>$[a]	4.61	-4.67	4.60	-3.41	5.60	-3.92
$\Delta\varepsilon$[b]	6.62	6.66	6.28	7.72	5.24	8.46
Energy[c]	4.15	4.22	3.71	4.71	3.27	5.37
Molecule	Pheo *a*			Chlo *a*		
Excitation	79→80	78→81	78→80	77→78	76→79	76→78
Weight	0.56	0.26	0.04	0.66	0.14	0.06
$<0\|x\|i\rightarrow a>$[a]	4.41	-3.24	-0.13	4.51	3.08	-0.93
$<0\|y\|i\rightarrow a>$[a]	1.58	-1.47	3.39	1.22	1.03	3.61
$\Delta\varepsilon$[b]	6.35	7.77	6.82	6.18	7.99	6.81
Energy[c]	3.87	4.91	4.23	3.68	5.09	4.23

[a] Transition moments of the configurations

[b] Orbital energy gap in eV

[c] Energy of the main configuration relative to that of the HF configuration.

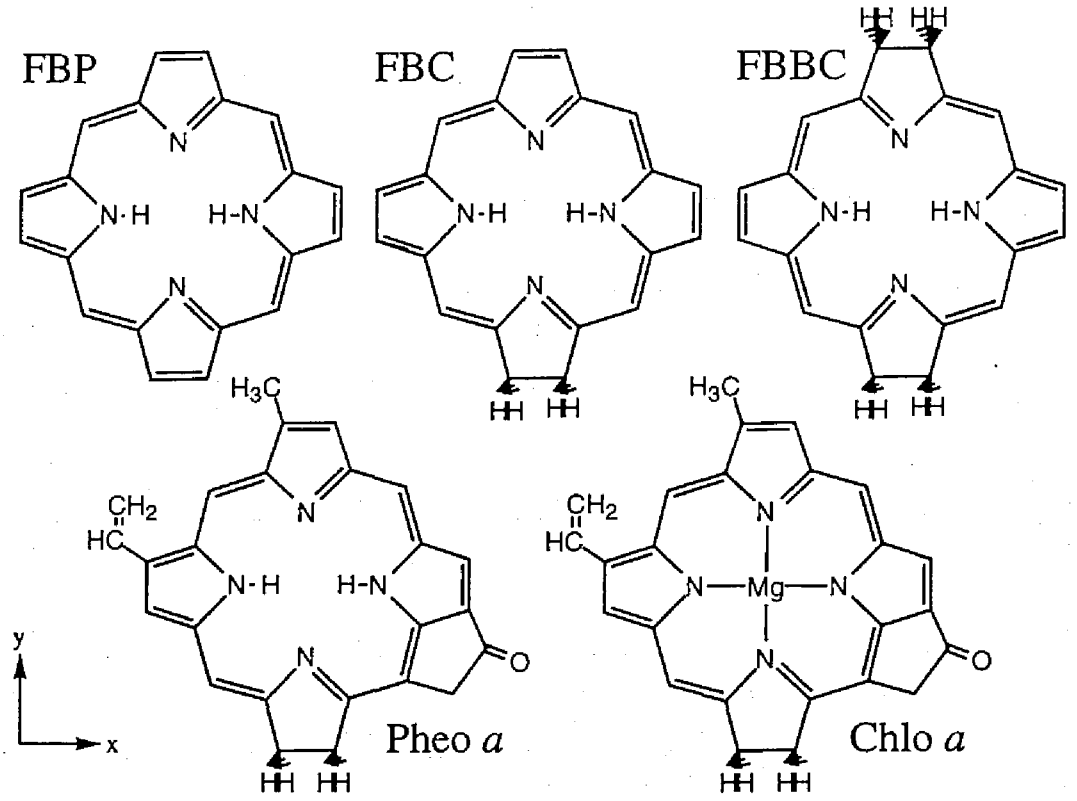

Figure 1. Molecular geometries of FBP, FBC, FBBC, Pheo *a*, and Chlo *a*. Some substituents in the X-ray structures of Pheo *a* and Chlo *a* are replaced by protons in the present calculations (see text).

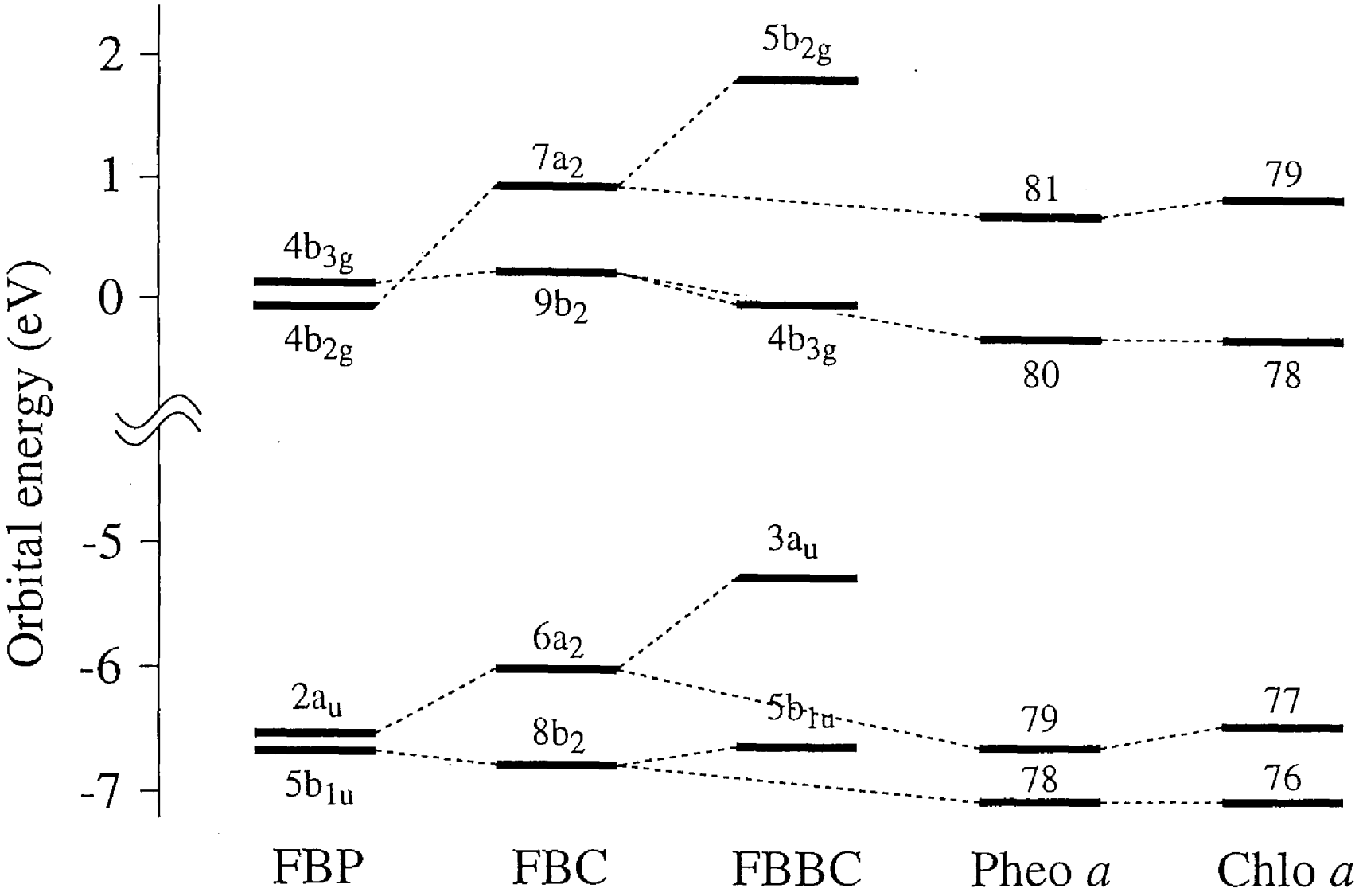

Figure 2. HF orbital energy levels of the "four orbitals" of FBP, FBC, FBBC, Pheo *a*, and Chlo *a*.

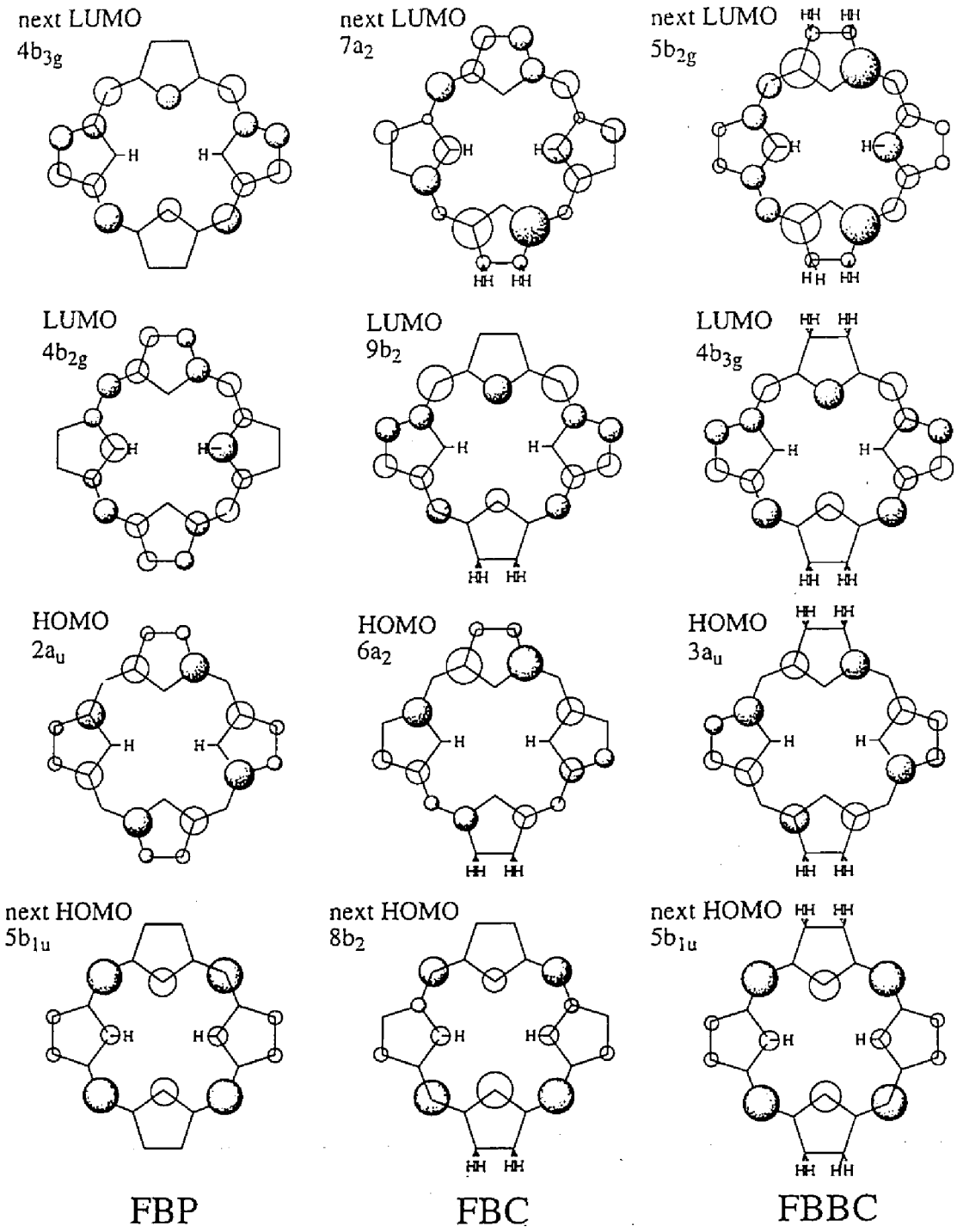

Figure 3. Illustration of the "four orbitals" of FBP, FBC, and FBBC.

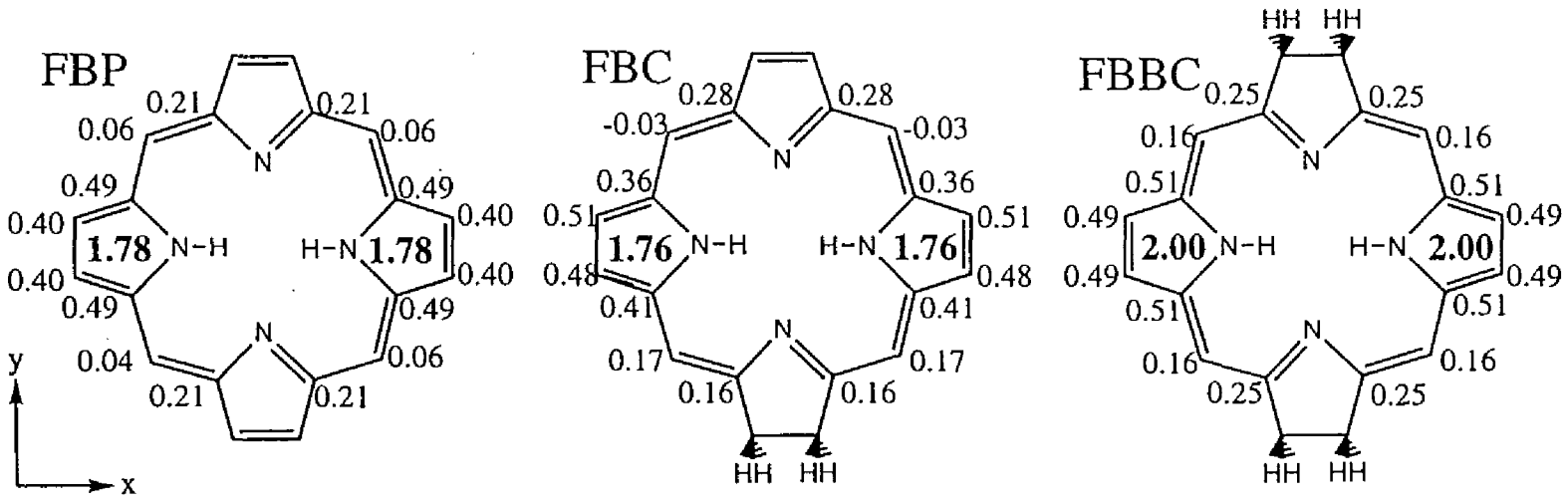

Figure 4. Population analysis for the transition moment of the HOMO→LUMO excitation configuration of FBC and FBBC and the HOMO→next-LUMO excitation configuration of FBP. Atoms with contributions larger than 0.01 are shown.

Part II

SAC-CI study on the excitation spectrum and the electron transfer reactions in the photosynthetic reaction center of *Rhodopseudomonas viridis*

Chapter 5

Excitation spectrum of the photosynthetic reaction center

Abstract

The excited states of the photosynthetic reaction center of *Rhodopseudomonas viridis* are clarified by the SAC-CI method. The theoretical excitaion spectrum successfully reproduced the experimental one in excitation energy, oscillator strength, and angle of transition moment and a theoretical assignment for the absorption spectrum is shown. Linear dichroism for the excited states is also taken into consideration for confirming the assignment. Dimerization effects seen in the excited states of special pair are explained by comparing with those of monomer. Protein effect on the excitation spectrum is calculated to be red-shifts of the peak positions in almost of all the states.

1. Introduction

Solar energy transduction to chemical energy is essentially important task for the survival of the life on the earth. This indispensable task is carried out by photosyntheses of green plants and some bacteria. The photosynthetic reaction center (RC) of *Rhodopseudomonas viridis* (*Rps. viridis*) is shown in Figure 1. The RC works for the transduction of the solar energy to driving forces of biochemical reactions. Excitation of special pair (P; bacteriochlorophyll *b* dimer) by a light absorption or an energy transfer cause a primary electron transfer at the RC, which is the first step of the photosynthesis. (See reference [1])

Thus far the interesting features of the electron transfer have been investigated by substantial efforts on this system. The long-range character [2], the high efficiency [1], and the unidirectionality [3,4] were experimentally found and they have been studied extensively due to both scientific interests and a technological applicability. However, almost all of the studies were concentrated on a dynamics caused by the first absorption. In Figure 2, the absorption spectrum of the RC of *Rps. viridis* [5] is shown. The spectrum has complex structure in both visible and near-infrared regions, which is indicating a possibility that the RC is workable by other absorptions. Namely, the each absorption is opening a channel for each dynamics. Recently, experimental results indicating new pathways of the electron transfer from B* of *Rhodobacter sphaeroides* were reported [6,7]. For investigating another dynamics, an understanding of the excited states is indispensable. The precise assignment of the spectrum would provide us a starting point for the investigation of the another feature of the electron transfer reaction in the RC.

Previously, some semi-empirical calculations for the excitation spectrum were reported [8-10]. Their theoretical spectra qualitatively

reproduced spectral feature but failed to reproduce the Q bands and linear dichroism (LD) data (angle of transition moment from C_2 axis of the RC)[9,10]. Although these works brought important information about the excited states, the theoretical assignment was not satisfactory due to lack of accuracy of approximations of their method.

In the present, ab initio electronic structure theory achieved chemical accuracy. The application of these method to large system as biochemicaly important system is one of the challenging frontier of quantum chemistry. The applicability to large systems is one of the important conditions which must be satisfied to be an useful theory. The SAC[11] /SAC-CI [12] method [13,14] is one of the accurate theories for the excited states, which describes electron correlations for ground and excited, ionized, anionized, and high-spin states. The SAC/SAC-CI method has been applied to many systems and established its accuracy and reliability [13,14]. In recent years, in order to apply the SAC-CI method to the excited states of the photosynthetic RC, we have developed algorithm and program. The SAC-CI method is successfully applied to the excited states of porphyrin compounds, free base porphin [15,16], Mg porphin [17], bacteriochlorin [18], and pheophytin [18] and showed its applicability to the excited states of such moderately large systems.

In this paper, we applied the SAC/SAC-CI method to the excited states of the RC of *Rps. viridis*. This study is aimed to assign the absorption spectrum and to understand the excited electronic structures of the RC. First, we describe the excited states of bacteriochlophyll *b* and show the assignment of the absorption spectrum in section 3. The excited states of P and the dimerization effects about energy level splitting and oscillator strength are described in section 4. In section 5, the SAC-CI assignment of the absorption and LD spectra and the electronic structure of the excited states are shown. Protein effect on the excitation spectrum, which

is introduced by a point charge model and a continuum model, is discussed in section 6.

2. Computational details

The structure of the RC of *Rps. viridis* [2] is shown in Figure 1, which shows the well-known symmetric alignment of the chromophores (L- and M-branches). For geometry of chromophores, a X-ray crystallographic structure [2] (1PRC in Brookhaven Data Bank [19]) is used. The present calculations are done for each chromophores, special pair (bacteriochlorophyll *b* dimer; P), two bacteriochlorophyll *b* (B_L and B_M), two bacteriopheophytin *b* (H_L and H_M), menaquinone (MQ), and ubiquinone (UQ), where the subscripts L and M denote chromophore belonging to L- and M-branches, respectively. For calculational efficiency, some substituents in the chromophores are simplified, except for the substituents which could π-conjugate with rings. The adopted models are shown in Figure 3. The labelling of the atoms and rings are also shown. Our previous calculations reproduced the absorption spectrum of the low-lying excited states instead of these simplifications [18].

The basis sets are common to these calculations. For C, N, and O atom, Huzinaga's (63/5)/[2s2p] sets [20] and for H atom, Huzinaga's (4)/[1s] set [21] is used. For Mg, Huzinaga's (533/5)/[5s/3p] set [20] plus two p-type polarization functions (ζ=0.045 and 0.143) and d-type polarization functions (ζ=1.01) are used.

Protein effect is introduced by a point charge model. The model contained about 30,000 atoms. The geometry of the heavy atoms in RC protein and cytochrome *c* are taken from the X-ray structure [2] (1PRC in Brookhaven Data Bank [19]). The ionized form is adopted for the ionizable residues, ASP, LYS, ARG, and GLU. For protein and waters,

the published charges [22,23] are used. For the chromophores, which are excluded from quantum-chemical calculation, Mulliken charge of HF orbitals are used.

In the SAC/SAC-CI calculations, the orbitals whose energy are in -0.7 ~ +0.7 a.u. are chosen for active space, in which at least 2p electrons are correlated. In our experience, this criteria would be enough to reproduce the low-lying excited states of porphyrin compounds [14-18]. In P, which is the largest molecule in the present calculation, 90 occupied and 220 unoccupied orbitals (total 310 orbitals) are taken into active space. Perturbation selection [15,24] is carried out in order to select double excitation operators. For the ground, excited, and electron attached states, the energy threshold, 1×10^{-5}, 1×10^{-6}, and 1×10^{-6} a.u. are used, respectively. For the ground, excited, and ionized states of P, the threshold of 3×10^{-6}, 2×10^{-7}, and 3×10^{-6} a.u. are used, respectively. All single excitations and the selected double excitations are included in the linked term. The dimension of the SAC/SAC-CI calculations are shown in Table 1. Correlation energies for the ground states of these compounds are also shown. Number of doubly excited configurations are rather reduced and the correlation energy of these molecule is relatively small from our previous calculations.

For Hartree-Fock SCF calculation, the HONDO version 8 program [25] and for the SAC/SAC-CI calculation, the development version [26] of SAC 85 [27] program is used. Parallel implementation is carried out for an integral transformation step which is the most time consuming in the present calculation.

3. Excited states of bacteriochlorophyll *b*

Here, we introduce the excited states of bacteriochlorophyll *b* monomer (BChl *b*) composing the one-side of P, in order to understand

the excited states of P more easily and to confirm the accuracy of the SAC-CI metnod. Figure. 4 shows the experimental [28] and the SAC-CI spectrum of BChl *b* and Table 2 shows the data for the excited states. The result reproduced the low-lying excited states of the experimental spectrum. The average error is 0.14 eV. The first excited state, 2^1A, is characterized as HOMO $\rightarrow$ LUMO excitation (π–π^*) in which HOMO-1 $\rightarrow$ LUMO+1 excitation (π–π^*) slightly mixes. In free base porphin (FBP) [15], these HOMO $\rightarrow$ LUMO and HOMO-1 $\rightarrow$ LUMO+1 degenerate and their transition moments are canceled out each other by the degenerate excitations [18,29]. In the case of BChl *b*, reductions of the C=C bonds in the pyrrole rings cause destabilizations of energy levels of the HOMO-1 and LUMO+1, which result in a larger intensity than that in FBP [18]. The second excited states, 3^1A, is characterized as HOMO-1 $\rightarrow$ LUMO excitation (π–π^*). The directions of the transition moments of the 2^1A and 3^1A states are perpendicular and parallel to the axes along the two reduced pyrrole rings, respectively.

4. Excited states of special pair (P)

In this section, the electronic structures of the excited states of P, especially dimerization effects are shown. The details of the assignment for the absorption spectrum of the RC are described in the latter section.

In Figure 5, the calculated energy levels of the excited states of P (the central column) are compared with those of BChl *b* (the second column from the left). The first excited states P(2^1A) are calculated to be at 1.40 eV and a red shift caused by the dimerization are reproduced. The reason of the red-shift is that the energy gap between the HOMO and LUMO decreases by the dimerization, due to HOMO-HOMO and LUMO-LUMO interactions between the two monomers. Under 3 eV region, total seven excited states of P are calculated, which consist of four exciton (Ex) and

three charge transfer (CT) states. In Table 3, net charges of the excited states of P are divided into the contribution by the each monomer, P_L and P_M. The difference of the electron population between the Ex and CT states is clearly seen in Table 3. In the CT states about a half of an electron move to the other monomer. This polarizing property would cause geometric relaxations of P in the CT states. The each monomer state splits into four states by the dimerization as shown in Figure 5; two Ex and two CT states, since two CT states (electron transfer to the other monomer) are newly included by the dimerization (details are shown in Appendix). The dotted lines connecting from dimer to monomer states shows the parent monomer state for the dimer states. Thus, P has eight states (four Ex and four CT states) originating from monomer 2 and 3^1A states.

As for the oscillator strength, the P(2 and 6^1A) states have large intensities in the excited states of P. In Table 4, the summary of the excited states of P are shown. The oscillator strengthes of the P(2 and 6 ^1A) states are 0.607 and 0.144, respectively. The reason why only these states have relatively large intensities is related to symmetry of P and properties of the monomer states. As mentioned above, P has a pseude-C_2 symmetry, though it is almost broken in the X-ray structure [2]. Then the excited states of P can be approximately assigned to the irreducible representations of C_2 symmetry as shown in Figure 5. The P(2 and 6 ^1A) states are belongs to B and A symmetries, respectively. In the B and A symmetries, the directions perpendicular and parallel to the C_2 axis are allowed, respectively. On the other hand, the monomer 2 and 3^1A states have a large "perpendicular" and a secondary large "parallel" transition moments, respectively as described above. Accordingly, states in B symmetry originating from the monomer 2^1A state, the P(2^1A) state, and states in A symmetry from the monomer 3^1A state, the P(6^1A) state, have

large transition moments. As seen in Table 3, the P(7^1A) state has a relatively large oscillator strength of 0.120, since, due to symmetry, the P(7^1A) state mixes with the HOMO $\rightarrow$ LUMO excitation which have a large transition moment.

5. Excitation spectrum of the reaction center

The absorption and LD spectra by Breton [5] and the SAC-CI method are shown in Figure 6. The experimentally observed peaks in the absorption spectrum are numbered from I to XIII. The dotted lines denote the proposed assignments in the present study. The excitation energy, oscillator strength, and angle of transition moment between the C_2 axis of the excited states are given in Table 4. Although the experimental spectrum has complex structure in a small energy range, the calculated spectrum reproduced the experimental one with the averaged error of 0.21 eV in excitation energy. Our assignments are grounded by excitation energy, oscillator strength, LD spectrum, and angle (θ) of transition dipole moment from the C_2 axis of the reaction center which are estimated experimentally by the LD spectrum [5]. Although we replaced inter-chromophore interaction to a classical coulomb interaction, the calculations reproduced the experimental values, which might indicate the adequacy of our approximation.

The first band I at 1.25 eV has been attributed to Q_y states of P, since there is no low-lying peak in the absorption spectrum of B and H monomer. This assignment are supported by the semi-empirical studies [8-10]. In the present calculation, the band I is also assigned to P(2^1A) state calculated at 1.4 eV, since the angle θ (85.1 deg.) is most close to the experimented one (90 deg.) [5] than those of the other candidates and a calculated large plus LD component seen in Figure 6 is also found in the experimental one [5]. Although the present calculation failed the energy

order of the first singlet excited state, the discrepancy with the experiment is 0.15 eV. The main configuration of the P(2^1A) state is HOMO(H) $\rightarrow$ LUMO(L) (π–π^*) excitation with a small mixing of H-1$\rightarrow$L+1 excitation. Due to in-phase (same-sign) coupling of these configurations, the P(2^1A) state is characterized as exciton (Ex) coupling of the Q_y state (H$\rightarrow$L excitation) of monomer (see Appendix). Comparing with the ground state of P(X^1A), about 0.1 electron is transferred from P_M to P_L as seen in Table 3. The P(2^1A) state has small charge transfer (CT) character due to configuration mixing of CT excitations to Ex ones. The intensity of the P(2^1A) state is 0.607, which is two times larger than that in B monomers. This enhancement is due to Ex character of the state; the additive contribution of the intensity of the two monomers (see Appendix).

Band II at 1.46 eV is observed as a small peak on a red-side shoulder of band III [5]. This peak has been attributed to an excited state of P, since this peak vanishes in the absorption spectrum of P^+ in oxidized RC [5]. The P(3^1A) state calculated at 1.62 eV should be assigned to the band II, since the angle θ (36.9 deg.) agrees well with the experimental one (30 deg.) and the energy separation from the first excited state (0.22 eV) is comparable with that in experiment (0.21 eV). The main configuration of the P(3^1A) state is H-1 $\rightarrow$ L (π–π^*) excitation with a small in-phase mixing of H $\rightarrow$ L+1 excitation, which is characterized as an exciton coupling of monomer Q_y state (H$\rightarrow$L excitation). The intensity of the P(3^1A) state is quite smaller than that of the P(2^1A) state, although these two state are both Ex states. The reason is that in C_2-fixed dimer, the P(3^1A) state belongs to A symmetry in which transition from the ground state is allowed only along a direction along C_2 axis and the H$\rightarrow$L excitation of the monomer has small intensity in this direction.

A strong peak, the band III (1.49 eV) has been ascribed to Q_y bands of B's and the bands IV (1.54 eV) and V (1.57 eV) to Q_y bands of H's, respectively [5]. Further, the band IV was attributed to H_L by an experimental result in which an illumination of λ>900 nm light to the RC bleached this peak due to a photoreduction of L-branch chromophores [30]. The present assignment supports the previous ones. The band III is assigned to the first excited states of B_M (2^1A) and B_L (2^1A) calculated at 1.35 and 1.45 eV, respectively, since the calculated angles θ, 64.3 and 67.2 deg. for B_M and B_L, respectively, and the plus LD components as seen in Figure 6 (b) are consistent with the experimental ones. These θ values and LD spectrum are useful to distinguish from the states originated from H's. The band IV and V are attributed to the first excited states H_L (2^1A) and H_M (2^1A) calculated at 1.59 and 1.75 eV, respectively. This assignment is rationalized by the θ values, 33.7 and 28.6 deg. and the large minus contributions in the LD spectrum as seen in Figure 6. It must be noted that the present result supports the energetic order of H_L and H_M which were proposed previously [30]. The orders of the intensity and LD value between H_L and H_M are consistent with the experiments [5]. The molecular structure of H's should be an origin of the order, since the gas phase result shown in Table 4 has the same the order of the states as that in protein. These four states are Q_y bands of B's and H's, whose main configurations are H $\rightarrow$ L (π–π^*) excitations.

We also calculated the excited states of four hemes, c-552, c-554, c-556, and c-559 by the SAC-CI method [a]. The hemes are included in cytochrome which locates next to the RC. The first excited state of c-552 is calculated at 1.50 eV, which is at blue-side of the first excited states of B_L and B_M [a]. The LD of the state is calculated to be a small negative value. In the experimental LD spectrum depicted in Figure. 6 (b), the blue-side shoulder of the large plus peak at 1.49 eV seems slightly

reduced. Then we propose this reduction is due to the first excited state of c-552. Thus, the present result indicates the order of the excited states for 1.4~1.6 eV region as

$$P(3^1A) < B_M(2^1A) < B_L(2^1A) < \text{c-552}(2^1A) < H_L(2^1A) < H_M(2^1A).$$

A small peak, band VI, is observed at 1.88 eV in the absorption spectrum and its LD has a negative contribution as seen in Figure 6 (b). In our knowledge, there is no assignment for this peak. This peak should be assigned to the second excited state of c-552, which is calculated at 1.83 eV [a]. Since the LD of this state is calculated to be a minus component, the assignment is consistent with the experimental fact.

Band VII is composed of at least two states from LD spectrum [5]. A peak at 1.8 eV was proposed to assign to H_L anion, since this peak increase its intensity in the absorption spectrum of the photoreduced RC [30]. We also calculated the electron attached states of H_L and the excitation energy of $X^2A(\infty \rightarrow L) \rightarrow 2^2A(\infty \rightarrow L)$ transition is calculated to be 1.4 eV. The discrepancy of 0.4 eV is somehow large, since a geometric relaxation effect on X^2A state are not considered in this calculation.

The blue-side shoulder (1.88eV) of band VII was proposed to be a Q_x component of P from circular dichroism (CD) spectra of oxidized RC [5]. We attribute $P(4^1A)$ state calculated at 2.10 eV to this shoulder. The calculated LD shows a slightly plus, which is consistent with the experimental one as seen Figure 6. The energy separation from the first singlet excited state of P in the theory and experiment [5] are 0.70 and 0.63 eV, respectively, which rationalize the assignment. The $P(4^1A)$ state is classified as a Q_x component, since the main configuration of the state, H-2 $\rightarrow$ L (π–π^*) excitation, is originate from monomer 3^1A state, H-1$\rightarrow$L excitation.

A broad band VIII composes a red-side shoulder of band IX. The LD experiment showed a characteristic large minus component as seen in Figure 6 and a specific small value (30 deg.) for the angle θ [5]. The present assignment of band VIII is P (6^1A) state calculated at 2.48 eV. Although the discrepancy between experiment, 0.48 eV, is rather large, the calculated angle (25.3 deg.) and the large minus LD value are close to the experiment [5]. The main configuration is H-3 → L excitation (π–π^*). The P (6^1A) state is classified to Q_x component of the excited state of P, since this transition is originate from monomer H-1 → L excitation.

The band IX and X observed at 2.04 and 2.07 eV are attributed to Q_x states of B_M (3^1A) and B_L (3^1A) states calculated at 2.17 and 2.23 eV, respectively. The present result supports the previous assignment [5] and the illuminated result [30]. The present results reproduced the LD spectrum and the angles θ for B_M (3^1A) and B_L (3^1A). The same energy order of the Q_x states of B is found in the gas phase calculation, which indicates that the molecular structure of B is the origin of the order of the states.

Bands XI, XII, and XIII observed 2.23, 2.28, and 2.32 eV have been attributed to Heme, H_L (Q_x), and H_M (Q_x), respectively [5,30]. The illuminated result [30] indicated lower H_L and higher H_M. The band XI might have two components, since the sharp peak of band XI vanishes and a shoulder remains in the oxidized state (P^+) absorption [5]. The sharp one has a characteristic minus LD. This component is ascribed to c-559 in the previous study [5]. In the SAC-CI result, the first excited state of c-554 is calculated at 2.38 eV with a relatively large minus LD value as shown in Figure 6. However, the excited state of P with minus LD is not calculated in this region (the 6^1A state has already assigned to the band VIII). The band XI should be assigned to c-554 and the reduction of intensity in the oxidized state spectrum [5] could be ascribed to an

accidental oxidation of c-554. The broad shoulder in the vicinity of the band XI might be assigned to P(7^1A), P(7^1A) and c-552(4^1A) states from the theoretical spectrum. For bands XII and XIII, H_L (3^1A) and H_M (3^1A) states calculated at 2.66 and 2.67 eV are assigned respectively, and the calculated energy order supported the previous experimental assignment [5,30]. The main configuration of the P (7^1A) state is H-1 $\rightarrow$ L excitation (π–π^*) which is CT coupling between monomer Q_x states. Net charge shown in Table 3 clearly shows its CT character; about 0.5 electron is transferred to P_L to P_M. The P (7^1A) state has relatively large intensity in comparison with other CT state, since the P (7^1A) state borrows its intensity from Ex state (2^1A) through configuration interaction. The H_L (3^1A) and H_M (3^1A) states are H-1 $\rightarrow$ L excitations (π–π^*).

In the energy region higher than the 2.5 eV, four excited states UQ(2^1A), P(8^1A), P(9^1A), and MQ(2^1A) with small intensity are calculated. P(8^1A) and P(9^1A) states, are calculated at 2.96 and 3.37 eV. They are intramolecular CT state in P as shown in Table 3. The UQ(2^1A) state calculated at 2.86 eV is H $\rightarrow$ L (π–π^*) excitation. The MQ(2^1A) state calculated at 3.44 eV is n–π^* excitation in which H $\rightarrow$ L (π–π^*) excitation strongly mixes.

6. Protein effect to the excited states

In the present calculation, protein effect is introduced by a point charge model. In Table 4, theoretical excitation energy, oscillator strength in the gas phase are compared with those by the point charge model. Almost all of the energy shift shown in Table 4 are minus values; red-shifts. The calculated energy shifts are at most -0.2 eV except for UQ, since the orbital energy gaps are not so much affected by the protein potential due to even shifts of the orbital energies.

As for UQ, the shift of the excitation energy is -0.5 eV, since the energy shift of HOMO is especially larger than that of LUMO. The energy shifts of the HOMO and LUMO are +1.73 and +0.79 eV, respectively. The reason of the larger shift of the HOMO is that the orbital has large amplitude in the negative-potential region generated by GLU L 212. Unfortunately the excitation energy shift of UQ can not be compared with experiment, since the absorption band of UQ is hidden by the strong and broad absorption due to protein or B bands of bacteriochlorophylls.

The excitation energy shifts of B's are relatively larger than that of the other chromophores. In the previous article, the absorption spectra of the RC and bacteriochlorophyll-*b* in ether were compared [32] and the red-shifts of Q_y and Q_x bands were observed. The present calculation reproduced the red-shifts. The energy shifts are -0.07 eV for the Q_y bands of B_L and B_M and -0.15 and -0.18 eV for the Q_X bands of B_L and B_M, respectively, which are comparable with the experimental values, -0.11 eV for the Q_y bands of B's, -0.11 eV for the Q_X bands of B_M, and -0.08 eV for the Q_x bands of B_L [5,28]. The reason of the red-shifts are explained by the orbital energy changes as in UQ. The Q_y and Q_X bands of B's are HOMO $\rightarrow$ LUMO and HOMO-1 $\rightarrow$ LUMO excitations, respectively. The orbital energy of the B_L and B_M are destabilized by negative electrostatic potential due to ASP M 182 and ASP L 155, respectively. However, the energy shifts of the LUMO's for B_L and B_M are relatively smaller than those of the HOMO's and HOMO-1's by about 0.2 eV, since the LUMO's avoid from the negative potential region. These difference causes the smaller energy gaps in protein than in gas phase.

The present point charge model does not take into account of the polarization effect of protein. This model might be adequate for Ex

states, since their dipole moments are enough small to neglect the effect on their energies. However, as shown in Table 3, CT state has 2 ~ 3 times larger dipole moment than those of Ex states in P.

The polarization effect is easily taken into consideration as an interaction of dipole moment of the state and the reaction field by using a continuum model, although this model has arbitrariness in the choice of the cavity. The polarization energy of electrons in protein molecules is written as [33,34],

$$\Delta E = -\frac{\eta^2 - 1}{a^3(2\eta^2 + 1)}\langle\mu\rangle\cdot\langle\mu\rangle \quad , \qquad (6\text{-}1)$$

where η is the solvent refractive index, μ is dipole moment of the state, and a is the effective radius of the spherical cavity. We used a value of 1.4266 for η (bulk property of cyclohexane) and 6.5 Å for a [9]. The estimated polarization energy for the states, ΔE(pol.), and the corrected excitation energy, EE(Pol.), are shown in Table 3. The polarization effect is large at CT states (about -0.1 ~ -0.2 eV) and the excitation energy of the CT states are red-shifted by -0.1 ~ -0.2 eV. Figure 5 also shows the stabilization of the CT states. The P (7^1A) state assigned to the band X shifted to the red-side by 0.22 eV and the error in excitation energy decreases to be 0.12 eV. The results indicate the importance of the polarization effect of surrounding medium in the CT state. In contrast, the polarization has no effect to the energy of the Ex states due to small dipole moments of the states.

The photosynthetic RC is included in a transmembrane protein [1,2] and should be feeling the membrane potential. In the present calculating model, the electric field due to the membrane potential is not considered. The polarization of electrons in chromophores is also one of the concern of protein effect. The chromophore's polarization energy is classically represented as

$$\Delta E = -\frac{1}{2}\sum_{i}^{atom} \alpha_i E_i^2 \quad , \qquad (6\text{-}2)$$

where α is atomic polarizability and E_i is a electric field on atom i. The electric field is roughly estimated to be 8.17×10^{-5} a.u., for which values of 40 Å (roughly estimated from X-ray structure of the RC [2]) and 0.168 V (potential in mitochondria [1]) are used for the membrane thickness and potential, respectively. Judging from Eq.6-2 and the estimated values of atomic polarizability [35], the electric field by the membrane is enough small not to affect the energy of the states.

7. Conclusion

The SAC/SAC-CI method is successfully applied to the excited states of the photosynthetic reaction center. The theoretical spectrum reproduced the experimental one in the excitation energy, the oscillator strength, and LD data. The averaged error of the excitation energy is 0.21 eV. The present results supports the experimented order of the Q-band peak positions between the L- and M-sides. for the B's and H's . A reliable assignments for the absorption spectrum are given, which would be a help of the photochemical study in the RC. The order of the excited states for 1.4~1.6 eV region is calculated to be

$P(3^1A) < B_M(2^1A) < B_L(2^1A) <$ c-552$(2^1A) < H_L(2^1A) < H_M(2^1A)$.

Dimerization effects on the excited states are studied. A red-shift of the first excited state by the dimerization is reproduced. The intramolecular CT states of P have large CT characters and a half of an electron is transferred to the other monomer in these states, which should cause large geometric relaxations and might have other electron transfer reaction in the RC.

Protein effect is taken into account by a point charge model. The protein effect on the excitation energy is calculated to be red-shift in

almost cases. Polarization effect of protein is estimated by a continuum model. The energy of the intramolecular CT states of P is stabilized by 0.2 eV. However, a precise examination for the protein effects should be considered by a more accurate treatment for protein molecule, which will be studied in the nest stage.

Appendix

We show brief explanation about the reason that configuration interactions (CI's) characterize the exciton (Ex) or the charge transfer (CT) natures of the excited states in P and the transition moment enhancement occurs in the first excited state of P. Since the electronic structure of P has pseudo-C_2 symmetry, we assume here an idealized C_2-fixed P; (1) HOMO-1(H-1), φ^D_{H-1}, and HOMO(H), φ^D_H, of P are strictly composed of in- and anti-phase mixing of H's of the monomers, φ^{M1}_H, and φ^{M2}_H, and LUMO(L), φ^D_L, and LUMO+1(L+1), φ^D_{L+1}, of P are composed of in- and anti-phase mixing of L's of the monomers, φ^{M1}_L and φ^{M2}_L, (2) due to C_2 symmetry, CI's between H→L and H-1→L+1 excitations (B symmetry) and between H-1→L and H→L+1 excitations (A symmetry) are symmetrically allowed, and (3) z-direction are set to C_2 axis and y-direction are set to be parallel to molecular plane of the monomers. Then, the molecular orbitals for H-1, H, L, and L+1 of P are written as

$$\varphi^D_{L+1} = N_{L+1}(\varphi^{M1}_L - \varphi^{M2}_L) \qquad \text{(A-1)}$$

$$\varphi^D_L = N_L(\varphi^{M1}_L + \varphi^{M2}_L) \qquad \text{(A-2)}$$

$$\varphi^D_H = N_H(\varphi^{M1}_H - \varphi^{M2}_H) \qquad \text{(A-3)}$$

$$\varphi^D_{H-1} = N_{H-1}(\varphi^{M1}_H + \varphi^{M2}_H), \qquad \text{(A-4)}$$

where N_x (x=H-1, H, ...) are normalization factors. Provided the monomer orbitals are orthonormal, N_x is $1/\sqrt{2}$ for all MOs. From eq. A-1 to 4, H→L and H-1→L+1 excited configurations belonging to B symmetry are written down to the monomer contributions.

$$\begin{aligned}\left\|\varphi_H^D(1)\varphi_L^D(2)\right\| &= \left\|N_H\{\varphi_H^{M1}(1)-\varphi_H^{M2}(1)\}N_L\{\varphi_L^{M1}(2)+\varphi_L^{M2}(2)\}\right\| \\ &= \left\|N_H N_L\varphi_H^{M1}(1)\varphi_L^{M1}(2)\right\|+\left\|N_H N_L\varphi_H^{M1}(1)\varphi_L^{M2}(2)\right\| \\ &\quad -\left\|N_H N_L\varphi_H^{M2}(1)\varphi_L^{M1}(2)\right\|-\left\|N_H N_L\varphi_H^{M2}(1)\varphi_L^{M2}(2)\right\|\end{aligned} \quad \text{(A-5)}$$

and

$$\begin{aligned}\left\|\varphi_{H-1}^D(1)\varphi_{L+1}^D(2)\right\| &= \left\|N_H\{\varphi_H^{M1}(1)+\varphi_H^{M2}(1)\}N_L\{\varphi_L^{M1}(2)-\varphi_L^{M2}(2)\}\right\| \\ &= \left\|N_H N_L\varphi_H^{M1}(1)\varphi_L^{M1}(2)\right\|-\left\|N_H N_L\varphi_H^{M1}(1)\varphi_L^{M2}(2)\right\| \\ &\quad +\left\|N_H N_L\varphi_H^{M2}(1)\varphi_L^{M1}(2)\right\|-\left\|N_H N_L\varphi_H^{M2}(1)\varphi_L^{M2}(2)\right\|\end{aligned}$$

.(A-6)

From eq. A-5 and 6, in-phase CI of the two excitations gives exciton (Ex) coupling of the monomers, due to canceling out the CT components.

$$\begin{aligned}&\left\|\varphi_H^D(1)\varphi_L^D(2)\right\|+\left\|\varphi_{H-1}^D(1)\varphi_{L+1}^D(2)\right\| \\ &= 2\left\|N_H N_L\varphi_H^{M1}(1)\varphi_L^{M1}(2)\right\|-2\left\|N_H N_L\varphi_H^{M2}(1)\varphi_L^{M2}(2)\right\|\end{aligned} \quad \text{(A-7)}$$

In the case the monomer MOs are orthonormal, eq. A-7 is simplified to

$$\begin{aligned}\Phi_{Ex}^{B-sym} &= \left\|\varphi_H^D(1)\varphi_L^D(2)\right\|+\left\|\varphi_{H-1}^D(1)\varphi_{L+1}^D(2)\right\| \\ &= \left\|\varphi_H^{M1}(1)\varphi_L^{M1}(2)\right\|-\left\|\varphi_H^{M2}(1)\varphi_L^{M2}(2)\right\|\end{aligned} \quad \text{(A-8)}$$

In the other hand, anti-phase CI gives charge transfer (CT) coupling, due to cancellation of Ex components.

$$\begin{aligned}\Phi_{CT}^{B-sym} &= \left\|\varphi_H^D(1)\varphi_L^D(2)\right\|-\left\|\varphi_{H-1}^D(1)\varphi_{L+1}^D(2)\right\| \\ &= \left\|\varphi_H^{M1}(1)\varphi_L^{M2}(2)\right\|-\left\|\varphi_H^{M2}(1)\varphi_L^{M1}(2)\right\|\end{aligned} \quad \text{(A-9)}$$

The CI between H→L+1 and H-1→L belonging to A symmetry gives the similar result; in- and anti-phase mixings give Ex and CT states, respectively.

Next we explain the enhancement of the transition dipole moment of the P(2^1A) state with this model. The P(2^1A) state is characterized as an Ex state in B symmetry. The transition dipole moment of the state is given as

$$\left\langle\Phi_g\left|R\right|\Phi_{Ex}^{B-sym}\right\rangle = \left\langle\varphi_H^{M1}\left|R\right|\varphi_L^{M1}\right\rangle-\left\langle\varphi_H^{M2}\left|R\right|\varphi_L^{M2}\right\rangle, \quad \text{(A-10)}$$

where R is dipole operator. The monomer H→L excitation has large transition dipole in y direction. From eq. A-10, since the matrix elements, $\langle \varphi_H^{M1} | y | \varphi_L^{M1} \rangle$ and $\langle \varphi_H^{M2} | y | \varphi_L^{M2} \rangle$, have different signs due to C_2 symmetry, the transition dipole moment of the Ex state in B symmetry, P(2^1A) state, is enhanced.

References

[1] D. Voet and J. G. Voet, Biochemistry second edition, chapter 22 (John Wiley & Sons, Inc., New York, 1995)

[2] J. Deisenhofer, O. Epp, K. Miki, R. Huber, and H. Michel, J. Mol. Bio. 180 (1984) 395.

[3] J. K. H. Hörber, W. Göbel, A. Ogrodnik, M. E. Michel-Beyerle, and F. W. Knapp, In Antennas and Reaction Centers of Photosynthetic Bacteria, M. E. Michel-Beyerle ed. Springer-Verlag, Berlin, 1985, pp.292.

[4] J. K. H. Hörber, W. Göbel, A. Ogrodnik, M. E. Michel-Beyerle, and R. J. Cogdell, FEBS Lett. 198 (1986) 268.

[5] J. Breton, Biochim. Biophys. Acta 810 (1985) 235.

[6] I. H. van Stokkum, L. M. P. Beekman, M. R. Jones, M. E. van Brederode, and R. van Grondelle, Biochemistry 36 (1997) 11360

[7] M. E. van Brederode, M. R. Jones, F. van Mourik, I. H. van Stokkum, and R. van Grondelle, Biochemistry 36 (1997) 6855

[8] W. W. Parson and A. Warshel, J. Am. Chem. Soc. 109 (1987) 6152.

[9] M. A. Thompson and M. C. Zerner, J. Am. Chem. Soc. 113 (1992) 8210.

[10] O. J. Scherer, C. Scharnagl, and S. F. Fischer, Chem. Phys. 197 (1995) 333.

[11] H. Nakatsuji and K. Hirao, J. Chem. Phys. 68 (1978) 2035.

[12] H. Nakatsuji, Chem. Phys. Letters 59 (1978) 362; 67 (1979) 329, 334.

[13] H. Nakatsuji, Acta Chim. Hung. 129 (1992) 719.

[14] H. Nakatsuji, ed. J. Leszczynski, Computational Chemistry, Vol. 2., (World Scientific, Singapore, 1996).

[15] H. Nakatsuji, J. Hasegawa, and M. Hada, J. Chem. Phys. 104 (1996) 2321.

[16] Y. Tokita, J. Hasegawa, and H. Nakatsuji, submitted to J. Phys. Chem.

[17] J. Hasegawa, M. Hada, M. Nonoguchi, and H. Nakatsuji, Chem. Phys. Letters 250 (1996) 437.

[18] J. Hasegawa, Y. Ozeki, K. Ohkawa, M. Hada, and H. Nakatsuji, J. Phys. Chem. B in press.

[19] E. E. Abola, F. C. Bernstein, S. H. Bryant, T. F. Koetzle, and J. Weng, Protein Data Bank, in Crystallographic Databases-Information Content, Software Systems, Scientific Applications, F. H. Allen, G. Bergerhoff, and R. Sievers, eds., Data Commission of the International Union of Crystallography, Bonn/Cambridge/Chester (1987) pp. 107-132.; F. C. Bernstein, T. F. Koetzle, G. J. B. Williams, E. F. Meyer, Jr., M. D. Brice, J. R. Rodgers, O. Kennard, T. Shimanouchi, and M. Tasumi, The Protein Data Bank: a Computer-based Archival File for Macromolecular Structures, J. Mol. Biol. 112 (1977) 535.

[20] S. Huzinaga, J. Andzelm, M. Klobukowski, E. Radzio-Andzelm, Y. Sakai, H. Tatewaki, Gaussian Basis Set for Molecular Calculations (Elsevier, NewYork, 1984).

[21] S. Huzinaga, J. Chem. Phys. 42 (1965) 1293.

[22] W. D. Cornell, P. Cieplak, C. I. Bayly, I. R. Gould, K. M. Merz, D. R.Freguson, D. C. Spellmeyer, T. Fox, J. W. Caldwell, and P. A. Kollman, J. Am. Chem. Soc. 117 (1995) 5197.

[23] W. L. Jorgensen, J. Chandrasekhar, J. D. Madura, R. W. Impey, and M. L. Klein, J. Chem. Phys. 79 (1983) 926.

[24] H. Nakatsuji, Chem. Phys. 75 (1983) 425.

[25] M. Dupuis, A. Farazdel, MOTECC-91, (Center for Scientific and Engineering Computations, IBM Corporation, 1991).

[26] H. Nakatsuji, M. Hada, M. Ehara, J. Hasegawa, T. Nakajima, H. Nakai, O. Kitao, K. Toyota, SAC/SAC-CI Program System (SAC-CI96)

for Calculating Ground, Excited, Ionized, and Electron Attached States and Singlet to Septet Spin Multiplicities, to be submitted.

[27] H. Nakatsuji, Program System for SAC and SAC-CI Calculations, Program Library No. 146(Y4/SAC), (Data Proccessing Center of Kyoto University, 1985), Program Library SAC85, No. 1396, (Computer Center of the Institute for Molecular Science, Okazaki, 1981).

[28] A. Scherz and W. W. Parson, Biochim. Biophys. Acta 766 (1984) 653.

[29] K. Toyota, J. Hasegawa, and H. Nakatsuji, Chem. Phys. Letters 250 (1996) 437.

[30] D. M. Tiede, Y. Choquet, and J. Breton, Biophys. J. 47 (1985) 443.

[31] K. Ohkawa, J. Hasegawa, and H. Nakatsuji, to be submitted.

[32] W. W. Parson, A. Scherz, and A. Warshel, in: Antennas and Reaction Center of Photosynthetic Bacteria, ed. M. E. Michel-Beyerle (Springer-Verlag, Berlin Heidelberg, 1985) p. 122.

[33] M. K. Karelson and M. C. Zerner, J. Phys. Chem. 96 (1992) 6949.

[34] L. Onsanger, J. Am. Chem. Soc. 58 (1936) 1486.

[35] H. Kashiwagi, F. Hirota, U. Nagashima, and T. Takada, Int. J. Quantum Chem. 30 (1986) 311.

Table I
Dimensions of the SAC/SAC-CI calculations[a].

Chromophore	P	B_M	B_L	H_M	H_L	MQ	UQ
Ground state[b]							
Before	196049700	7149870	7661654	6228684	6228684	1023165	1677195
After	37549	7570	7582	7298	7983	5021	4347
Excited state							
Before	196049700	7149870	7661654	6228684	6228684	1023165	1677195
After	226726	37140	45188	40968	43165	28630	32948
Ionized state							
Before	1782090	—	—	—	—	—	—
After	9902	—	—	—	—	—	—
Electron attached state							
Before	—	340290	356174	296436	296436	75896	111691
After	—	25330	25627	24300	24096	15599	16938

[a] Calculations with protein model

[b] Correlation energies for the ground states of P, B_M, B_L, H_M, H_L, MQ, and UQ are -0.15752, -0.12277, -0.11546, -0.13499, -0.15073, -0.13538, and -0.88780 a.u., respectively.

Table 2
Excited states of BChl *b* monomer calculated by the SAC/SAC-CI method

State	SAC/SAC-CI			Exptl.[a]	
	Main configuration[b] (C≥0.2)	Excitation energy (eV)	Oscillator strength[c]	Excitation energy[c] (eV)	
2^1A	-0.91(H→L)+0.21(H-1→L+1)	1.52	0.395 y	1.60	y
3^1A	-0.88(H-1→L)-0.32(H→L+1)	2.34	0.179 x	2.15	x
4^1A	-0.89(H-2→L)-0.15(H-3→L)	3.53	0.0129 x		

[a] Ref. [28]
[b] H and L denote HOMO and LUMO, respectively.
[c] "x" and "y" are directions of transition moment which are parallel and perpendicular to the axis along the two reduced pyrrole rings.

Table 3
Character for the excited states of special pair (P) calculated by the SAC/SAC-CI method (in protein model).

State	Character[a]	Net charge		Dipole moment (Debye)	ΔE (Pol.)[c] (eV)	ΔEE (Pol.)[d] (eV)	EE (Pol.)[e] (eV)	EE(Exp.) (eV)
		P_L[b]	P_M[b]					
X^1A	—	-0.075	0.075	5.45	-0.01	—	—	
2^1A	Ex	-0.179	0.179	3.60	-0.01	+0.01	1.41	1.25 (I)
3^1A	Ex	-0.019	0.019	7.55	-0.03	-0.01	1.61	1.46 (II)
4^1A	Ex	-0.197	0.197	5.75	-0.02	0.00	2.10	1.88 (VII)
5^1A	CT	-0.674	0.674	18.00	-0.07	-0.05	2.31	
6^1A	Ex	0.043	-0.043	8.48	-0.04	-0.02	2.46	2.00 (VIII)
7^1A	CT	0.506	-0.506	22.25	-0.24	-0.22	2.35	2.23 (XI)
8^1A	CT	-0.675	0.675	16.65	-0.12	-0.10	2.86	
9^1A	CT	0.539	-0.539	20.00	-0.20	-0.18	3.19	

[a] "Ex" and "CT" denote exciton and charge transfer excited states, respectively.
[b] "P_L" and "P_M" denote bacteriochlorophyll monomer constructing P, respectively.
[c] Change of energy due to polarization effect of protein by a continuum model.
[d] Change of excitation energy due to polarization effect of protein by a continuum model.
[e] Excitation energy including polarization effect of protein by a continuum model.

Table 4
Singlet excited states of chromophores in photosynthetic reaction center of *Rhodopseudomonas viridis*.

Chromophores[a]	SAC-CI (gas phase)			SAC-CI (in protein)						Exptl.[e]	
	State	Excitation Energy (eV)	Oscillator strength	State	Main configuration[b] (|CI|≥0.3)	Excitation energy (eV)	Energy shift[c] (eV)	Oscillator strength	Linear dichroism (deg)[d]	Excitation Energy[f] (eV)	Linear dichroism (deg)[d]
P	2^1A	1.42	0.673	2^1A	0.88(H→L)	1.40	-0.01	0.607	85.1	1.25 (I)	90
P	3^1A	1.63	0.067	3^1A	-0.85(H-1→L)	1.62	-0.01	0.090	36.9	1.46 (II)	30
B_M	2^1A	1.42	0.335	2^1A	-0.92(H→L)	1.35	-0.07	0.363	64.3	1.49 (III)	70
B_L	2^1A	1.52	0.372	2^1A	0.92(H→L)	1.45	-0.07	0.406	67.2	1.49 (III)	70
H_L	2^1A	1.65	0.317	2^1A	-0.87(H→L)-0.34(H-1→L+1)	1.59	-0.06	0.323	33.7	1.54 (IV)	40
H_M	2^1A	1.67	0.284	2^1A	-0.87(H-1→L)	1.75	+0.08	0.283	28.6	1.57 (V)	40
P	4^1A	2.18	0.100	4^1A	-0.89(H-2→L)	2.10	-0.08	0.088	61.0	1.88 (VII)	
P	6^1A	2.61	0.181	6^1A	0.70(H-3→L)-0.37(H-2→L+1)	2.48	-0.13	0.144	25.3	2.00 (VIII)	30
B_M	3^1A	2.32	0.125	3^1A	0.88(H-1→L)	2.17	-0.15	0.149	79.8	2.04 (IX)	70
B_L	3^1A	2.41	0.140	3^1A	-0.87(H-1→L)-0.30(H-1→L+1)	2.23	-0.18	0.148	77.1	2.07 (X)	70
P	5^1A	2.22	0.070	5^1A	-0.88(H→L+1)	2.37	+0.15	0.038	87.4		
P	7^1A	2.52	0.083	7^1A	-0.83(H-1→L+1)	2.57	+0.05	0.120	71.5	2.23 (XI)	
H_L	3^1A	2.67	0.103	3^1A	-0.84(H-1→L)-0.44(H-1→L+1)	2.66	-0.01	0.091	61.6	2.28 (XII)	70
H_M	3^1A	2.67	0.090	3^1A	0.82(H-1→L)+0.47(H-1→L+1)	2.67	0.00	0.113	53.6	2.32 (XIII)	70
UQ	4^1A	3.85	0.018	2^1A	0.92(H→L)	2.86	-1.01	0.001	76.8		
P	8^1A	3.15	0.006	8^1A	0.80(H-2→L+1)+0.38(H-3→L)	2.96	-0.19	0.013	35.6		
P	9^1A	3.34	0.009	9^1A	0.78(H-3→L+1)+0.37(H-3→L)	3.37	+0.03	0.018	84.7		
MQ	2^1A	3.52	0.000	2^1A	0.74(H-4→L)+0.45(H→L)	3.44	-0.08	0.002	32.0		

[a] P, B, and H denote special-pair, bacteriochlorophyll, and bacteriopheophytin, respectively. L and M denote chromophore in L and M branch, respectively.
[b] H and L denotes HOMO and LUMO, respectively.
[c] Energy shift between excitation energies in protein and in gas phase. Plus and minus signs denote blue and red shifts, respectively.
[d] Angle of the transition moment vector with the pseudo-C_2 axis of the reaction center.
[e] Reference 5
[f] Number in the parenthesis is labelling of the absorption in Figure 3.

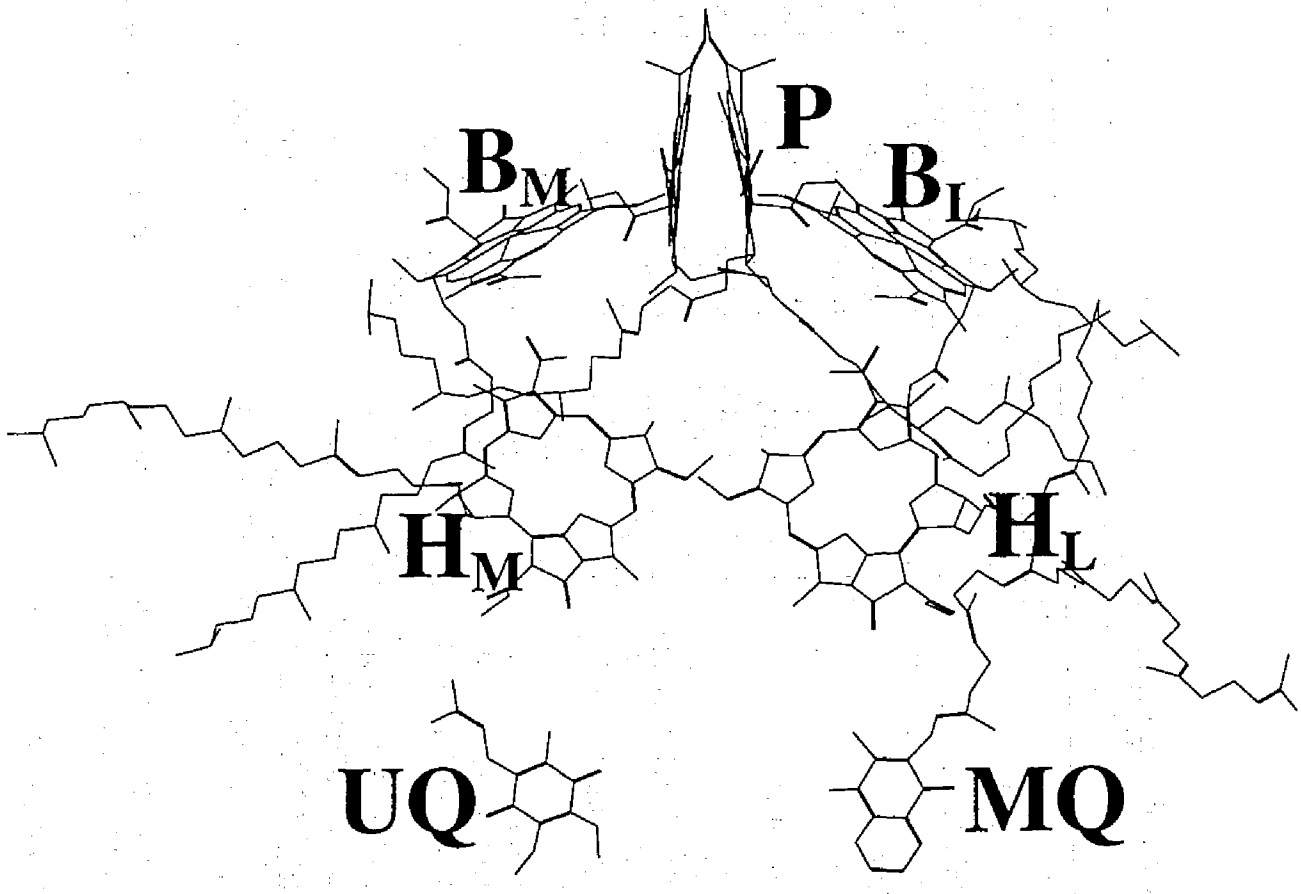

Figure 1. Structure of the chromophores in the photosynthetic reaction center of *Rps. viridis*. The nuclear coordinates are taken from ref. 2.

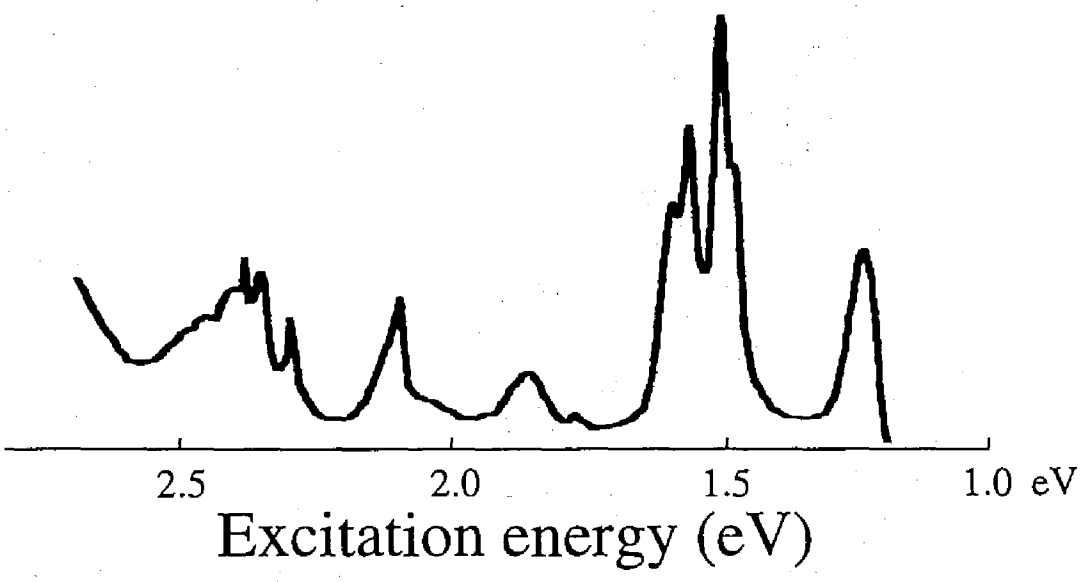

Fig. 2 Absorption spectrum of *Rhodopseudomonas viridis* reaction center[5]

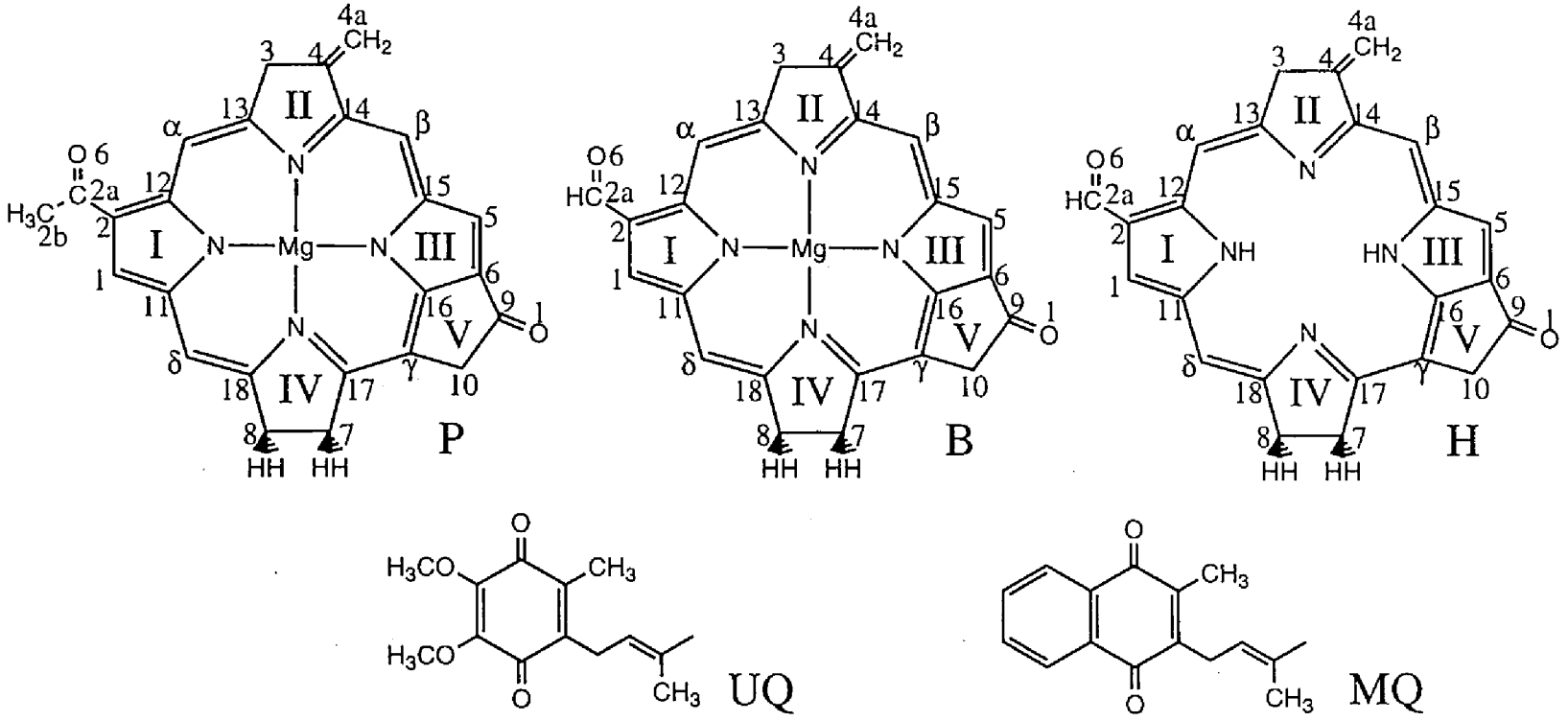

Figure 3. Calculational models for P, B, H, UQ and MQ. For P, only monomer is shown. Some substituents in the X-ray structures are replaced by protons in the present calculations (see text). Labelling of the atoms for P, B, and H is also shown.

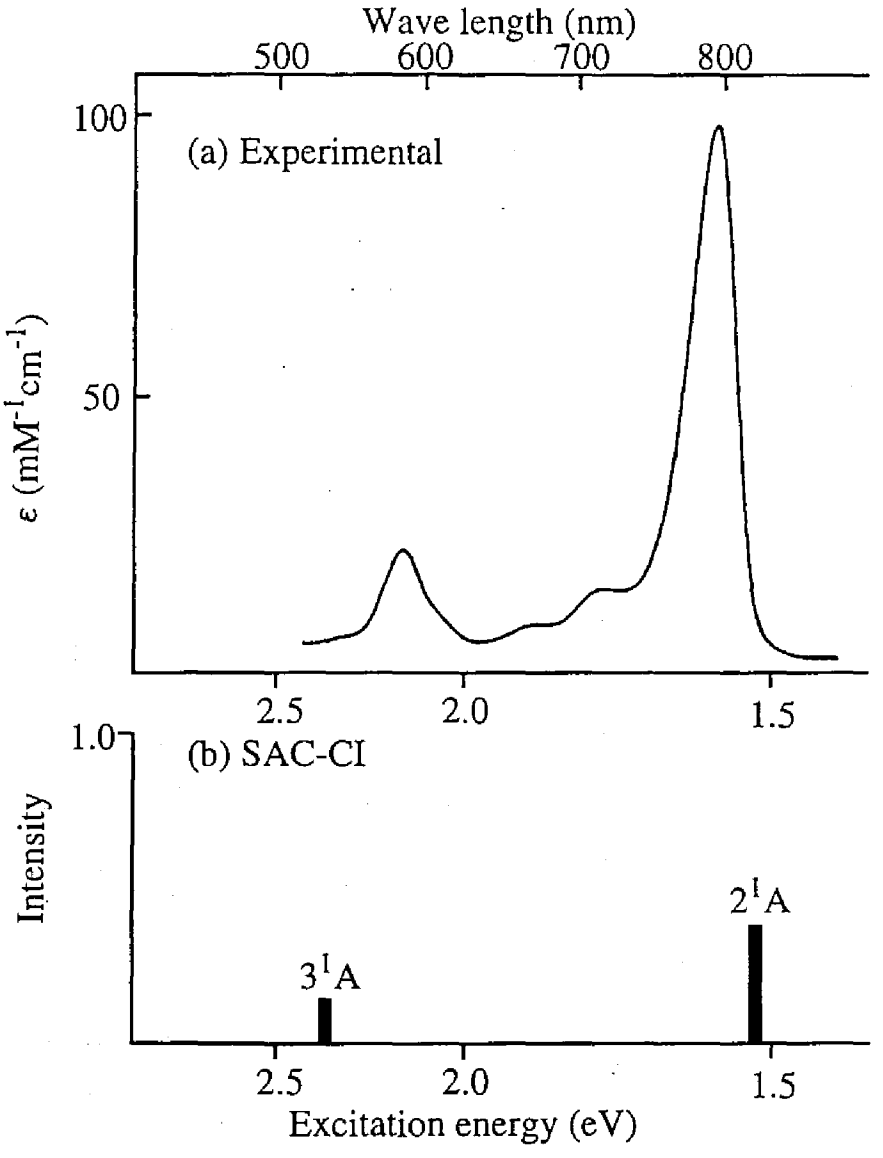

Fig. 4. Electronic spectra for BChl *b* monomer.
(a) Absorption spectrum for BChl *b* monomer [28].
(b) Theoretical spectrum calculated by the SAC/SAC-CI method.

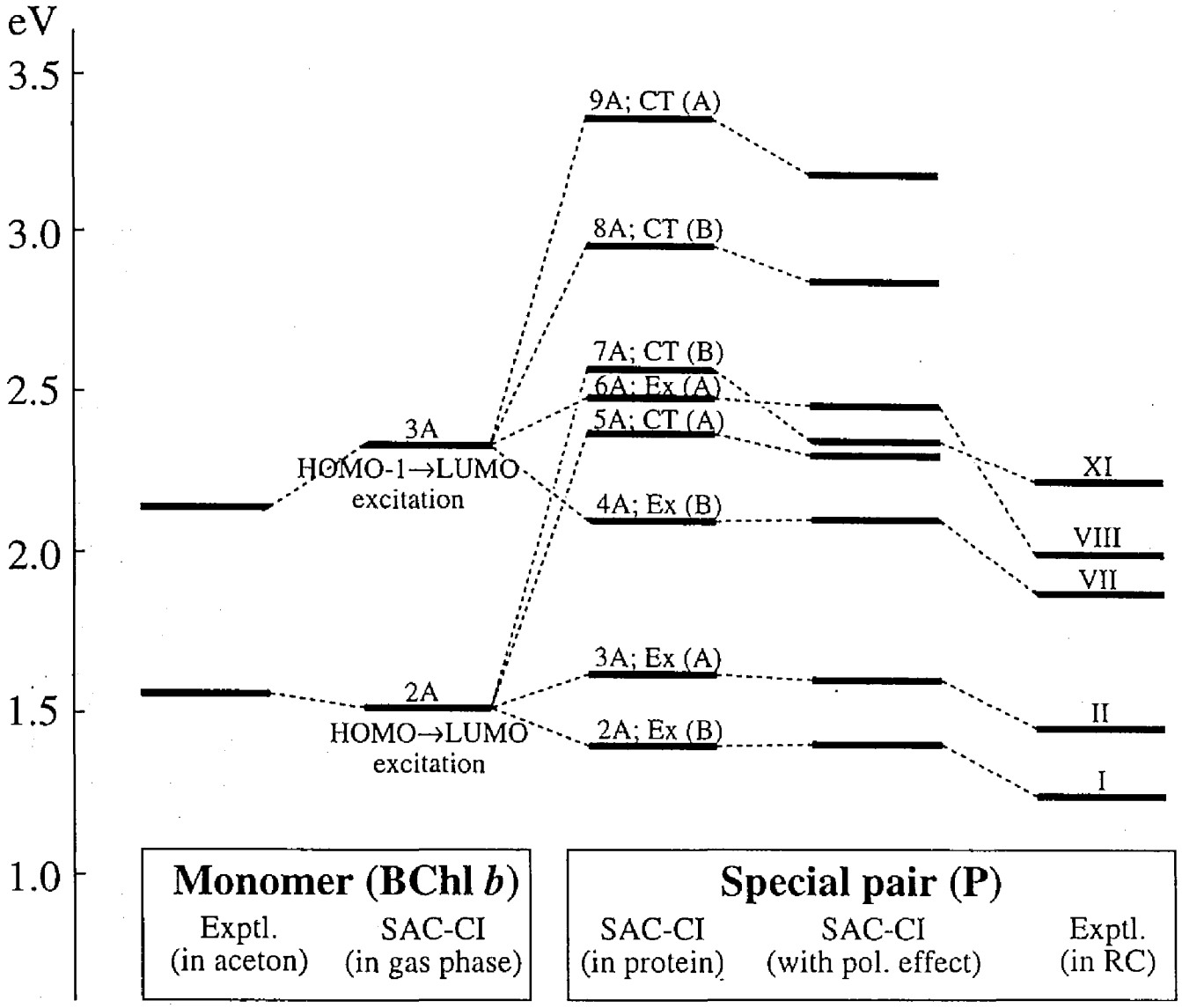

Fig. 5 Energy levels of the excited states of BChl *b* and special pair (P; BChl *b* dimer) calculated by the SAC-CI method, which are compared with those by experiments [5,28]. "Ex" and "CT" in the central column denote exciton and charge transfer characters of the excited states of P. "A" and "B" in the parentheses in the central column denote irreducible representations to which the excited states of P approximately belong. Polarization effects on the excited states of P are also shown.

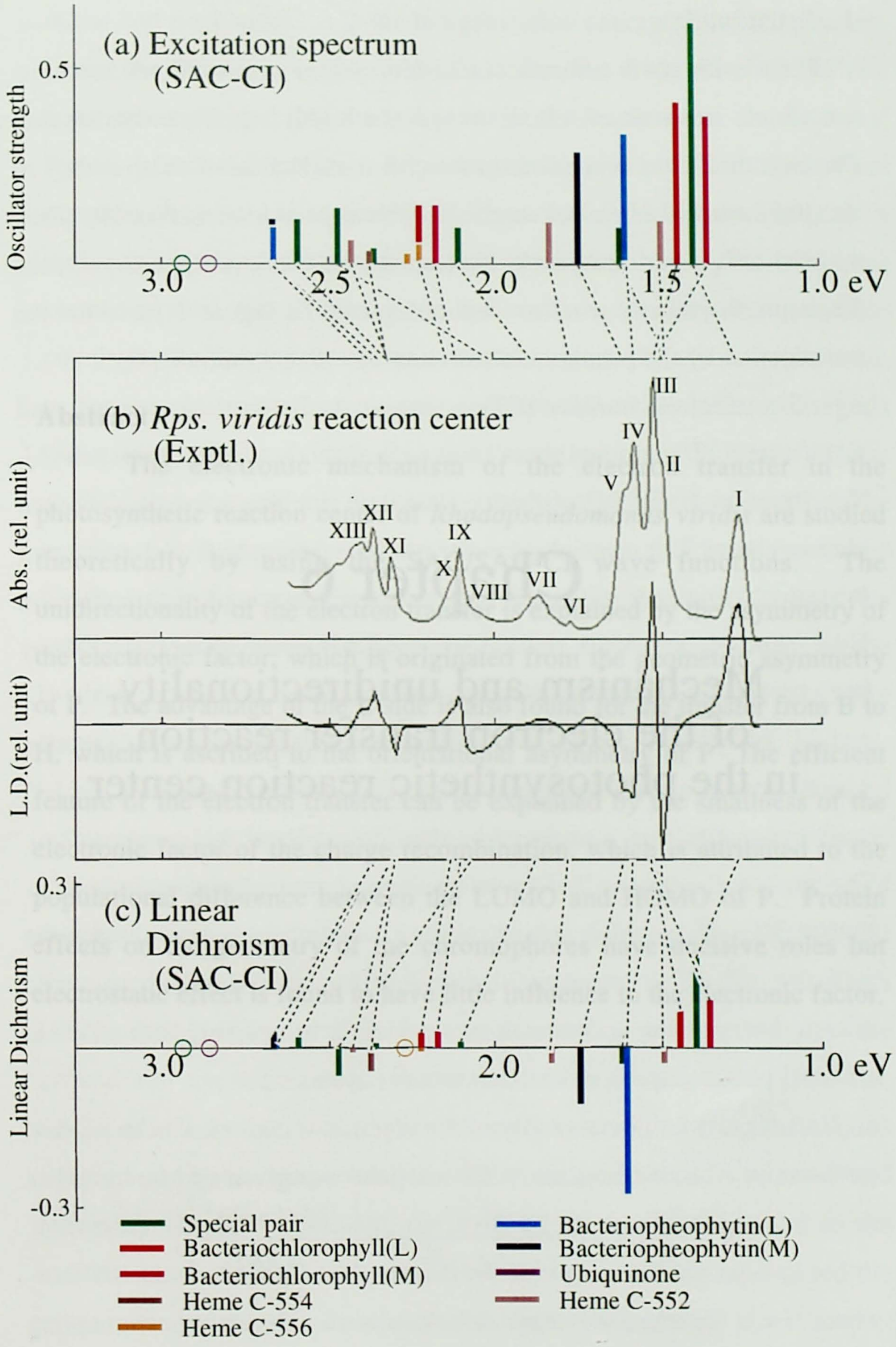

Fig. 6 Absorption and linear dichroism spectra of the RC. (a) Theoretical excitaion spectrum calculated by the SAC-CI method. (b)Experimental absorption and linear dichroism spectra [5]. (c) Theoretical linear dichroism spectrum calculated by the SAC-CI method.

Chapter 6

Mechanism and unidirectionality of the electron transfer reaction in the photosynthetic reaction center

Abstract

The electronic mechanism of the electron transfer in the photosynthetic reaction center of *Rhodopseudomonas viridis* are studied theoretically by using the SAC/SAC-CI wave functions. The unidirectionality of the electron transfer is explained by the asymmetry of the electronic factor, which is originated from the geometric asymmetry of P. The advantage of the L-side is also found for the transfer from B to H, which is ascribed to the orientational asymmetry of P The efficient feature of the electron transfer can be explained by the smallness of the electronic factor of the charge recombination, which is attributed to the populational difference between the LUMO and HOMO of P. Protein effects on the geometry of the chromophores have decisive roles but electrostatic effect is found to have little influence to the electronic factor.

1. Introduction

Photosynthesis is a chemical reaction system which utilizes sunshine, on which survival of the lives on the earth significantly depend. Photosynthesis has a important role of a transduction of solar energy to driving forced of chemical reactions. *Rhodopseudomonas viridis* (*Rps. viridis*) are one of the purple bacteria which carry out photosynthesis. Their photosynthetic reaction center depicted in Figure 1 performs the transduction by the primary electron transfer. (See reference [1])

The electron transfer (ET) is known to be fast, long-range, and significantly efficient and there is no such elaborate artificial system [1]. The structure of the RC of *Rps. viridis* was elucidated to contain seven chromophores [2]: special pair (P; bacteriochlorophyll *b* dimer), two bacteriochlorophylls *b* (B_L and B_M), two bacteriopheophytins *b* (H_L and H_M), menaquinone (MQ), and ubiquinone (UQ) as shown in Fig. 1. They have pseudo C_2 symmetric alignment which compose two passways (L- and M- branches) for the ET and they are included in the RC protein which consists of 1200 residues. Another interesting feature of the ET, unidirectionality, was also found by the time-resolved fluorescence [3,4]. The excited electron at P is transferred asymmetrically almost along L-branch, $P \rightarrow H_L \rightarrow MQ$, in spite of the C_2 alignment. Accordingly, the study on the ET is meaningful not only for satisfying our scientific interest but also for understanding a principle to construct the efficient artificial photosynthetic or electron transfer systems.

Thus far, the unidirectionality of the electron transfer has been studied extensively. The rate constant of ET reactions was given by Marcus [5] as

$$k = \frac{2\pi}{\hbar}|H_{IF}|^2 \frac{1}{(4\pi\lambda RT)^{1/2}} \exp\left\{-\frac{(\Delta G+\lambda)^2}{4\lambda RT}\right\},$$

where H_{IF} is the transfer integral which expresses the electronic coupling between initial and final states. ΔG is the free energy difference between

initial and final states. λ is the reorganization energy of the ET reaction. Under the adequacy of the above formula, the discussions on the rate constant are divided into the energetics of the reaction and the electronic factor, the transfer integral. Regarding to the energetics, semi-empirical quantum-chemical calculations [6,7], electrostatic calculations [8,9], and a molecular dynamics simulation [10] were reported. These studies concluded that the ET along the L-branch is energetically favorable mainly due to the protein electrostatic effects [6,8-10]. In the other hand, as for the electronic factor, some calculations of the transfer integrals using semi-empirical wave functions were reported [7,8,11]. These studies also showed the electronic advantage of the L-side ET. The asymmetries in geometry and electronic population of P were mentioned for the origin of the unidirectionality. However, the clarification of the unidirectionality have not been confirmed, since the accuracy of the methods employed in these studies would be unsatisfactory for treating transitions among the electronic excited states.

At the present, ab initio electronic structure theory achieved chemical accuracy. The application of these method to large systems as biochemicaly important systems is one of the challenging frontier of quantum chemistry. In order to be an useful theory, the applicability of these method to a large system must be satisfied. The SAC[12] /SAC-CI [13] method [14] is one of the accurate electron correlation theory for the ground and excited, ionized, anionized, and high-spin states [15]. The SAC/SAC-CI method was applied to many system including the excited states of porphyrin compounds [15,16-19] and established its accuracy and reliability [14,15]. Recently, the SAC-CI method was applied to the excited states of the photosynthetic RC and successfully reproduced the experimental absorption and linear dichroism spectra [20].

In this paper, we applied the SAC/SAC-CI method to the ET reactions in the RC of *Rps. viridis*. In this study, we utilizes the SAC-CI wave functions which succeeded in the application for the excited states of the RC [20]. This study is aimed to understand the dynamics of the ET reactions in terms of the electronic factor and to clarify the origin of the asymmetric feature of the reactions. Since the ET is a transition among the electronic states, the analysis of the transfer integrals could provide us another picture of the reactions. Further, the theoretical approach to an experimentally unobserved ET's would provide an important information for the design of an effective ET system. In section 3, the calculational detail of the transfer integral is shown. The analyses on the unidirectionality and the efficiency based on the transfer integrals calculated by the SAC/SAC-CI wave functions are shown in section 4.

2. Calculation of transfer integral

In this section, we explain the calculational detail of the transfer integral from the SAC/SAC-CI wave functions of chromophores. Here, the calculation of the transfer integral of the reaction, $P^*B \rightarrow P^+B^-$, is shown as an example. First, the SAC or SAC-CI wave functions of P*, P^+, B, and B^- are prepared as

$$P^*: \quad \Psi_{EX}^{P} = R^{P}\exp(S^{P})\Phi_0^{P}, \tag{2-1}$$

$$P^+: \quad \Psi_{I}^{P} = I^{P}\exp(S^{P})\Phi_0^{P}, \tag{2-2}$$

$$B: \quad \Psi_{G}^{B} = \exp(S^{B})\Phi_0^{B}, \tag{2-3}$$

$$B^-: \quad \Psi_{EA}^{B} = E^{B}\exp(S^{B})\Phi_0^{B}, \tag{2-4}$$

where $\Phi_0^{P} = \|\phi_1^{P}\phi_2^{P}\cdots\phi_{N_P}^{P}\|$ and $\Phi_0^{B} = \|\phi_1^{B}\phi_2^{B}\cdots\phi_{N_B}^{B}\|$. R, I, and E operators are the excitators for the singlet excited, ionized, and electron attached states, respectively. S operator is the excitation operator for the ground state. For simplicity, the summations of the operators are omitted. For the SAC/SAC-CI wave functions utilized above, those which

was calculated in the previous study for the excited states of the RC [20] are used. The brief explanation for the computational detail of the SAC/SAC-CI wave functions are shown in the latter section.

The initial and final states of the reactions, P*B and P^+B^-, are defined as the product of the wave functions of the fragment states (2-1) ~ (2-4).

$$P^*B: \quad \Psi^{P^*B} \cong \Psi^P_{EX}\Psi^B_G = R^P \exp\left(S^P + S^B\right)\Phi_0^{P+B} \qquad (2\text{-}5)$$

$$P^+B^-: \quad \Psi^{P^+B^-} \cong \Psi^P_I\Psi^B_{EA} = I^P E^B \exp\left(S^P + S^B\right)\Phi_0^{P+B} \qquad (2\text{-}6)$$

Here, $\Phi_0^{P+B} = \left\|\phi_1^P\phi_2^P\cdots\phi_{N_P}^P\phi_1^B\phi_2^B\cdots\phi_{N_B}^B\right\|$.

Since the operator $I^P E^B$ is not a singlet excitation operator, the R_I^{P+B} operator is introduced for spin-symmetry adaptation.

$$P^+B^-: \quad \Psi^{P^+B^-} = R^{P+B}\exp\left(S^P + S^B\right)\Phi_0^{P+B} \qquad (2\text{-}6')$$

The detail is shown in appendix.

Finally, the transfer integral of the reactions is defined as

$$P^*B \rightarrow P^+B^-: \quad \left\langle \Psi^{P^*B} \middle| H \middle| \Psi^{P^+B^-} \right\rangle. \qquad (2\text{-}7)$$

Similarly for the other ET reaction, $P^+B^-H \rightarrow P^+BH^-$ and $P^+B^- \rightarrow PB$, the transfer integrals are defined as

$$P^+B^-H \rightarrow P^+BH^-: \quad \left\langle \Psi^{BH^-} \middle| H \middle| \Psi^{B^-H} \right\rangle \qquad (2\text{-}8)$$

$$P^+B^- \rightarrow PB: \quad \left\langle \Psi^{P^+B^-} \middle| H \middle| \Psi^{PB} \right\rangle. \qquad (2\text{-}9)$$

In the practical calculation, orthonormal LMO's are assumed, which neglect intermolecular MO overlaps, since the overlaps are calculated to be very small (at most 10^{-4} order). For the sake of simplicity, the configurations having coefficients larger than 0.1 in the SAC/SAC-CI wave functions, are considered.

3. Computational detail

In this section, the computations for the SAC/SAC-CI wave functions used above is explained briefly. For details, see reference 20. For the geometry of chromophores, a X-ray crystallographic structure of *Rps. viridis* [2] (1PRC in Brookhaven Data Bank [21]) is used. For calculational efficiency, some substituents in the chromophores are simplified as shown in Figure 2, except for the substituents which could π-conjugate with rings. The labeling of the atoms and rings are also shown. Our previous calculations reproduced at least the absorption spectrum of the low-lying excited states of the RC, under these simplifications [20]. For the basis set, C, N, and O atom, Huzinaga's (63/5)/[2s2p] sets [22] and for H atom, Huzinaga's (4)/[1s] set [23] is used. For Mg, Huzinaga's (533/5)/[5s/3p] set [24] plus two p-type polarization functions (ζ=0.045 and 0.143) and d-type polarization functions (ζ=1.01) are used [20]. Protein effect is introduced by a point charge model. The charges reported previously [24,25] for protein and waters or Hartree-Fock populations for chromophores are placed at the atom centers [2,21]. For the SAC/SAC-CI wave functions for the ground and excited states of the chromophores, those calculated for the excitation spectrum are used [20]. For the ionized and electron-attached states, additional SAC-CI calculations were performed with the same condition as those for the excited states [20]. At least 2p-electrons are correlated and perturbation selection [16,26] is carried out in order to select double excitation operators. For the ground and electron attached states, the energy threshold, 1×10^{-5} and 1×10^{-6} a.u. are used, respectively. For the ground and ionized states of P, the threshold of 3×10^{-6} and 3×10^{-6} a.u. are used, respectively. All single excitations and the selected double excitations are included in the linked term. The dimension of the SAC/SAC-CI calculations are shown in Table 1. For Hartree-Fock SCF calculation, the

HONDO version 8 program [27] and for the SAC/SAC-CI calculation, the development version [28] of SAC 85 [29] program is used.

4. Electronic mechanism of the ET reactions in the RC of *Rps. viridis*

In this section, the reaction rate of the ET in the RC of *Rps. viridis* are discussed in the respect of the electronic factor. The reactions described here are the ET from P to B and from B to H along both L- and M- branches and the charge recombination (CR) from B to P and from H to P. In Figure 3, the calculated electronic factors, $|H_{IF}|^2$, in protein and gas phase are shown for each branch. These values are proportional to the ET rate constant. Only the electronic factors which are larger than 1.00 are shown. The energy levels are estimated by using the previous study [30] (colored green) and the SAC-CI calculated excitation energies, ionization energies, and electron affinities. The values in the parenthesis are estimated electronic factor from experimental data in a previous study [31]. The theoretical transfer integrals for the ET, P $\rightarrow$ B and B $\rightarrow$ H, are 25.2×10^{-9} and 104.4×10^{-9} (with protein effect), respectively and they are similar to the estimated ones, 21×10^{-9} and 72×10^{-9} a.u., respectively. These results indicate the adequacy of the theoretical electronic factor.

The ET reaction from P to H is described as the following. First, P* is generated by a direct photoexcitation or an energy transfer from antenna protein [1]. The P* would be relaxed to the first excited state, $P(2^1A)$, by an internal conversion as described in Kasha's rule. The ET reaction from $P(2^1A)$ state to $P^+(1^2A)B^-(1^2A)$ state would occur along the L-branch, since the electronic factor of the L-side is about 15 times larger than that of the M-side as shown in Figure 3. The nature of the transfer is characterized as LUMO(P) $\rightarrow$ LUMO(B_L). The unidirectionality is

originated from the asymmetry of the electronic factor, since the calculated electronic part of branching ratio $|H_L/H_M|^2 \approx 15$ in protein ($|H_L/H_M|^2 \approx 35$ in gas phase) is enough large to explain that from experiments $k_L/k_M > 5$ [8]. Here, the above consideration is based on the sequential mechanism, since the energy of the intermediate radical pair, P^+B^-, was experimentally estimated to be lower than that of the P* state [30,32]. Even if the ET occurred faster than the internal conversion, the L-side would be also preferable to the M-side due to the largeness of the electronic factors. The successive ET from $P^+(1^2A)B^-(1^2A)$ state to $P^+(1^2A)H^-(1^2A)$ would proceed along the L-branch. The nature of the transfer is characterized as $LUMO(B_L) \rightarrow LUMO(H_L)$. The competitive reaction to the ET from B to H is the CR reaction from $P^+(1^2A)B^-(1^2A)$ state to the ground state of PBH, $LUMO(B_L) \rightarrow HOMO(P)$. According to the electronic factor, the CR is much less preferable to the ET, since the electronic factor of the CR is only about 4 percent of that of the ET. This smallness of the electronic factor of the CR is the electronic origin of the high-efficiency of the ET. After the ET to H, the excited electron would be transferred to MQ [1]. The side reaction of the ET to MQ is the CR to ground state, PBH. The electronic factor of the ET to MQ was reported to be 0.48×10^{-9} a.u. in the previous article [33]. On the other hand, the electronic factor of the CR reaction by the superexchange mechanism is evaluated to be 0.053×10^{-9} a.u. [34], which is enough small to explain the high-efficiency of the ET from H to MQ.

5. Analysis of the transfer integral

In Table 2, the electronic factors, $|H_{IF}|^2$, for the ET reactions, P*B $\rightarrow P^+B^-$, in various approximations are shown. In order to understand the accuracy of Fock approximation, the transfer integrals by Fock approximation are compared with those by total hamiltonian, within a

single-configuration approximation. Table 2 shows that the values by the Fock approximation are quite similar to those by the total hamiltonian, which indicates the adequacy of the Fock approximation in this system. In the multi-configuration case, the configuration interaction effect introduced by the SAC/SAC-CI method is examined. In Table 2, the inclusion of the configuration interaction effect by the SAC/SAC-CI method reduces the value of the transfer integrals, which makes the transfer integral close to the values estimated from experiments [31,35]. The ratios between L- and M-branch are also shown in Table 1. For P*B $\rightarrow P^{+}B^{-}$, the SAC-CI reduces the L/M rate by 3/4. Although the Fock approximation appears somehow qualitative, it has a decisive role for the transfer integral. Further, it is useful for the analysis and brief estimation of the transfer integral due to its economical advantage.

6. Electronic factor of the ET from P to B

The unidirectionality of the ET reaction from P to B is originated from the asymmetry of the electronic factor between L- and M-branches as shown in Figure 3. Comparing the electronic factor in protein and in gas phase, the unidirectionality could be explained without protein effect. Protein effect is not an origin of the asymmetry of the electronic factor. In order to understand the asymmetry origin, the element of the electronic factor in the gas phase is further analyzed. Since Fock matrix element, f_{ij}, (i≡LUMO of B and j≡LUMO of P), has a decisive role in the transfer integral H_{IF} as shown in the previous section, this element is decomposed into the atomic contributions of atoms belonging to B as,

$$f_{ij} = \sum_{X \in B} \sum_{r \in X} \sum_{s \in P} C_{ri}^{*} C_{sj} f_{rs} = \sum_{X \in B} f_X , \qquad (6\text{-}1)$$

where f_x is the contribution of atom X,C is MO coefficient and f_{rs} (r ∈ B and s ∈ P) is AO Fock matrix element. From an inspection of eq. 6-1,

conditions for f_{ij} to be large are the following. The first one is a proximity condition. In order that f_{rs} have a large value, the atomic orbitals r and s should be nearly located, since f_{rs} significantly depends on the distance between r and s. The second one is a MO coefficient condition. Even if the f_{rs} is large, contribution to f_{ij} would be reduced, when the product of the MO coefficient $C_{ri}{}^{*}C_{sj}$ is small. The third one is nodal effects which originates from nodes of the MO's. Summation over the AO's and the atoms could cancel their contribution each other, if the MO coefficients have opposite signs. This cancellation could have a large effect to the total Fock matrix element, in the case that the donor or acceptor orbitals have nodal structure as porphyrin compounds.

The result for the decomposition of f_{ij}, (i≡LUMO of B and j≡LUMO of P) is shown in Figure 4 (a). There is also asymmetry between L- and M-sides and the atomic contribution is large in the B_L. The origin of the asymmetry lies in the difference of the contributions at the rings III and II of B's as shown in Figure 4 (a). The largest contribution is derived from the 6-carbon (See Figure 2 for the atomic labeling) in the ring III of B_L and its value is 10.8×10^{-5} hartree. On the other hand, the largest contribution in B_M is -6.4×10^{-5} hartree of the β-carbon.

The asymmetry in the molecular arrangement of P was reported previously [8,11], which we also show in Figure 5. The rings III of B_L and B_M are close to the vicinity of the ring I of the P_M and P_L, respectively. The distances from the rings III of B_L and B_M to the rings I of the P_M and P_L are 6.89 and 7.41 Å (center-to-center distance), respectively and the L-side is more closer than the M-side by 0.5 Å. The rings II of B_L and B_M are close to the rings V of P_L and P_M, respectively. Especially, the 4a-carbon (See Figure 2 for the atomic labeling) of B_L locates at 4.7 Å from the γ-carbon of P_L. However in this case, the

distances between the L- and M-sides are similar: 7.13 and 7.14 Å, respectively.

In Figure 5, MO populations of the LUMO's of P and B's are shown, which are the donor and acceptor orbitals, respectively. Regarding to B's, the population is almost symmetric between L- and M-sides and some amplitude are calculated at the 5- and 6- carbons of the ring III. However, the 4- and 4a- carbons of the ring II have little population in both B's. In the case of P, the population is gathering in the vicinity of the rings I of P_L and P_M. Further, the population of P has a slight asymmetry, which is slightly localized to the P_L. The rings I and V of P_L have larger amplitudes than those of P_M.

Considering the geometric and wave functional informations described above, the asymmetry in the ring III contribution of B's is mainly attributed to the geometric asymmetry. The rings III of B's and I of P, which have some MO amplitudes, are closer in L-side than in M-side. Due to the proximity condition, the L-side has a larger electronic factor than the M-side. The proximity condition have a priority over the MO coefficient condition in this case, since the orbital amplitude on the rings I are slightly larger in P_L and in P_M. As for the ring II, The origin of the asymmetry lies in MO coefficient asymmetry. As seen in Figure 5, the LUMO of P is slightly localized in P_L and the γ-carbon of P_L, which lay close to the 4- and 4a-carbons of B_L, has some population. In this case, the distances between the ring I of B_L and V of P_L is similar to that between B_M and P_M as described above. Accordingly, the contribution of the 4a- and 4-carbon is larger in the L-side due to the MO coefficient condition.

7. Electronic factor of the ET from B to H

The calculated electronic factor for the ET from B to H is also larger in the L-side than in the M-side. As the same way as the previous subsection, the Fock matrix element f_{ij} (i≡LUMO of H and j≡LUMO of B) is decomposed into the atomic contribution of H's. The result is shown in Figure 7. The largest contribution to f_{ij} is 42.92×10^{-5} and 24.95×10^{-5} hartree from 1-carbon at the ring I in H_L and H_M, respectively. This difference is the main reason for the asymmetry in the electronic factor between L- and M-sides.

In Figure 7 (a) and (b), the MO populations of the LUMO's of B and H in the L- and M-branches, respectively, are shown. The origin of the asymmetry do not lie in the MO asymmetry, since the MO population is quite symmetric between L- and M-sides. Another important fact found in these figures is that in both the L- and M-sides, H's and B's are aligned as the most populated rings I are adjacent each other. The Fock matrix element f_{ij} could be large due to fulfilling the MO coefficient condition. This effect is apparently seen in the values of the electronic factors, which is twice as large as that for P to B in the case of the L-side. In a previous semi-empirical study [7], the electronic factor for the ET's, P $\rightarrow$ B and B $\rightarrow$ H, were calculated to be equal, which seems out of physical intuition in the respect of the MO coefficient condition.

In comparison with the geometry between the two sides, the distances between the four nitrogens center of B and H are 10.67 and 10.59 Å for the L- and M-sides, respectively and the L-side is slightly distant as shown in Figure 7. However, the orientations of the H_L and H_M are somehow different. The distance between the 1-carbons of B and H, which have the largest amplitude in their LUMO's, are 5.03 and 5.46 Å in the L- and M-sides, respectively. The L-side is more distant by 0.4 Å than the M-side. This orientation asymmetry could be derived from the specific protein environment surrounding H's. H_L has a glutamate side chain (GLU L104)

near the carbonyl group at the ring V. The GLU L104 is thought to have a hydrogen bond with the oxygen of the carbonyl group [36,37] and might be controlling the orientation of the H_L, since in the M-side, GLU L104 is replaced to valine (M131) [2,8] which has no polar group. The orientational difference affects the atomic contribution asymmetry of the 1-carbon and results in the asymmetry of the total Fock element.

The importance of the nodal condition is indicated in Figure 6. The atomic contributions between the 1- and 2-carbons in the ring I of H's have opposite signs and cancel each other. The LUMO of H's have a node between the 1- and 2-carbons, which makes their contributions different signs.

8. Electronic factor of the CR from B to P

The electronic factor of the CR from B_L to P is rather small than that of the ET as shown in Figure 3, although the both reactions transfer electron between the same chromophores. In this case, the HOMO and LUMO of P must be compared, since the ET occurs from the LUMO of P to the LUMO of B and the CR from the LUMO of B to HOMO of P. The Fock matrix element, f_{ij} (i≡LUMO of B and j≡HOMO of P), is also analyzed by the decomposition and compared with the ET reaction in Figure 4 (b). The ring III contribution is rather reduced, which affects the reduction of the electronic factor.

In Figure 8, MO population of the HOMO of P is compared with that of LUMO. Population of the HOMO of P is significantly different from that of LUMO of P. The HOMO is delocalized in the whole chromophore and the maximum is seen in the vicinity of the rings II and III of P_M, which is well separated from the ring III of B_L. The population in the vicinity of the ring I of P_M is significantly reduced. The MO coefficient condition is much less fulfilled in the CR than the ET. Accordingly, these

populational difference causes the asymmetry of the electronic factor, which would be one of the important reason of the efficient ET in the RC.

9. Protein effect to the electronic factor

Protein effects on the ET reaction are classified into three; a structural effect which controls the chromophore alignment, an electrostatic effect to the electronic structure of chromophores, and an electronic effect to the electronic factor through protein wave functions. In the RC, the structural effect has definitive roles in the ET as described before. The unidirectionality and the large electronic factor of the ET from B_L to H_L are originated from the geometrical asymmetry between L- and M-branches. The electrostatic effect of protein, which is taken into account by a point charge model, is shown to have a minor effect on the electronic factor of the ET, since, the differences of the electronic factor in gas phase and protein model are calculated to be small. The unidirectionality could be explained without introducing protein effect. However, we note that on the energetics of the ET, the protein electrostatic effect would have a contribution to the unidirectionality as reported in the previous articles [38,39]. The electronic effect of protein has also a minor effect to the ET in the RC, since the unidirectionality could be explained without borrowing the wave functions of protein. The bacteriochrophylls included in the RC are powerful donor and acceptor, since they have higher HOMO and lower LUMO levels than those of protein.

10. Conclusion

The electronic mechanism of the electron transfer in the photosynthetic reaction center of *Rhodopseudomonas viridis* are studied by using the SAC/SAC-CI wavefunctions which include the electron

correlations of the chromophores. The electronic factors of the electron transfers and charge recombinations are calculated and analyzed

The unidirectionality of the electron transfer is explained by the asymmetry of the electronic factor. The advantage of the L-side is shown for the transfers both from P to B and from B to H. The ratios of the electronic factor are 15.2 and 6.56 for P $\rightarrow$ B and B $\dashrightarrow$ H, respectively. The efficient feature of the electron transfer can be explained by the smallness of the electronic factor of the charge recombination.

The electronic factors are analyzed by the decomposition to the atomic contributions. In order to have a large electronic factor, three conditions should be required; the proximity condition, the MO coefficient condition, and the nodal effect. The asymmetry of the electronic factor of the electron transfer from P to B is ascribed to the geometric asymmetry of P (the proximity condition). The distance between the rings I of P_M and III of B_L which fulfill the MO coefficient condition are closer by 0.5 Å than that in M-side. The asymmetry in the ET from B to H is also ascribed to the geometric asymmetry (the proximity condition). In this case, the orientational asymmetry of the H's have a definitive role. The smallness of the CR electronic factor is attributed to the difference in the MO populations between the LUMO and HOMO of P (the MO coefficient condition). The considerable nodal effect is found in the transfer integrals for B to H transfers, in which the contributions from the adjacent atoms are canceled by the node in the LUMO's of H.

Protein effect on the geometry of the RC have a decisive role in the electron transfer mechanism. The difference of the molecular structures between L- and M-branches introduces asymmetric alignment to P and H's through intermolecular interactions. On the other hand, protein electrostatic effect to the electron distribution is found to be small and have little influence to the electronic factor asymmetry. Present result

explains the unidirectional character without invoking the electronic wave function of protein.

Appendix

The CT state, P^+B^-, defined as eq. 2-6 is not a pure singlet state, since the state is defined as the product of the two doublet wave functions, P^+ and B^-. In eq. 2-6, the operators, I^P and E^B, are excitator for the ionized and electron attached states including one and two electron processes.

$$I^{\mathrm{P}} = \sum_{I}^{\mathrm{P}} C_I^{\mathrm{P}}(S) I_I^{\mathrm{P}}(S) + \sum_{I}^{\mathrm{P}} \sum_{J}^{\mathrm{P}} C_{IJ}^{\mathrm{P}}(D) I_I^{\mathrm{P}}(S) R_J^{\mathrm{P}}(S)$$
$$= \sum_{I}^{\mathrm{P}} I_I^{\mathrm{P}}(S) \left\{ C_I^{\mathrm{P}}(S) + \sum_{J}^{\mathrm{P}} C_{IJ}^{\mathrm{P}}(D) R_J^{\mathrm{P}}(S) \right\} \qquad \text{(A-1)}$$

$$E^{\mathrm{B}} = \sum_{I}^{\mathrm{B}} C_I^{\mathrm{B}}(S) E_I^{\mathrm{B}}(S) + \sum_{I}^{\mathrm{B}} \sum_{J}^{\mathrm{B}} C_{IJ}^{\mathrm{B}}(D) E_I^{\mathrm{B}}(S) R_J^{\mathrm{B}}(S)$$
$$= \sum_{I}^{\mathrm{B}} E_I^{\mathrm{B}}(S) \left\{ C_I^{\mathrm{B}}(S) + \sum_{J}^{\mathrm{B}} C_{IJ}^{\mathrm{B}}(D) R_J^{\mathrm{B}}(S) \right\} \qquad \text{(A-2)}$$

Here, $I_I^{\mathrm{P}}(S)$, $E_I^{\mathrm{B}}(S)$, and $R_J^{\mathrm{P}}(S)$ are one-electron excitators for the ionized, electron attached, and singlet excited states. $C_I^{\mathrm{P}}(S)$ and $C_I^{\mathrm{B}}(S)$ denote SAC-CI coefficients for the one-electron excitators and $C_{IJ}^{\mathrm{P}}(D)$ and $C_{IJ}^{\mathrm{B}}(D)$ denotes those for the two-electron excitators. Using eq. A-1 and 2, the eq. 2-6 is rewritten as

$$\Psi^{\mathrm{P^+B^-}} = \sum_{I}^{\mathrm{P}} \sum_{K}^{\mathrm{B}} I_I^{\mathrm{P}}(S) E_K^{\mathrm{B}}(S) \left\{ C_I^{\mathrm{P}}(S) + \sum_{J}^{\mathrm{P}} C_{IJ}^{\mathrm{P}}(D) R_J^{\mathrm{P}}(S) \right\}$$
$$\times \left\{ C_K^{\mathrm{B}}(S) + \sum_{L}^{\mathrm{B}} C_{KL}^{\mathrm{B}}(D) R_L^{\mathrm{B}}(S) \right\} \exp\left(S^{\mathrm{P}} + S^{\mathrm{B}}\right) \Phi_0^{\mathrm{P+B}}. \qquad \text{(A-3)}$$

Here, the products of the excitator, $I_I^{\mathrm{P}}(S) E_K^{\mathrm{B}}(S)$, are written as

$$I_I^{\mathrm{P}}(S) E_K^{\mathrm{B}}(S) = a_{i\alpha} a_{a\alpha}^{\dagger} \qquad \text{(A-4)}$$

Since A-4 is not a singlet operator, the spin contamination occurs in A-3. For the spin-symmetry adaptation, the $R_I^{\mathrm{P+B}}(S)$ operator is introduced, in which the beta counterpart is added into A-4.

$$R_I^{\mathrm{P+B}}(S) \equiv \frac{1}{\sqrt{2}} (a_{i\alpha} a_{a\alpha}^{\dagger} + a_{i\beta} a_{a\beta}^{\dagger}) \qquad \text{(A-5)}$$

Then a pure singlet state for the P^+B^- state is obtained as,

$$\Psi^{P^+B^-} = \sum_{I}^{P+B} R_I^{P+B}(S)\left\{C_I^P(S) + \sum_{J}^{P} C_{IJ}^P(D)R_J^P(S)\right\}$$
$$\times\left\{C_I^B(S) + \sum_{J}^{B} C_{IJ}^B(D)R_J^B(S)\right\}\exp\left(S^P + S^B\right)\Phi_0^{P+B} \quad \text{(A-6)}$$

References

[1] D. Voet and J. G. Voet, Biochemistry second edition, chapter 22 (John Wiley & Sons, Inc., New York, 1995)

[2] J. Deisenhofer, O. Epp, K. Miki, R. Huber, and H. Michel, J. Mol. Bio. 180 (1984) 395.

[3] J. K. H. Hörber, W. Göbel, A. Ogrodnik, M. E. Michel-Beyerle, and F. W. Knapp, In Antennas and Reaction Centers of Photosynthetic Bacteria, M. E. Michel-Beyerle ed. Springer-Verlag, Berlin, 1985, pp.292.

[4] J. K. H. Hörber, W. Göbel, A. Ogrodnik, M. E. Michel-Beyerle, and R. J. Cogdell, FEBS Lett. 198 (1986) 268.

[5] R. A. Marcus and N. Sutin, Biochim. Biophys. Acta 811 (1985) 265

[6] M. A. Thompson and M. C. Zerner, J. Am. Chem. Soc. 113 (1992) 8210.

[7] O. J. Scherer, C. Scharnagl, and S. F. Fischer, Chem. Phys. 197 (1995) 333.

[8] M. E. Michel-Beyerle, M. Plato, J. Deisenhofer, H. Michel, M. Bixon, and J. Jortner, Biochim. Biophys. Acta 932 (1988) 52.

[9] M. R. Gunner, A. Nicholls, and B. Honig, J. Phys. Chem. 100 (1996) 4277.

[10] M. Marchi, J. N. Gehlen, D. Chandler, and M. D. Newton, J. Am. Chem. Soc. 115 (1993) 4178.

[11] M. Plato, K. Möbius, M. E. Michel-Beyerle, M. Bixon, and J. Jortner, J. Am. Chem. Soc. 110 (1988) 7279.

[12] H. Nakatsuji and K. Hirao, J. Chem. Phys. 68 (1978) 2035.

[13] H. Nakatsuji, Chem. Phys. Letters 59 (1978) 362; 67 (1979) 329, 334.

[14] H. Nakatsuji, Acta Chim. Hung. 129 (1992) 719.

[15] H. Nakatsuji, ed. J. Leszczynski, Computational Chemistry, Vol. 2., (World Scientific, Singapore, 1996).

[16] H. Nakatsuji, J. Hasegawa, and M. Hada, J. Chem. Phys. 104 (1996) 2321.

[17] Y. Tokita, J. Hasegawa, and H. Nakatsuji, submitted to J. Phys. Chem.

[18] J. Hasegawa, M. Hada, M. Nonogushi, and H. Nakatsuji, Chem. Phys. Letters, 250 (1996) 159.

[19] J. Hasegawa, Y. Ozeki, K. Ohkawa, M. Hada, and H. Nakatsuji, J. Phys. Chem. B in press.

[20] J. Hasegawa, K. Ohkawa, and H. Nakatsuji, to be submitted.

[21] E. E. Abola, F. C. Bernstein, S. H. Bryant, T. F. Koetzle, and J. Weng, Protein Data Bank, in Crystallographic Databases-Information Content, Software Systems, Scientific Applications, F. H. Allen, G. Bergerhoff, and R. Sievers, eds., Data Commission of the International Union of Crystallography, Bonn/Cambridge/Chester (1987) pp. 107-132.; F. C. Bernstein, T. F. Koetzle, G. J. B. Williams, E. F. Meyer, Jr., M. D. Brice, J. R. Rodgers, O. Kennard, T. Shimanouchi, and M. Tasumi, The Protein Data Bank: a Computer-based Archival File for Macromolecular Structures, J. Mol. Biol. 112 (1977) 535.

[22] S. Huzinaga, J. Andzelm, M. Klobukowski, E. Radzio-Andzelm, Y. Sakai, H. Tatewaki, Gaussian Basis Set for Molecular Calculations (Elsevier, NewYork, 1984).

[23] S. Huzinaga, J. Chem. Phys. 42 (1965) 1293.

[24] W. D. Cornell, P. Cieplak, C. I. Bayly, I. R. Gould, K. M. Merz, D. R.Freguson, D. C. Spellmeyer, T. Fox, J. W. Caldwell, and P. A. Kollman, J. Am. Chem. Soc. 117 (1995) 5197.

[25] W. L. Jorgensen, J. Chandrasekhar, J. D. Madura, R. W. Impey, and M. L. Klein, J. Chem. Phys. 79 (1983) 926.

[26] H. Nakatsuji, Chem. Phys. 75 (1983) 425.
[27] M. Dupuis, A. Farazdel, MOTECC-91, (Center for Scientific and Engineering Computations, IBM Corporation, 1991).
[28] H. Nakatsuji, M. Hada, M. Ehara, J. Hasegawa, T. Nakajima, H. Nakai, O. Kitao, K. Toyota, SAC/SAC-CI Program System (SAC-CI96) for Calculating Ground, Excited, Ionized, and Electron Attached States and Singlet to Septet Spin Multiplicities, to be submitted.
[29] H. Nakatsuji, Program System for SAC and SAC-CI Calculations, Program Library No. 146(Y4/SAC), (Data Proccessing Center of Kyoto University, 1985), Program Library SAC85, No. 1396, (Computer Center of the Institute for Molecular Science, Okazaki, 1981).
[30] S. Schmidt, T. Arlt, P. Hamm, H. Huber, T. Nägele, J. Wachtveitl, M. Meyer, H. Scheer, and W. Zinth, Chem. Phys. Letters 223 (1994) 116.
[31] S. Tanaka and R. A. Marcus, J. Phys. Chem. B. 101 (1997) 5031.
[32] S. Schmidt, T. Arlt, P. Hamm, H. Huber, T. Nägele, J. Wachtveitl, M. Meyer, H. Scheer, and W. Zinth, Spectrochim. Acta 51A (1995) 1565.
[33] M. R. Gunner and P. L. Dutton, J. Am. Chem. Soc. 111 (1989) 3400.
[34] The transfer integral of the CR reaction from $P^+(1^1A)H^-(1^1A)$ state (≡ state 3) to the ground state (≡ state 0) would be evaluated by the superexchange mechanism, since $P^+(1^1A)B^-(1^1A)$ state (≡ state 2) should be energetically higher than the $P^+(1^1A)H^-(1^1A)$ state. The transfer integral formula is expressed as

$$H_{30} = \frac{H_{32}H_{20}}{\Delta E_{32}},$$

where H_{mn}'s denote the transfer integral between state m and n. ΔE_{32} is the energy difference between states 3 and 2. In this case, only state 2 is considered as an virtual intermediate state and for ΔE_{32} the value previously reported [30] is used.

[35] M. Bixon, J. Jortner, and M. E. Michel-Beyerle, The Photosynthetic Bacterial Reaction Center, J. Breton and A. Verméglio eds. (Plenum Press, New York, 1992).

[36] M. Lutz and B. Robert, In Antennas and Reaction Centers of Photosynthetic Bacteria, M. E. Michel-Beyerle ed. Springer-Verlag, Berlin, 1985, pp. 138.

[37] G. Feher, R. A. Isaacson, M. Y. Okamura, and W. Lubitz, Biophys. J. 51 (1987) 337a.

[38] M. R. Gunner, A. Nicholls, and B. Honig, J. Phys. Chem. 100 (1996) 4277.

[39] W. W. Parson, Z. T. Chu, and A. Warshel, Biochim. Biophys. Acta 1017 (1990) 251.

Table 1
Dimensions of the SAC/SAC-CI calculations[a].

Chromophore	P	B_M	B_L	H_M	H_L	MQ	UQ
Ground state[b]							
Before	196049700	7149870	7661654	6228684	6228684	1023165	1677195
After	37549	7570	7582	7298	7983	5021	4347
Ionized state							
Before	1782090	—	—	—	—	—	—
After	9902	—	—	—	—	—	—
Electron attached state							
Before	—	340290	356174	296436	296436	75896	111691
After	—	25330	25627	24300	24096	15599	16938

[a] Calculations with protein model

[b] Correlation energies for the ground states of P, B_M, B_L, H_M, H_L, MQ, and UQ are -0.15752, -0.12277, -0.11546, -0.13499, -0.15073, -0.13538, and -0.88780 a.u., respectively.

Table 2
Electronic factors[a] $|H_{IF}|^2$ ($\times 10^{-9}$) in a.u. with some approximations

Approximation	P → B			B → H		
	L	M	L / M	L	M	L / M
Single-configuration approximation						
F[b]	37.36	1.83	20.42	116.96	17.96	6.51
H[c]	37.13	1.85	20.07	116.96	17.96	6.51
Multi-configuration						
SAC-CI	25.21	1.65	15.27	104.43	15.93	6.56
Estimated values from an experiment						
	21[d],14[e]			72[d],54[e]		

[a] Electronic factors calculated with a protein model
[b] Fock approximation for total hamiltonian
[c] Total hamiltonian
[d] Reference 31
[e] Reference 35

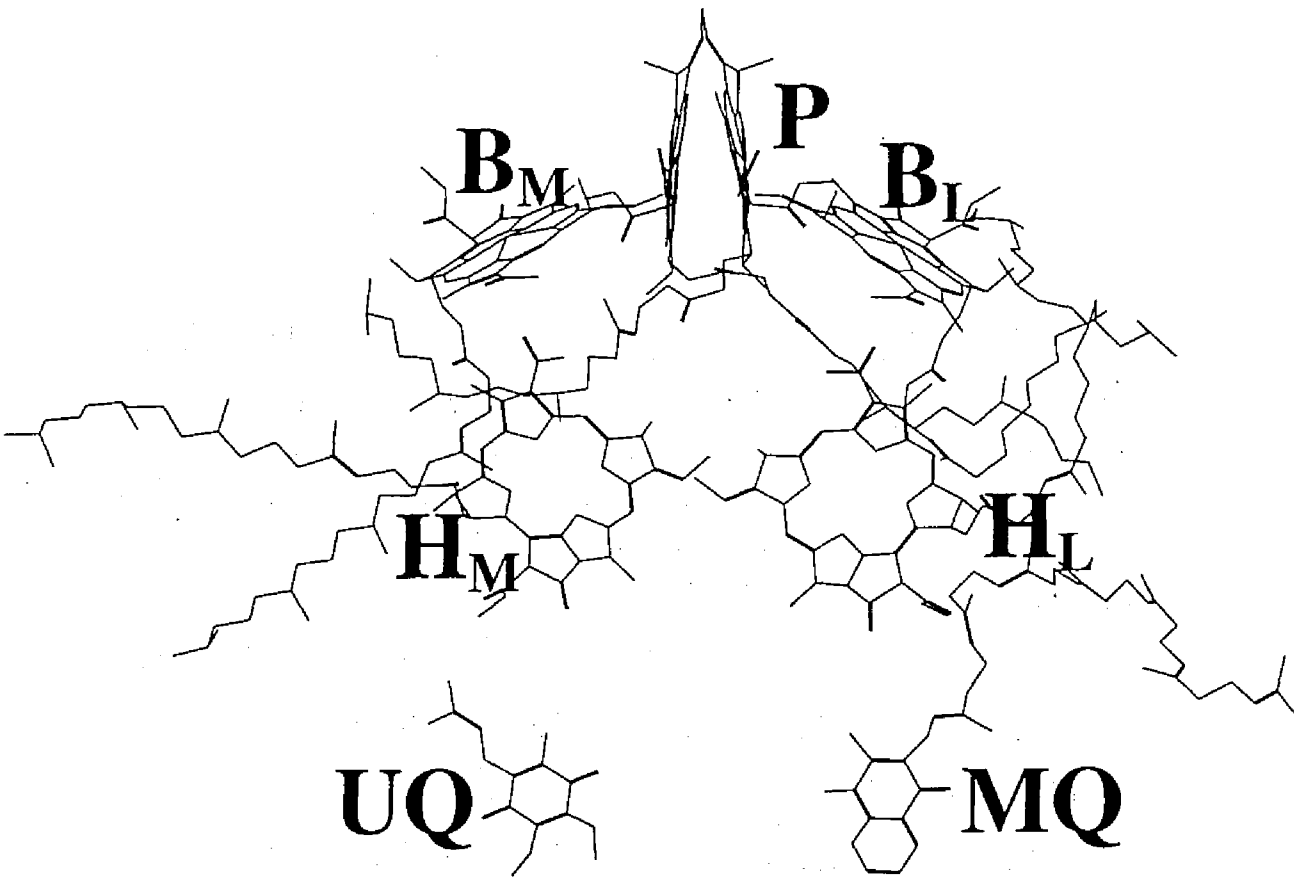

Figure 1. Structure of the chromophores in the photosynthetic reaction center of *Rps. viridis*. The nuclear coordinates are taken from ref. 2.

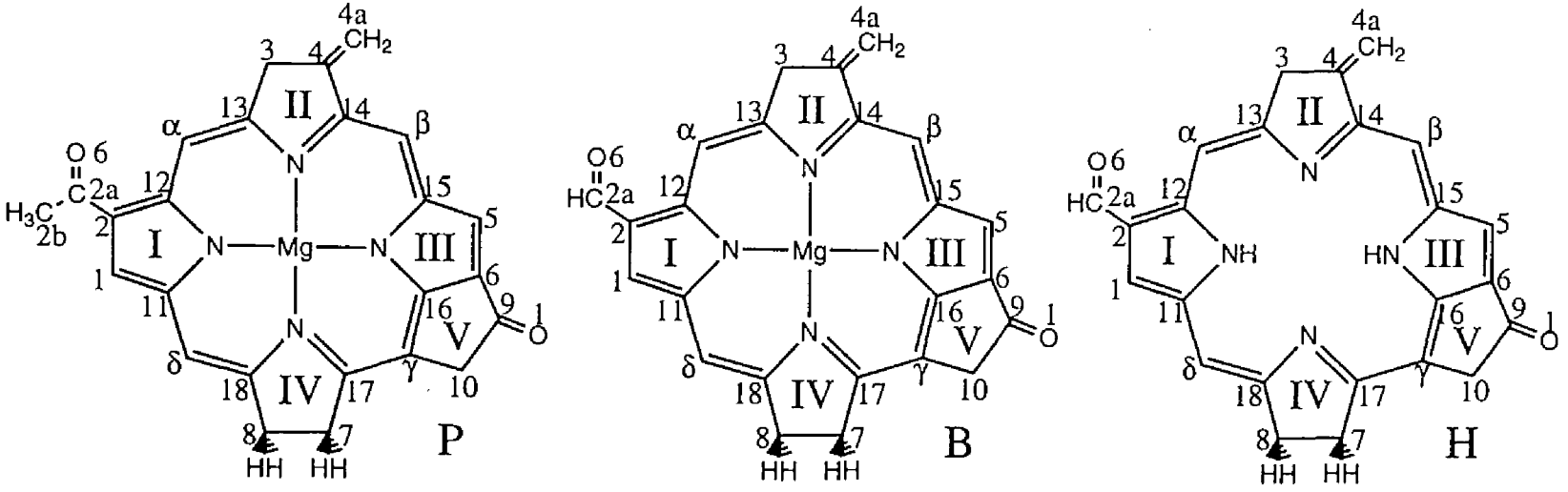

Figure 2. Calculational models for P, B, and H. For P, only monomer is shown. Some substituents in the X-ray structure are replaced by protons in the present calculations (see text). Labelings of the atoms for P, B, and H are also shown.

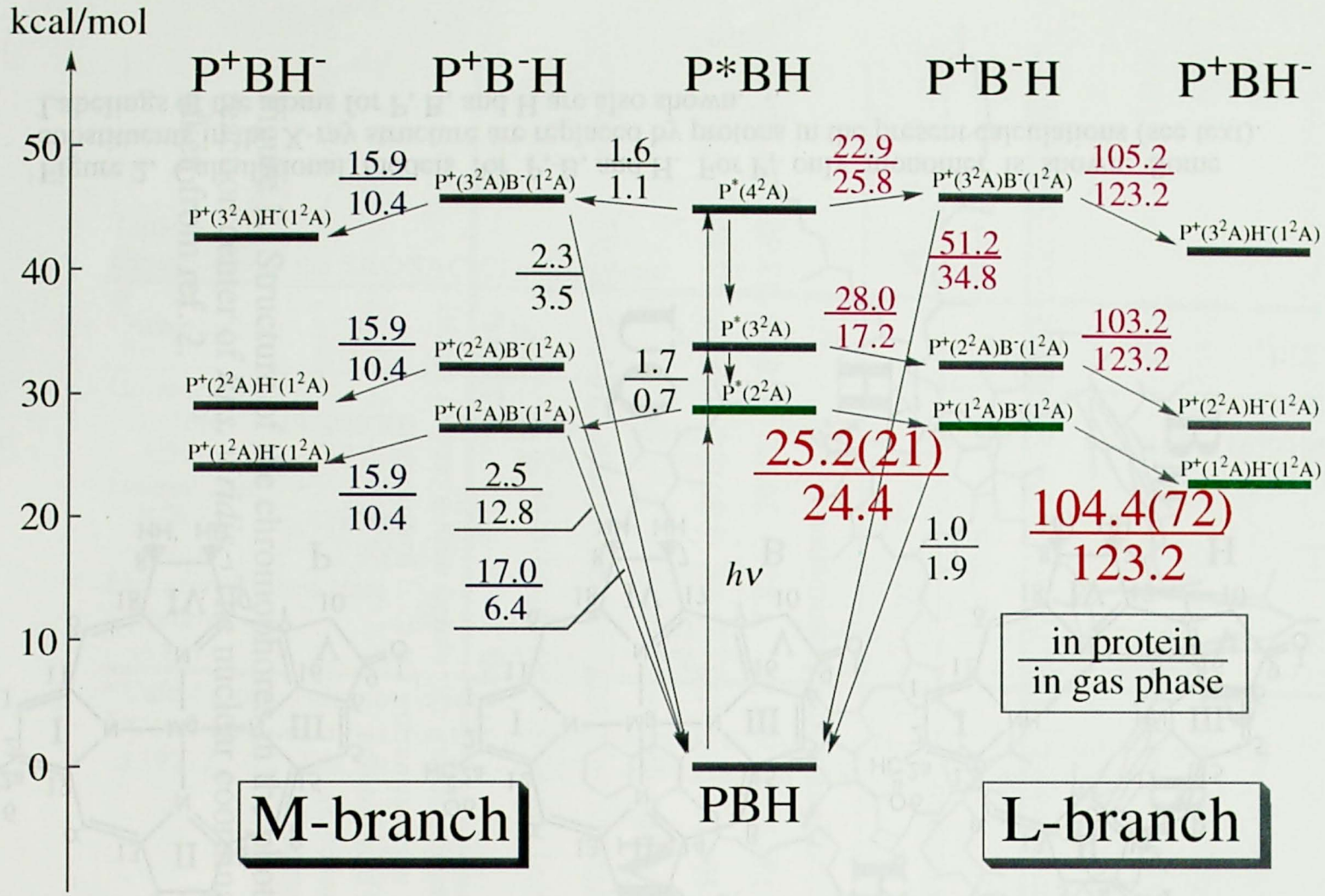

Figure 3. Electronic factors, $|H_{IF}|^2$, ($\times 10^{-9}$ in a.u.) of the electron transfer reactions (in protein / in gas phase) in the photosynthetic reaction center. Energy levels of the states are estimated by using an experimental result [30] (colored green) and the SAC-CI calculated excitation energies, ionization energies and electron affinities. Numbers in the parentheses are an estimated values [31].

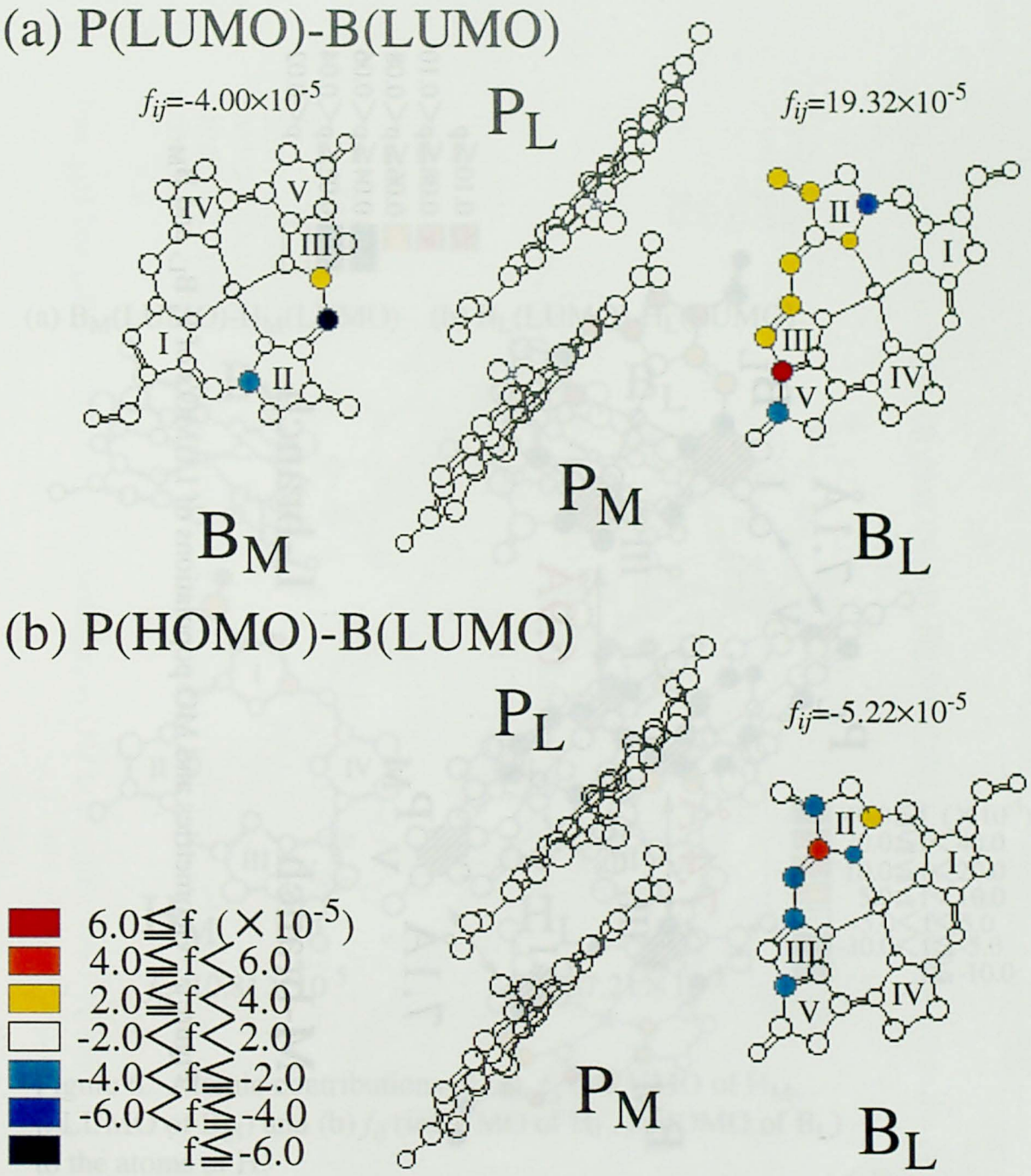

Figure 4. Atomic contributions of (a) f_{ij} (i≡LUMO of B, j≡LUMO of P) and (b) f_{ij} (i≡LUMO of B, j≡HOMO of P) to the atoms of B.

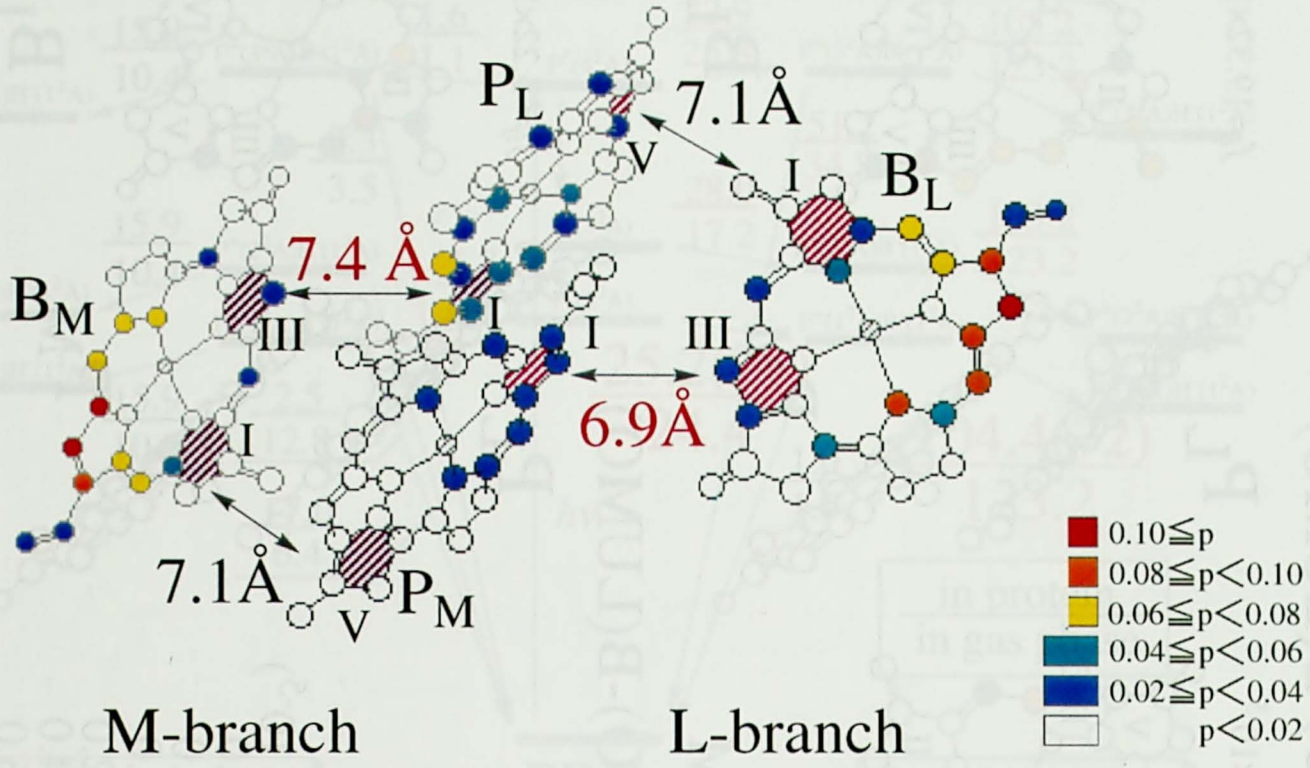

Figure 5. Geometries and MO populations of LUMO's of P, B_L, and B_M.

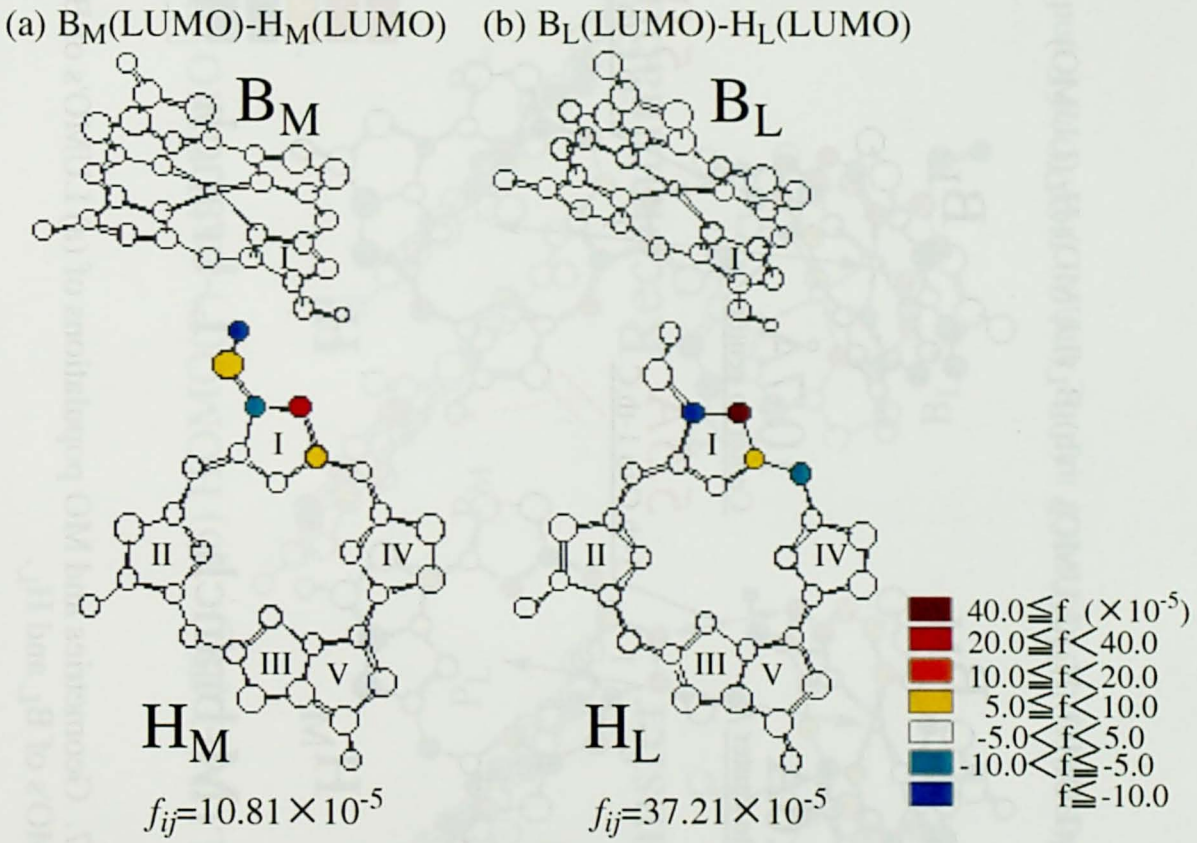

Figure 6. Atomic contributions of (a) f_{ij} (i≡LUMO of H_M, j≡LUMO of B_M) and (b) f_{ij} (i≡LUMO of H_L, j≡HOMO of B_L) to the atoms of H.

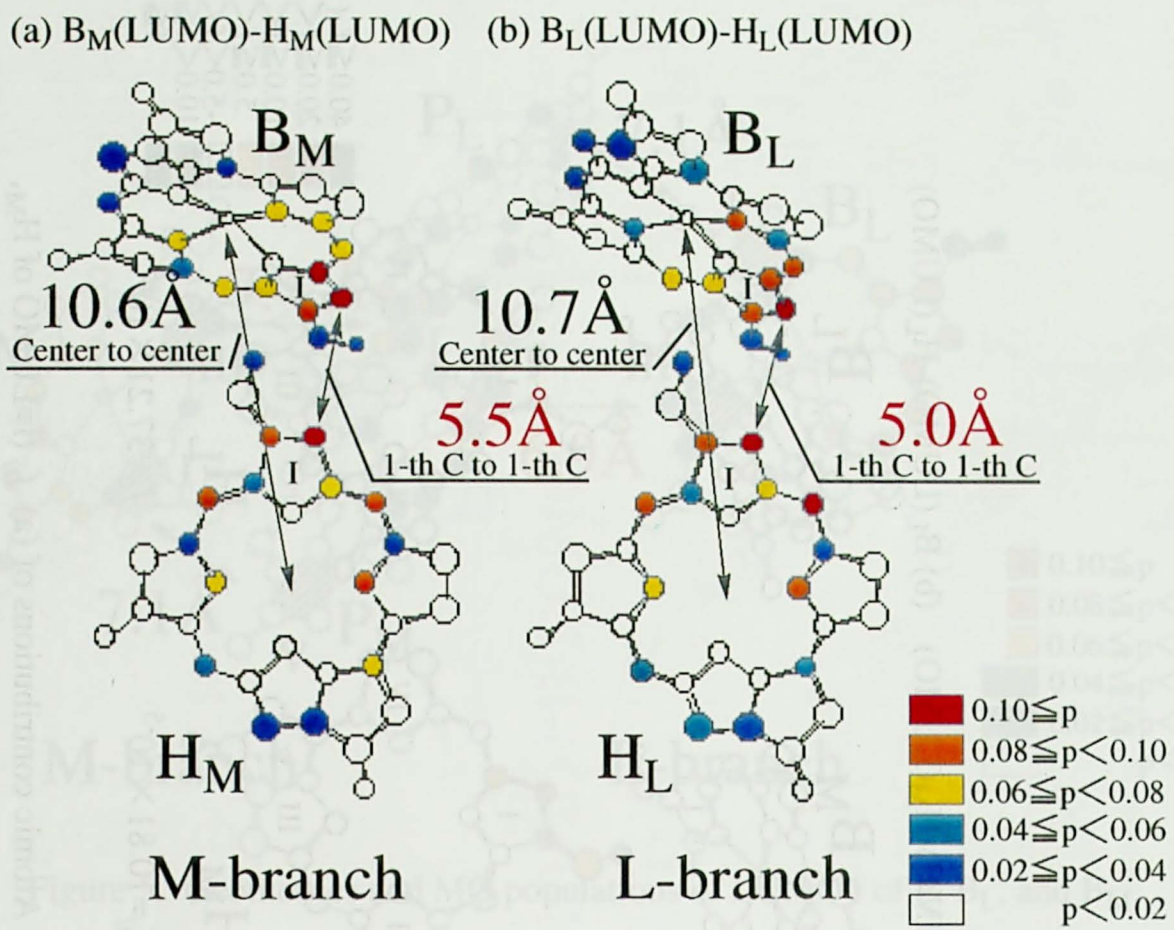

Figure 7. Geometries and MO populations of (a) LUMO's of B_M and H_M, and (b)LUMO's of B_L and H_L.

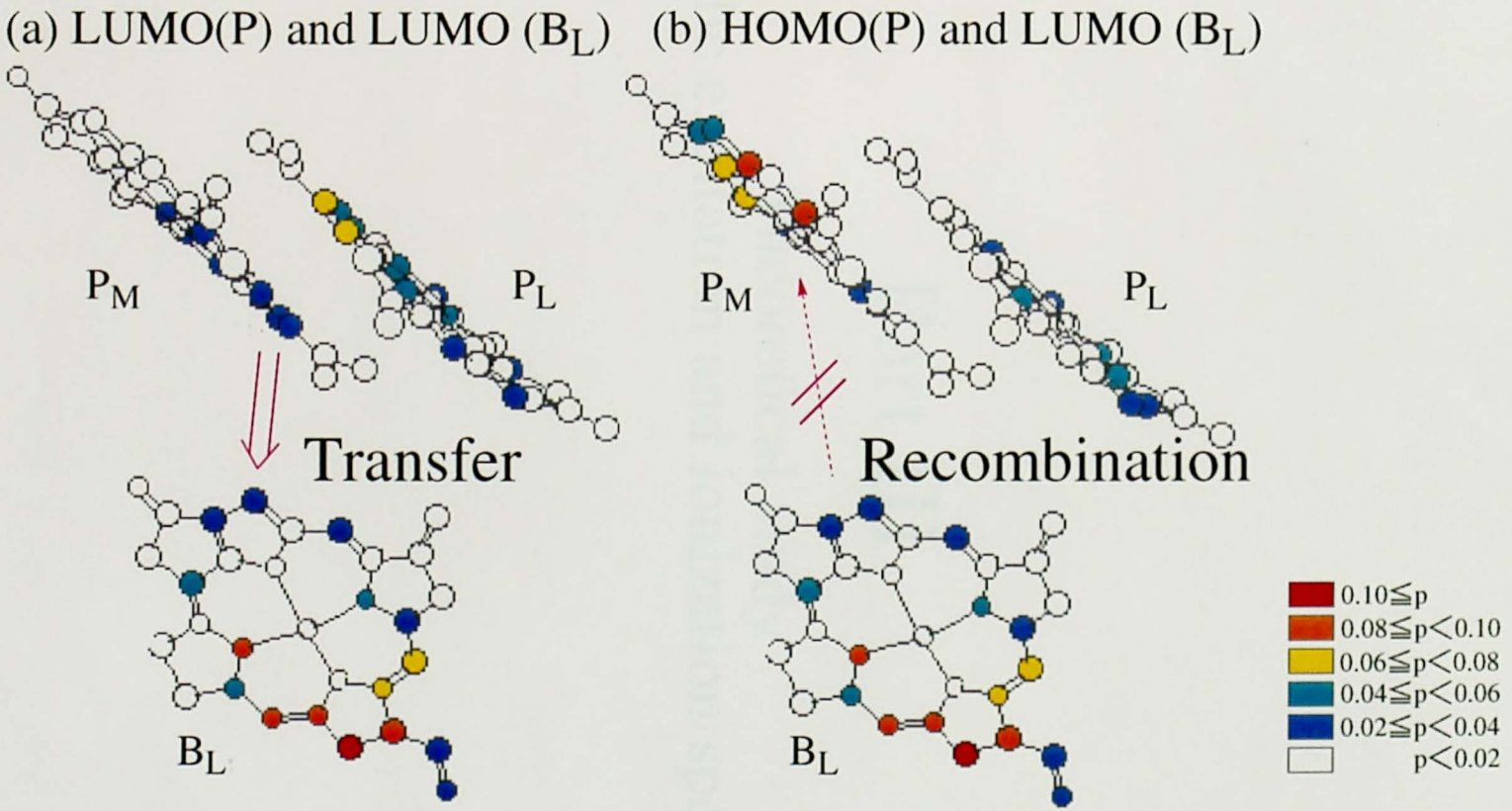

Figure 8. MO populations of (a) LUMO's of P and B_L and (b) HOMO of P and LUMO of B_L.

Part III

Theoretical study on the excitation and ionization spectra

Chapter 7

Theoretical study on the ionized states of ethylene by the SAC-CI (general-*R*) method

Abstract

The SAC(symmetry adapted cluster)/SAC-CI(configuration interaction) general-*R* method is successfully applied to the photoelectron spectrum of ethylene. The theoretical spectrum satisfactorily reproduces the outer- and inner-valence regions of the spectrum. The exponential generation (EG) algorithm followed by the perturbation selection (PS) is shown to be useful in the generation of small and yet effective higher-excitation operators for the SAC-CI general-*R* method. The peak at 23.7 eV is assigned to the "twinning" ionized states, the 2^2A_g and 3^2A_g states, and the peak at 27.4 eV is attributed to the 6^2A_g and 7^2A_g states. In the energy region around 31 eV, some ionized states are suggested to locate with small intensities. The 1^2B_{3g} state obtains its intensity by the initial state configuration interaction.

1. Introduction

Ethylene has long been a key molecule in the experimental [1-8] and theoretical [1,8-14] studies of photoelectron spectra. The assignments of the outer-valence ionizations are now well established [1,8-14], but some problems still exist in the assignment of the shake-up peaks in the inner-valence region of the spectrum [8-14]. Different theoretical assignments [8-14] were reported for the peak at 23.7 eV; "twinning" [8,10,11] (two ionized states compose the peak) and "non-twinning" ones [9,12-14] (single ionized state composes the peak). For the quite small hump at 31 eV, the SAC-CI theoretical assignment were proposed previously [12,13], but the accuracy of the calculations were not satisfactory, since only the single and double (SD) ionization operators were included in the linked term.

The reason of the complexity in the theoretical calculations of the inner-valence ionization spectra lies in their multi-electron nature: simultanious ionization and excitation process. For quantitative descriptions of such processes, large computational efforts are generally required, since the number of excitation operators increase markedly for the higher-order excitations [8,14]. However, we believe that the number of the excitation operators which are really necessary for quantitative calculations should be limited and can be generated by the exponential generation (EG) algorithm [15]. The description of such state must be improved dramatically by including such excitation operators. In our SAC [16] /SAC-CI [17] method [18,19], such important higher-excitation operators are included in the linked terms by the general-R (g-R) algorithm [20] in addition to the single and double excitation operators in the SD-R method.

The spirit of the EG algorithm is that the important higher-excitation operators must be the produsts of the lower important excitation operators [15]. The EG algorithm is a selective generation method of the higher-excitation operators from the lower-order ones. The SAC-CI calculations including such higher excitation operators (general-*R*) have been shown to give results close to the full-CI ones with small numbers of operators [20-22]. On the other hand, the perturbation selection (PS) procedure [23] is also a reliable method of selection, so that we have proposed a combined use of the EG and perturbation selection [22,23]. We first do EG for higher excitation operators and then do PS with respect to the main configurations. The PS alone without EG is too time consuming for calculations of moderate-size molecules.

In this report, the SAC-CI (g-*R*) method with the EG + PS for higher-excitation operators is applied to the ionized states of ethylene. The assignment of the photoelectron spectrum in both the outer- and inner-valence regions are given and compared with the previous experimental and theoretical results.

2. Computational detail

We calculate vertical ionization energies of ethylene using experimental geometry [24]. The basis sets of calculations are as follows: for carbon, Huzinaga-Dunning (9s5p)/[5s3p] set [25] plus d-polarization function (α=0.75) [12] and for hydrogen, Huzinaga-Dunning (4s)/[3s] set [26] plus p-polarization function (α=0.95), and at the center of the C=C bond, the s, p, and d functions (α=1.4, 0.5, and 1.02, respectively) [27] are used. The number of the SCF MO's are 74. The SAC-CI g-*R* calculations are performed within the active space composed of the 6 occupied and 61 unoccupied MO's: the 1s orbitals of carbon and some

higher virtual MO's are eliminated from the active space. In the SAC-CI (g-*R*) method, the EG algorithm [15] is used for the generation of the triple and quadruple excitation operators. A preliminary SD-CI calculations were carried out to select the operators for the EG and the thresholds for the EG, $\{\lambda^{S}_{MM}, \lambda^{D}_{MM}\}$, are set to {0.005, 0.04}. The superscripts, "S" and "D", denote single and double excitation operators, respectively, and the subscript, "MM" , denotes the product of the excitation operators. The excitation operators whose SD-CI coefficients are larger than the above thresholds are chosen as the operators for the EG. In the present calculations, about 6000 operators from single to quadruple excitations are generated for each symmetry. The B_{1g} and A_u states which are known not to exist in the energy region lower than 30 eV of the photoelectron spectrum [8] are excluded from the calculations. The generated configurations are further selected by the perturbation selection prodedure with the threshold of 1×10^{-5} hartree for the main configurations chosen from the SD-CI results. Table 1 shows the results of the selections. All single (ionization) operators and selected higher operators (PS for doubles and EG + PS for triples and quadruples) are included in the linked term. Table 1 shows that many of the operators generated by the EG are further selected by the PS, which shows the effectiveness of the EG algorithm.

The SCF MO's are calculated by HONDO version 8 program [28]. For the SAC-CI calculations, the development version [29] of the SAC85 program [30] are used.

3. Result and discussion

The SCF MOs of ethylene are expressed as

$$(\text{core})^4(2a_g)^2(2b_{1u})^2(1b_{3u})^2(3a_g)^2(1b_{2g})^2(1b_{2u})^2(1b_{3g})^0(3b_{1u})^0\cdots,$$

where the number in the superscript shows the occupation number. The natures of the $2a_g$, $2b_{1u}$, $3a_g$, and $3b_{1u}$ MO's are $2s\sigma$, $2s\sigma^*$, $2p\sigma$ and $2p\sigma^*$, respectively, the $1b_{3u}$ and $1b_{2g}$ MO's are in-plane $2p\pi_i$ and $2p\pi_i^*$ characters, respectively, and the $1b_{2u}$ and $1b_{3g}$ MO's are out-of-plane $2p\pi_o$ and $2p\pi_o^*$ characters, respectively, where the subscripts i and o denote in-plane and out-of-plane, respectively.

In Table 2, the ionization energies, monopole intensities, and main configurations of the ionized states are summarized. The calculated monopole intensity includes both final-state configuration interaction (FSCI) and initial state configuration interaction (ISCI) [31]. The experimental ionization potentials and the previous SAC-CI(SD-*R*) [12], 2ph-TDA [10], and MRSDCI [8] results are also shown. In the previous SAC-CI (SD-*R*) calculations [12], the intensities were calculated including only the FSCI. The ionized states whose intensities are less than 0.001 are not shown.

In Figure 1, the experimental photoelectron spectrum (PES) and the present theoretical spectrum are shown. For the experimental spectrum, we adopt the spectra measured by Bieri et. al. [7] (10 ~ 25 eV) and Gelius [5] (25 eV ~; expanded along the vertical axis). The bars connecting among experimental peaks represent the primary-satellite relationships obtained by the present calculations. The present results reproduce well the experimental PES in both the outer- and inner-valence regions.

The primary peaks observed at 10.51, 12.85, 14.66, 15.87, and 19.23 eV [4] are assigned to 1^2B_{2u}, 1^2B_{2g}, 1^2A_g, 1^2B_{3u}, and 1^2B_{1u} states calculated at 10.20, 12.75, 14.50, 15.83, and 19.18 eV, respectively. The average discrepancy between the experiment and theory is 0.13 eV. This assignment is the same as the previous one [1,8-14]. They represent almost pure one-electron processes. The 1^2B_{2u}, 1^2B_{2g}, 1^2A_g, 1^2B_{3u} states are the ionization of the carbon 2p electrons in the outer-valence orbitals,

$1b_{2u}$, $1b_{2g}$, $3a_g$, and $1b_{3u}$, respectively. The 1^2B_{1u} state is the ionization from the $2b_{1u}$ orbital ($2s\sigma^*$).

There have been a controversy on the assignment of the peak observed at 23.7 eV as mentioned in the introduction: "twinning" or "non-twinning" [8-14]. The present result supports "twinning" results proposed in Refs 8, 10, and 11. This peak is assigned to the two ionized states, 2^2A_g and 3^2A_g states calculated at 23.54 and 24.55 eV, respectively. The main configuration of the 2^2A_g state is 2h-1p state, $(1b_{2u})^{-2}(4a_g)^1$, to which 1h state, $(2a_g)^{-1}$, strongly mixes. The 3^2A_g state is the counterpart of the 2^2A_g state. In addition, many triple-excited configurations also mix as sub-configurations. The origin of the "twinning" state is a strong mixing between the 2h-1p and 1h configurations and the intensities of these states arises from the $(2a_g)^{-1}$ configuration. In other words, the primary peak of the ionization from the $2a_g$ MO splits into two by the mixing of the 2h-1p state $(1b_{2u})^{-2}(4a_g)^1$.

A comparison with the previous calculations indicates that the electron correlations take a large part in the "twinning" phenomenon and that the inclusion of the small but important higher-excitation operators by the SAC-CI (g-*R*) method greatly improve the description of the states. Recently, a large-scale MRSDCI calculation with a large basis set [8] was reported, in which the "twinning" was reproduced by using state-averaged natural orbitals as a reference function but not by the SCF MO's. Further, the previous "non-twinning" results by the SAC-CI (SD-*R*) method [12,13], in which the 2^2A_g state was calculated to be an one-electron process, are dramatically improved in the present g-*R* calculation by the inclusion of the 3,4-ple excitations as linked term and 5,6-ple excitation as unlinked terms.

The very weak peak observed at 27~30 eV region is assigned to 6^2A_g and 7^2A_g states calculated at 28.05 and 29.60 eV, respectively. This

assignment is the same as in 2ph-TDA [10] and MRSDCI [8]. The main configuration of these states is $(2b_{1u})^{-1}(1b_{2u})^{-1}(1b_{3g})^{1}$ and other double and triple excitations strongly mix in it. The intensity of the states are borrowed from the $(2a_g)^{-1}$ configuration.

A quite small hump was observed at 31 eV in the PES [5] and the previous 2ph-TDA [10] results showed some ^2A_g exist in this region. The present result also suggests the existence of some low-intensity ionized states, which belong not only to the ^2A_g states but also to the states in the other symmetries. In Fig. 2, the ionized states whose intensities are larger than 0.001 are shown. The 10^2B_{1u}, 11^2B_{2u}, 12^2A_g, and 14^2B_{3u} states are calculated at 31.47, 31.65, 32.07, and 33.29 eV, respectively, and many other ionized states with very small intensities are calculated in this region. The intensities of these states are due to the configuration mixings with the 1h states, though they are small.

In the recent high resolution PES [8], a new correlation peak was observed at 21.4 eV. In the MRSDCI calculation [8], the four ionized states were carefully attributed to this new peak. Among them, the 2^2B_{1u} and 3^2B_{3u} states calculated at 20.34 and 20.22 eV, respectively, had relatively large intensities [8]. Our result propose to assign the new peak to 2^2B_{1u} state calculated at 20.98 eV, a satellite band of the 1^2B_{1u} state. The main configuration is $(2b_{2u})^{-1}(3a_g)^{-1}(1b_{3g})^{1}$. The 3^2B_{3u} state calculated at 22.84 eV is attributed to the lower-energy side shoulder of the primary peak at 23.7 eV as described below. The 2ph-TDA method [10] led to a similar result; the 2^2B_{1u} and 3^2B_{3u} state were calculated at 20.32 eV and 23.22 eV, respectively.

The 3^2B_{3u} and 4^2B_{1u} states calculated at 22.84 and 25.21 eV, respectively, are suggested to be the lower and higher side shoulder of the peak at 23.7 eV. The 3^2B_{3u} and 4^2B_{1u} states are the satellite peaks belonging to the main peaks at 15.87 and 19.23 eV, respectively.

In the present calculation, many other ionized states with small intensities are calculated. The 1^2B_{3g} state is calculated at 17.55 eV and locates at the shoulder of the primary peak at 15.87 eV. The nature of the state is $(1b_{2u})^{-2}(1b_{3g})^1$. We note that the B_{3g} symmetry have no 1h state, which means there is no primary peak to borrow intensity. The observed intensity is a result of the initial state configuration interaction (ISCI) [29]. In the ground-state SAC wave function, the double excitations, $(1b_{2u})^{-2}(1b_{3g})^2$ and $(1b_{2u})^{-2}(1b_{3g})^1(2b_{3g})^1$ have relatively large coefficients. The first one is the double excitation from HOMO to LUMO, which often becomes important in π-conjugated systems. The $(1b_{2u})^{-2}(1b_{3g})^1$ configuration has its intensity from these two configurations. The 10^2B_{3g} state calculated at 30.02 eV also has small intensity through ISCI effect.

In Table 2, the previous results by SAC-CI (SD-*R*) [12], 2ph-TDA [10], and MRSDCI [8] are also shown. The previous SAC-CI (SD-*R*) calculations in 1984 with the basis of [5s2p1d/2s] plus three bond centered functions were quite efficient, since the dimension of the calculations were less than one hundred in each symmetry, and gave accurate results for the primary peaks. However, since the calculations did not include higher-excitation operators and the ISCI effect, the ionization potentials in the inner-valence region were overestimated and "non-twinning" result was led for the peak at 23.7 eV. The 2ph-TDA calculations with the DZP basis were reported in 1978. Although the results underestimated the ionization potentials by about 0.8 eV for the entire spectrum, the energy separations among the ionized states were reproduced well. Recently, a quite large MRSDCI calculations with the basis of [6s7p3d1f/5s2p1d] plus four bond centered functions was reported. This is the best calculation so far made and the results reproduced the detailed spectral features. Although the dimensions of the present SAC-CI (g-*R*) calculations are

quite small (about 4000~5000 configurations in each symmetry) in comparison with this MRSDCI calculation, the results are comparable as seen from Table 1. This result shows the SAC-CI (g-*R*) method based on the EG + PS algorithm is quite effective for the study of the multi-electron processes involved in the photoelectron spectra.

References

[1] K. Kimura, S. Katsumata, Y. Achiba, T. Yamazaki, and S. Iwata, Handbook of He I Photoelectron Spectra of Fundamental Organic Molecules (Japan scientific societies press, Tokyo, 1981).

[2] J. H. D. Eland, Int. J. Mass Spectrom. Ion Phys., 2 (1969) 471.

[3] G. R. Branton, D. C. Frost, T. Makita, C. A. McDowell, and I. A. Stenhouse, J. Chem. Phys. 52 (1970) 802.

[4] D. W. Turner, C. Baker, A. D. Baker, and C. R. Brundle, Molecular Photoelectron Spectro Scopy (Wiley-Interscience, London, 1970).

[5] U. Gelius, J. Electron. Spectrosc. Relat. Phenom. 5 (1974) 985.

[6] M. S. Banna and D. A. Shirley, J. Electron Spectroscl 8 (1976) 255.

[7] G. Bieri and L. Asbrink, J. Electon. Spectros. Relat. Phenom., 20 (1980) 149.

[8] S. J. Desjardins, A. D. O. Bawagan, Z. F. Liu, K. H. Tan, Y. Wang, and E. R. Davidson J. Chem. Phys. 103 (1995) 6385.

[9] R. L. Martin and E. R. Davidson, Chem. Phys. Letters 51 (1977) 237.

[10] L. S. Cederbaum, W. Domke, J. Scirmer, W. von Niessen, G. H. F. Diercksen, and W. P. Kraemer, J. Chem. Phys. 69 (1978) 1591.

[11] J. Baker, Chem. Phys. Letters. 101 (1983) 136.

[12] H. Nakatsuji, J. Chem. Phys. 80 (1984) 3703.

[13] H. Wasada and K. Hirao, Chem. Phys. 138 (1989) 277.

[14] C. W. Murray and E. R. Davidson, Chem. Phys. Letters 190 (1992) 231.

[15] H. Nakatsuji, J. Chem. Phys. 83 (1985) 5743.

[16] H. Nakatsuji and K. Hirao, J. Chem. Phys. 68 (1978) 2035.

[17] H. Nakatsuji, Chem. Phys. Letters 59 (1978) 362, 67 (1979) 329,334.

[18] H. Nakatsuji, Acta Chim. Hung. 129 (1992) 719.

[19] H. Nakatsuji, in: Computational Chemistry, vol. 2, ed. J. Leszczynski (World Scientific, 1997)

[20] H. Nakatsuji, Chem. Phys. Letters 177 (1991) 331.

[21] H. Nakatsuji, J. Chem. Phys. 94 (1991) 6716.

[22] M. Ehara and H. Nakatsuji, Chem. Phys. Letters. in press.

[23] H. Nakatsuji, Chem. Phys. 75 (1983) 425.

[24] J. H. Callomon, E. Hirota, K. Kuchitsu, W. J. Lafferty, A. G. Maki, and C. S. Pote, LANDOLT-BÖRNSTEIN, vol. 7, ed. K. -H. Hellwege (Springer-Verlag, Berlin, 1976) p.179.

[25] S.Huzinaga, J.Andzelm, M.Klobukowski, E.Radzio-Andzelm, Y.Sakai, H. Tatewaki, Gaussian basis set for Molecular Calculations (Elsevier, New York, 1984).

[26] S.Huzinaga, J. Chem. Phys. 42 (1965) 1293.

[27] R. J. Buenker and S. D. Peyerimhoff, Chem. Phys. 9 (1976) 75.

[28] M.Dupuis and A.Farazdel, MOTECC-91 (Center for Scientific and Engineering Computations, IBM Corporation, 191).

[29] H. Nakatsuji, M. Hada, M. Ehara, J. Hasegawa, T. Nakajima, H. Nakai, O. Kitao, K. Toyota, SAC/SAC-CI Program System (SAC-CI96) for Calculating Ground, Excited, Ionized, and Electron Attached States and Singlet to Septet Spin Multiplicities, to be submitted.

[30] H. Nakatsuji, Program System for SAC and SAC-CI Calculations, Program Library No. 146(Y4/SAC), (Data Proccessing Center of Kyoto University, 1985), Program Library SAC85, No. 1396, (Computer Center of the Instutute for Molecular Science, Okazaki, 1981).

[31] R. L. Martin and D. A. Shirley, J. Chem. Phys. 64 (1974) 3685.

Table 1
Dimensions of the SAC/SAC-CI (general-*R*) calculations for ethylene.

State	Number of configurations (EG[a] + PS[b] / EG[a])				
	Order of excitations				Total
	1	2	3	4	
Singlet ground state					
A_g	64 / 64	3176 / 9453			3241 / 9518
Ionized states					
A_g	2 / 2	283 / 340	3516 / 4481	1005 / 1823	4806 / 6646
B_{2g}	1 / 1	244 / 324	3392 / 4518	970 / 1893	4607 / 6736
B_{3g}	0 / 0	185 / 224	3024 / 4189	980 / 1961	4189 / 6374
B_{1u}	1 / 1	263 / 340	3511 / 4608	854 / 1842	4629 / 6791
B_{2u}	1 / 1	179 / 224	2928 / 4043	859 / 1940	3967 / 6208
B_{3u}	1 / 1	247 / 326	3621 / 4545	1025 / 1896	4894 / 6768

[a] EG denotes exponential generation.
[b] PS denotes perturbation selection.

Table 2
Ionized states of ethylene having intensities larger than 0.001 in the photoelectron spectrum.

State	SAC-CI (general-R)			Expt1.[a]	SAC-CI(SD-R)[b]	2ph-TDA[c]	MRSDCI[d]
	Main configuration ($\|C\|\geq 0.3$)	IP(eV)	Intensity[e]	IP(eV)	IP(eV)	IP(eV)	IP(eV)
1^2B_{2u}	$-0.96(1b_{2u})^{-1}$	10.20	0.926	10.51(s)[f]	10.25	9.74	10.38
1^2B_{2g}	$-0.95(1b_{2g})^{-1}$	12.75	0.899	12.85(s)[f]	12.78	12.13	12.91
1^2A_g	$0.93(3a_g)^{-1}$	14.50	0.890	14.66(s)[f]	14.50	13.77	14.66
1^2B_{3u}	$-0.88(1b_{3u})^{-1}-0.33(1b_{2g})^{-1}(1b_{2u})^{-1}(1b_{3g})^1$	15.83	0.765	15.87(s)[f]	15.93	15.02	16.02
1^2B_{3g}	$0.91(1b_{2u})^{-2}(1b_{3g})^1-0.34(1b_{2u})^{-2}(2b_{3g})^1$	17.55	0.009				17.2
2^2B_{3u}	$0.82(1b_{2g})^{-1}(1b_{2u})^{-1}(1b_{3g})^1+0.37(1b_{2g})^{-1}(1b_{2u})^{-1}(1b_{3g})^1$	18.53	0.012			17.82	18.32
1^2B_{1u}	$0.82(2b_{1u})^{-1}-0.34(2b_{2u})^{-1}(3a_g)^{-1}(1b_{3g})^1$	19.18	0.666	19.23(s)[f]	19.32	18.34	19.24
2^2B_{1u}	$-0.82(2b_{2u})^{-1}(3a_g)^{-1}(1b_{3g})^1-0.32(2b_{2u})^{-1}(3a_g)^{-1}(1b_{3g})^1$ $+0.31(2b_{2u})^{-1}(3a_g)^{-1}(2b_{3g})^1$	20.98	0.021	21.4(w)[d]	23.45	20.32	20.34
2^2B_{2g}	$-0.82(1b_{3u})^{-1}(1b_{2u})^{-1}(1b_{3g})^1-0.37(1b_{3u})^{-1}(1b_{2u})^{-1}(1b_{3g})^1$	22.38	0.001				21.91
3^2B_{3u}	$-0.81(1b_{2g})^{-1}(1b_{2u})^{-1}(1b_{3g})^1+0.30(1b_{3u})^{-1}(1b_{2u})^{-2}(1b_{3g})^2$	22.84	0.048		25.86	23.22	22.22
2^2A_g	$0.68(1b_{2u})^{-2}(4a_g)^1-0.46(2a_g)^{-1}$	23.54	0.209	23.7(m)[g]	24.37	23.10	23.3
3^2B_{1u}	$0.86(1b_{2u})^{-2}(3b_{1u})^1$	24.45	0.003				23.44
3^2A_g	$0.72(1b_{2u})^{-2}(4a_g)^1+0.42(2a_g)^{-1}$	24.55	0.177	23.7(m)[g]	26.97	23.83	24.5
4^2B_{1u}	$0.79(2b_{2u})^{-1}(3a_g)^{-1}(1b_{3g})^1$	25.21	0.053			25.58	24.34
3^2B_{2g}	$0.71(1b_{3u})^{-1}(1b_{2u})^{-1}(1b_{3g})^1+0.54(1b_{2g})^{-1}(1b_{2u})^{-2}(1b_{3g})^2$	25.79	0.004				24.21
3^2B_{2u}	$-0.51(1b_{2u})^{-2}(2b_{2u})^1-0.41(1b_{3u})^{-1}(1b_{2u})^{-1}(2b_{3u})^1$ $+0.37(3a_g)^{-1}(1b_{2u})^{-1}(4a_g)^1-0.37(1b_{2g})^{-1}(1b_{2u})^{-1}(2b_{2g})^1$	26.56	0.001				23.78
4^2A_g	$-0.81(1b_{2u})^{-2}(5a_g)^1$ $+0.32(2b_{1u})^{-1}(1b_{2u})^{-1}(1b_{3g})^1$	27.08	0.002				27.06
4^2B_{2u}	$-0.83(1b_{2u})^{-2}(2b_{2u})^1$	27.46	0.002				
5^2B_{3u}	$0.84(1b_{2g})^{-2}(2b_{3u})^1$	27.66	0.001				
6^2B_{1u}	$0.72(1b_{2g})^{-2}(3b_{1u})^1+0.37(1b_{2g})^{-2}(4b_{1u})^1$	27.87	0.002				
6^2A_g	$-0.62(2b_{1u})^{-1}(1b_{2u})^{-1}(1b_{3g})^1-0.53(1b_{2u})^{-2}(5a_g)^1$	28.05	0.077	27.4(w)[g]		26.95	27.7
5^2B_{2g}	$-0.81(1b_{2g})^{-1}(1b_{2u})^{-1}(2b_{2u})^1$	29.08	0.002				
6^2B_{2g}	$-0.50(1b_{2g})^{-1}(1b_{2u})^{-1}(2b_{2u})^1+0.40(3a_g)^{-1}(1b_{2g})^{-1}(4a_g)^1$	29.57	0.002				
7^2A_g	$-0.64(2b_{1u})^{-1}(1b_{2u})^{-1}(1b_{3g})^1-0.52(3a_g)^{-1}(1b_{2u})^{-2}(1b_{3g})^2$	29.60	0.050	27.4(w)[g]		28.02	28.7
7^2B_{2g}	$-0.51(1b_{2g})^{-1}(1b_{2u})^{-1}(2b_{2u})^1-0.41(1b_{2g})^{-1}(1b_{2u})^{-1}(2b_{2u})^1$ $-0.37(3a_g)^{-1}(1b_{2g})^{-1}(4a_g)^1-0.33(3a_g)^{-1}(1b_{2g})^{-1}(4a_g)^1$	29.79	0.003				
10^2B_{3g}	$-0.85(1b_{2u})^{-2}(2b_{3g})^1$	30.02	0.008				
7^2B_{3u}	$0.66(3a_g)^{-1}(1b_{2g})^{-1}(3b_{1u})^1+0.34(3a_g)^{-1}(1b_{2g})^{-1}(4b_{1u})^1$	30.15	0.001				

	$-0.33(3a_g)^{-2}(2b_{3u})^1$			
8^2B_{1u}	$-0.55(1b_{2g})^{-2}(3b_{1u})^1+0.47(1b_{2g})^{-2}(4b_{1u})^1$	30.27	0.002	
	$+0.41(1b_{2g})^{-1}(1b_{3u})^{-1}(4a_g)^1$			
8^2B_{2g}	$-0.67(3a_g)^{-1}(1b_{2g})^{-1}(4a_g)^1+0.38(1b_{2g})^{-1}(1b_{2u})^{-1}(2b_{2u})^1$	30.31	0.002	
8^2A_g	$-0.71(1b_{2g})^{-2}(5a_g)^1$	30.90	0.001	
	$-0.34(1b_{3u})^{-1}(1b_{2g})^{-1}(3b_{1u})^1+0.32(1b_{2g})^{-2}(4a_g)^1$			
9^2B_{2u}	$-0.68(1b_{2g})^{-1}(1b_{2u})^{-1}(2b_{2g})^1+0.34(3a_g)^{-1}(1b_{2u})^{-1}(5a_g)^1$	30.94	0.002	
	$+0.31(1b_{3u})^{-1}(1b_{2u})^{-1}(2b_{3u})^1$			
10^2B_{2u}	$0.61(1b_{3u})^{-1}(1b_{2u})^{-1}(2b_{3u})^1-0.43(1b_{2g})^{-1}(1b_{2u})^{-1}(2b_{2g})^1$	31.11	0.001	
	$+0.33(1b_{3u})^{-1}(1b_{2u})^{-1}(2b_{3u})^1$			
10^2B_{1u}	$-0.70(3a_g)^{-1}(1b_{2g})^{-1}(2b_{3u})^1+0.30(1b_{2g})^{-1}(1b_{3u})^{-1}(4a_g)^1$	31.47	0.005	
10^2A_g	$-0.49(3ag)^{-2}(4a_g)^1-0.35(1b_{2g})^{-2}(5a_g)^1$	31.53	0.003	
	$+0.35(1b_{3u})^{-1}(3a_g)^{-1}(2b_{3u})^1$			
11^2B_{2u}	$-0.62(1b_{3u})^{-1}(1b_{2u})^{-1}(2b_{3u})^1-0.44(1b_{2g})^{-1}(1b_{2u})^{-1}(2b_{2g})^1$	31.65	0.011	~31(w)[h]
10^2B_{3u}	$0.74(1b_{2g})^{-2}(3b_{3u})^1$	31.76	0.001	
11^2A_g	$0.83(1b_{2u})^{-2}(6a_g)^1$	31.99	0.003	
12^2A_g	$0.62(1b_{2u})^{-2}(6a_g)^1-0.45(1b_{2u})^{-1}(3a_g)^{-1}(2b_{2u})^1$	32.07	0.010	~31(w)[h]
11^2B_{1u}	$0.62(1b_{2g})^{-2}(4b_{1u})^1+0.44(1b_{2g})^{-1}(1b3u)^{-1}(4a_g)^1$	32.20	0.004	
10^2B_{2g}	$-0.60(1b_{3u})^{-1}(1b_{2g})^{-1}(2b_{3u})^1-0.32(3a_g)^{-1}(1b_{2g})^{-1}(5a_g)^1$	32.20	0.002	
	$+0.32(3a_g)^{-1}(1b_{2g})^{-1}(5a_g)^1$			
11^2B_{3u}	$0.67(1b_{2g})^{-1}(1b_{2u})^{-1}(2b_{3g})^1$	32.21	0.002	
12^2B_{3u}	$-0.42(3a_g)^{-1}(1b_{2g})^{-1}(3b_{1u})^1-0.40(3a_g)^{-2}(2b_{3u})^1$	32.75	0.001	
	$-0.33(1b_{2g})^{-2}(3b_{3u})^1+0.32(1b_{3u})^{-1}(3a_g)^{-1}(4a_g)^1$			
11^2B_{2g}	$0.42(1b_{2g})^{-1}(1b_{2u})^{-2}(1b3g)^2$	32.81	0.004	
13^2B_{3u}	$-0.37(3a_g)^{-2}(2b_{3u})^1-0.35(1b_{3u})^{-1}(1b_{2u})^{-1}(2b_{2u})^1$	33.09	0.002	
	$+0.33(1b_{3u})^{-2}(2b_{3u})^1$			
13^2B_{1u}	$-0.69(1b_{2u})^{-1}(2a_g)^{-1}(1b_{3g})^1+0.40(1b_{3u})^{-2}(2b_{1u})^{-1}(1b_{3g})^2$	33.23	0.003	
14^2B_{3u}	$0.49(1b_{3u})^{-1}(3a_g)^{-1}(4a_g)^1+0.33(2b_{1u})^{-1}(1b_{2g})^{-1}(4a_g)^1$	33.29	0.005	
	$-0.31(1b_{3u})^{-1}(1b_{2u})^{-1}(2b_{2u})^1$			
14^2B_{2g}	$+0.48(1b_{2g})^{-2}(2b_{3u})^1+0.40(3a_g)^{-1}(1b_{2g})^{-1}(5a_g)^1$	33.94	0.001	
	$-0.37(1b_{3u})^{-1}(3a_g)^{-1}(3b_{1u})^1$			

[a] The characters in the parentheses, "s", "m", and "w" denote the intensities of the peaks, strong, medium, and weak, respectively.
[b] Reference 12. [c] Reference 10. [d] Reference 8. [e] Monopole intensity including the final-state and initial-state configuration interactions.
[f] Reference 4. [g] Reference 6. [h]. Reference 5.

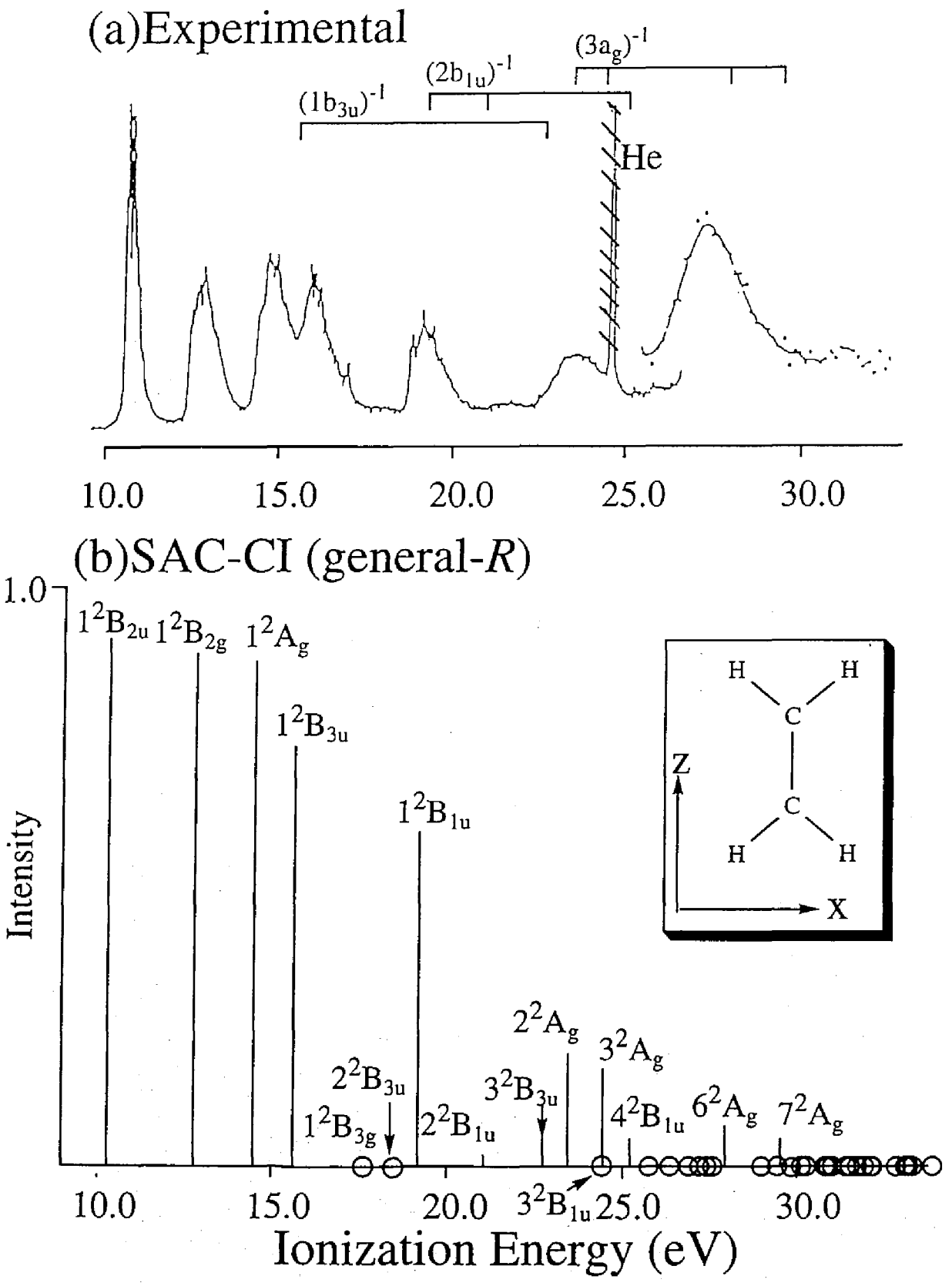

Fig. 1. Ionization spectra for ethylene. (a)Photoelectron spectra from Refs 7 (10 ~ 25 eV) and 5 (25 eV ~; expanded along the vertical axis). The bars connecting the observed peaks show the primary-satellite relationships found in the present calculations. (b)Theoretical spectrum calculated by the SAC-CI (general-*R*) method. Ionized states whose intensities are larger than 0.001 are shown.

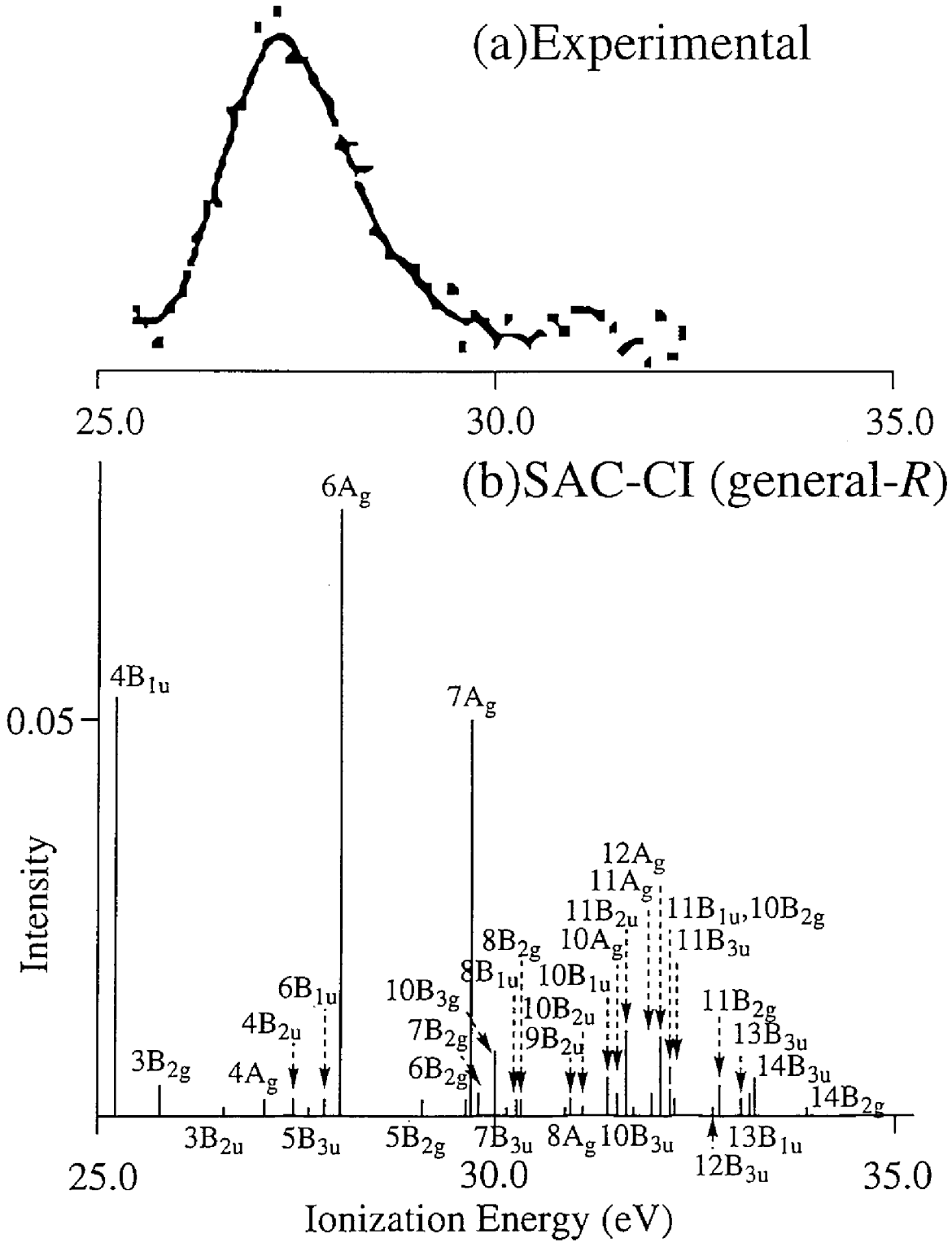

Fig. 2. Inner-valence ionization spectra for ethylene. (a)Photoelectron spectra from Ref 5 (25 eV ~). (b)Theoretical spectrum calculated by the SAC-CI (general-*R*) method. Ionized states whose intensities are larger than 0.001 are shown.

Chapter 8

SAC-CI study on the electronic spectrum of TcO_4^-

Summary. Theoretical electronic spectrum of TcO_4^- calculated by the SAC(symmetry adapted cluster)/SAC-CI method is presented. The spectrum is in good agreement with the experimental one. The observed peaks are assigned and the existence of several absorptions in the energy region higher than that observed is predicted. The difference and the similarity between the electronic spectra of TcO_4^- and MnO_4^- are clarified. The spectral difference between TcO_4^- and MnO_4^- is due to a remarkably high energy shift of the 3^1T2 state of TcO_4^-.

Key wards: TcO_4^- — SAC/SAC-CI method — Electronic spectrum — Excited state

1.Introduction

Four coordinated oxo-metal complexes are important as oxidizing agent. Their visible and ultraviolet spectra have been reported[1], and theoretical assignments[2] were attempted by Ziegler et al. in 1976. Some complexes show interesting photochemistry as observed for MnO_4^-[3,4]. We have studied the electronic spectra of the tetraoxo metal complexes, CrO_4^{2-}[5], MoO_4^{2-}[6], MnO_4^-[7], RuO_4[8], OsO_4[8], and also CrO_2Cl_2[9] by the SAC (symmetry adapted cluster)[10] and the SAC-CI (symmetry adapted cluster-configuration interaction)[11] method[12]. We have investigated the similarity and the difference in the electronic spectra of these tetraoxo metal complexes[5]. It has been shown that a sufficient inclusion of electron correlations for both ground and excited states are important for reliable ab initio assignments of the spectra.

Technetium belongs to the group VIIA metal as manganese and TcO_4^- is also a strong oxidizing reagent[13]. However, the electronic spectrum[14] of TcO_4^- shown in Figure 1 is very different from that of MnO_4^-. The peaks of TcO_4^- lie in a higher energy region than those of MnO_4^-. TcO_4^- does not have a broad band like that of MnO_4^- at 3.47 eV, and the energy separation between Band I and II in MnO_4^- is larger than that of TcO_4^-. The correspondence between Band IIIs of these compounds is unclear.

In this study, we calculate the ground and excited states of TcO_4^- by the SAC/SAC-CI theory and present a theoretical assignment of the observed spectrum and a prediction of the peaks so far not observed. We analyze the bonding nature of the ground and excited states and compare the natures of the excited states with those of the other oxo-metal complexes studied previously[5-9].

2. Computational details

The geometry of TcO_4^- is fixed to the Td symmetry with the Tc-O bond distance of 1.71 Å adopted from the experimental data of X-ray crystallography[15].

The gaussian basis set we use in this work is valence DZ and TZ levels. We use for Tc the (16s10p7d)/[7s3p3d] set[16] and the two polarization p-functions with the exponents α=0.028 and 0.086[16], and for O the (9s5p)/[4s2p] set[16]. From our experience[5-9], this basis set would reliably describe the valence excited states of this molecule.

The HF orbitals calculated by the HONDO program[17] are used as reference orbitals. Electron correlations in the ground state are treated by the SAC[10] method and those in the excited states by the SAC-CI method[11] with the use of the program SAC85[18]. The space of the active orbitals must be sufficiently large to accurately describe the valence excitations. The active space of the present SAC/SAC-CI calculations consists of 12 higher occupied orbitals and 36 lower unoccupied orbitals: all valence-type occupied and unoccupied orbitals are included. For the linked term, all single excitations and double excitations selected by the perturbative method[19] are included. The main configurations whose coefficients are larger than 0.1 in the 12 lower solutions in a preliminary SE-CI calculations in each symmetry are used as the reference configurations for the perturbation selection[19]. The energy thresholds $\lambda_g = 4.0 \times 10^{-5}$ hartree for the ground state and $\lambda_e = 7.0 \times 10^{-5}$ hartree for the excited states are used in the present calculation. The numbers of the linked configurations are shown in Table I.

3. Results and discussions

3.1. Ground state of TcO_4^-

The SCF orbital sequence and the orbital characters are shown in Table II. The plus (+) and minus (-) signs denote the bonding and antibonding combinations, respectively. The lowest three valence orbitals 1e, $1t_2$, and $1a_1$ are the bonding MOs between the 4d orbitals of Tc and the 2p orbitals of O. The higher occupied orbitals $2t_2$ and $1t_1$ are nonbonding MOs mainly composed of the oxygen 2p orbitals. In particular, the highest occupied MO (HOMO) $1t_1$ is completely localized on oxygens. The lowest unoccupied MO (LUMO) 2e and the higher unoccupied $4t_2$ MO are antibonding between the Tc 4d and the O 2p orbitals. These antibonding MOs have larger amplitudes on Tc than on O. The unoccupied $2a_1$ and $3t_2$ MOs are the nonbonding MOs mainly composed of the Tc 5s and 5p orbitals, respectively.

Comparing with RuO_4[8] and MoO_4^{2-}[6], which are isoelectronic with TcO_4^-, orbital energies of the valence occupied MOs are shifted by about +7.5 and -8.0 eV, respectively. Further, the energy shifts are larger for the bonding orbitals than for the ligand orbitals by about 1 eV. The bonding MOs having larger amplitudes on the metal than the ligand MOs feel the change of the nuclear charge more sensitively.

Table III shows the total energies, Mulliken atomic orbital populations and net charges of TcO_4^- calculated by the HF and SAC methods. By including electron correlations, the ionicity of the Tc-O bond is much relaxed, and the relaxation is largest on the Tc 4d orbitals. Table IV shows the occupation numbers of the natural orbitals of the SAC wave function. In comparison with the HF ones, the occupations of the $1t_1$ and $2t_2$ MOs decrease more than those of the other occupied orbitals. In the

unoccupied MOs, the occupancies of the 2e and $2a_1$ MOs increase by including electron correlations. These changes in the occupation numbers result in an increase of the Tc 4d occupations and a decrease of the O 2p occupations as shown in Table III. Similar relaxation was also found in our previous studies on MnO_4^-, CrO_4^{2-}, etc.[5-9], so this phenomenon seems to be quite general.

3.2 Excited states of TcO_4^-

Figure 1 shows the experimental electronic spectrum of TcO_4^- together with that of the related complex, MnO_4^-[14]. In the spectrum of TcO_4^-, there are two strong peaks at 4.27 and 5.00 eV (Band I and Band II) and a weak peak at 6.59 eV (Band III). These peaks would be due to the allowed transitions. As compared with the electronic spectrum of MnO_4^-, (1) the peaks of TcO_4^- shift entirely to higher energy region, (2) Band I and II are different from those of MnO_4^- in both the energy splitting and intensity, (3) in MnO_4^-, the Band IIa and IIb are due to the different excited states[7], but in TcO_4^- we do not know how many states there are in Band II, and (4) the strong peak of MnO_4^- at 6.5 eV is not observed for TcO_4^- in the observed energy region.

We summarize in Table V the SAC/SAC-CI results for the singlet excitation energy, oscillator strength, and the net charges on Tc and O. In the T_d symmetry only the transitions to the $^1T_2$ states are dipole-allowed. The SAC/SAC-CI theoretical spectrum for TcO_4^- is shown in Figure 2 and compared with the experimental spectrum. The theoretical spectrum reproduces well the excitation energies and the intensities of the observed peaks in 4 ~ 6 eV region. From Table V the excited states in TcO_4^- may be divided into two regions (Region A and Region B). Region A is 3.0 ~

7.2 eV and Region B is above Region A. The 1 ~ 3 $^1T_2$ states in Region A are characterized as the transitions from the ligand to the anti-bonding MOs and 4 ~ 6 $^1T_2$ states in Region B as the transitions from the ligand to the metal. Though all the states are the charge transfer states from O to Tc, the amount of transferred charge is larger in Region B than in Region A. This trend is similar to that in MnO_4^-.

Next we discuss more details of the absorptions. Based on the present calculation, the observed Bands I, II, and III are assigned to 1^1T_2, 2^1T_2, and 3^1T_2 states, respectively, by comparing the experimental and theoretical spectra in both the excitation energy and the intensity. This assignment is the same as that by Ziegler et al.[2] with the Hartree-Fock-Slater discrete variational method.

Band I corresponds to the first dipole-allowed excited state 1^1T_2 ($1t_1 \rightarrow 2e$), and the fine structure spacing of about 0.1 eV represents the vibrational structure in the excited state. The first observed peak of MnO_4^- has the same nature as that of TcO_4^-, as seen from the corresponding diagram given in Figure 3.

Band II and Band III are due to the allowed states of 2^1T_2 ($2t_2 \rightarrow 2e$) and 3^1T_2 ($1t_1 \rightarrow 4t_2$), respectively. This assignment is different from that for MnO_4^-, since in MnO_4^-, the 2^1T_2 and 3^1T_2 states constitute Band II[7]. In Figure 1, Band II of MnO_4^- is thus divided into Band IIa and IIb. Furthermore, the natures of Bands II and III of TcO_4^- are just the reverse of those of Bands IIa and IIb of MnO_4^-, as shown in the corresponding diagram in Figure 3.

state		MnO_4^-		TcO_4^-
2^1T_2	$\leftrightarrow$	Band IIb	$\leftrightarrow$	Band II
3^1T_2	$\leftrightarrow$	Band IIa	$\leftrightarrow$	Band III

The existence of the vibrational structure in Band IIb of MnO_4^- is consistent with that of Band II of TcO_4^-. The energy separation between

Band II and III in TcO_4^- is much larger than that between Band IIa and IIb in MnO_4^-, though the corresponding excited states have similar nature. It is due to a remarkably high energy shift of the 3^1T_2 states ($1t_1 \rightarrow 4t_2$) in TcO_4^-, and this shift is easily explained from the orbital energy levels shown in Figure 4. The orbital energy difference between the $1t_1$ and $4t_2$ MOs in TcO_4^- is much larger than that in MnO_4^-. The $4t_2$ MO of TcO_4^- lies in high energy, since the anti-bonding interaction between metal and ligand is larger in TcO_4^- than in MnO_4^-. This is because the Tc 4d orbital is more diffuse than the Mn 3d orbital and then the metal-ligand overlap interaction is larger in TcO_4^- than in MnO_4^-.

In the previous study on the photochemical decomposition reaction of MnO_4^-[4], 1^1T_2 and 3^1T_2 states are shown to play important roles. Though no report for the photo reaction of TcO_4^- is found, the 1^1T_2 and 2^1T_2 states are expected to be important as photochemical reaction channels, since in TcO_4^-, these states correspond to the 1^1T_2 and 3^1T_2 states of MnO_4^-.

For the energy region higher than Band III, there is no experimental data for the electronic absorption of TcO_4^-. However, as seen from Table V, we can predict an existence of the three dipole-allowed electronic states 4^1T_2, 5^1T_2, and 6^1T_2, whose excitation energies are calculated at 7.45, 7.56, and 8.19 eV, respectively, and the intensities to be weak, weak, and strong, respectively. The 4^1T_2 state has a mixed nature of L $\rightarrow$ A and L $\rightarrow$ M transitions, and the intensity is low. The 5^1T_2 and 6^1T_2 states originate from the L to M ($2t_2 \rightarrow 2a_1$) excitation, and so a larger amount of electronic charge on O is transferred to the metal than in the 1 ~ 4^1T_2 states in Region A as seen from Table V. The 4^1T_2 state lies just on the border of Region A and Region B, since as seen from Table V, the nature of the transition switches from L $\rightarrow$ A to L $\rightarrow$ M on this state and

the amount of charge transferred from ligand to metal is median between those in Region A and Region B.

The peaks of the 5^1T_2 and 6^1T_2 states calculated at 7.45 and 7.56 eV for TcO_4^- would correspond to the peak III of MnO_4^- shown in Figure 1. In particular, the 6^1T_2 state of TcO_4^- has a large intensity of 0.0339 so that it would correspond to the strong peak (Band IV) observed at 6.5 eV for MnO_4^- (Figure 1). In comparison with our previous results for CrO_4^{2-} [5], the 6^1T_2 state of TcO_4^- has the same character as the 5^1T_2 state of CrO_4^{2-}, which gives a strong peak at 6.0 ~ 7.0 eV[20]. The $4\sim6^1T_2$ states may lie higher than the first ionization potential, since they are excitations from the orbitals lower than $1t_1$ (HOMO). Thus, we propose to examine a new band system in the higher energy region (7.5 ~ 8.0 eV) of the TcO_4^- spectrum.

In the electronic spectra of $LiMnO_4 \cdot 3H_2O$ and $Ba(MnO_4)_2 \cdot 3H_2O$, a weak absorption called "Teltow band" was observed[21] in the red side of 1^1T_2 state. This band was calculated to be a symmetry forbidden 1^1T_1 state in our previous work[5,7]. This state can be observed by a symmetry lowering from T_d to C_{3v} in its crystal. For TcO_4^-, the 1^1T_1 state is calculated at 3.83 eV and has the same nature as the symmetry allowed 1^1T_2 state calculated at 4.28 eV (Band I), the excitation from ligand to antibonding MO ($2t_1 \rightarrow 2e$). In this class of complexes like MnO_4^-, CrO_4^-, and so forth, the 1^1T_1 and 1^1T_2 states originate from the same MO excitations and the 1^1T_1 state is always at the red side of the 1^1T_2 state, though the energy itself is different for different complexes. The energy difference between the 1^1T_1 and 1^1T_2 states is roughly due to the difference in the exchange integrals.

Compared with MnO_4^-, all the peaks observed for TcO_4^- are shifted to higher energy region by 1.5 ~ 2.6 eV, as seen from Figure 3. This is

roughly explained as follows[5]. In the frozen orbital approximation, the HF excitation energy may be expressed as

$$\Delta E_{i\rightarrow a} = \varepsilon_a - \varepsilon_i - J_{ia} + 2K_{ia}$$

Because the transitions are from ligand to metal, the transitions are affected by the metal-ligand bond length. Since the Tc-O bond is longer than the Mn-O bond, the J_{ia} values of TcO_4^- should be smaller than those of MnO_4^-.

4. Conclusion

In this study, we have applied the SAC/SAC-CI method to the ground and excited states of TcO_4^-. For the ground state, the electron correlation works to relax the ionicity of the M-O bond. For the excited states, the observed three absorption peaks in the electronic spectrum are assigned to the lower three dipole-allowed $^1T_2$ states. Further, the existence of the weak and strong peaks in the energy region higher than the observed one is predicted. The similarity and the difference in the electronic spectra of TcO_4^- and MnO_4^- are clarified. The Band II in the spectrum of TcO_4^- is quite different from the corresponding band in the MnO_4^- spectrum, as seen in Figure 1. The reason is the remarkably high energy shift of the 3^1T_2 state ($1t_1\rightarrow 4t_2$) of TcO_4^-, and is due to the larger antibonding nature of the $4t_2$ MOs of TcO_4^- than that of MnO_4^-.

References

1 Carrington A, Symmons MC (1963) Chem Rev 63:443

2 Ziegler T, Rauk A, Baerends EJ (1976) Chem Phys 16:209

3 Lee DG, Moylan CR, Hayashi T, Brauman JI (1987) J Am Chem Soc 109:3003

4 Nakai H, Nakatsuji H (1994) J Mol Struct (Theochem) 311:141

5 Jitsuhiro S, Nakai H, Hada M, Nakatsuji H (1994) J Chem Phys 101:1029

6 Nakatsuji H, Saito S (1990) J Chem Phys 93:1865

7 Nakai H, Ohmori Y, Nakatsuji H (1991) J Chem Phys 95:8287

8 Nakatsuji H, Saito S (1991) Int J Quant Chem 39:93

9 Yasuda K, Nakatsuji H (1993) J Chem Phys 99:1945

10 Nakatsuji H, Hirao K (1978) J Chem Phys 68:2035

11 Nakatsuji H (1978) Chem Phys Lett 59:362; (1979) Chem Phys Lett 67:329, 334

12 Nakatsuji H (1992) Acta Chim Hung 129:719

13 Colton R, Peacock RD (1962) Quart Rev Chem Soc 16:299

14 Mullen P, Schwochau K, Jørgensen CK (1969) Chem Phys Lett 3:49

15 Krebs B, Hasse KD (1976) Acta Cryst B32:1334

16 Huzinaga S, Andzelm J, Klobukowski M, Radzio-Andzelm E, Sakai E, Tatewaki H (1984) Gaussian Basis Set for Molecular Calculations, Elsevier, New York

17 Dupuis M, Farazdel A (1991) MOTECC-91; Center for Scientific and Engineering Computations, IBM Corporation

18 Nakatsuji H (1985) Program System for SAC and SAC-CI Calculations, Program Library No.146 (Y4/SAC), (1981) Data Processing Center of Kyoto University; Program Library SAC85 No.1396, Computer Center of the Institute for Molecular Science

19 Nakatsuji H (1983) Chem Phys 75:425

20 Johnson LW, McGynn SP (1970) Chem Phys Lett 7:618

21 Johnson LW, Hughes E, McGynn SP (1971) J Chem Phys 35:4476

Table 1. Dimensions of the SAC/SAC-CI calculations of TcO_4^-

Symmetry	After selection	Before selection
Ground state : SAC		
$^1A_1$	3686	23809
Excited state[a] : SAC-CI		
$^1A_1$	7444	23809
$^1A_2$	6676	23280
$^1B_1$	7191	23436

[a] $^1B_2$ states are degenerate with $^1B_1$ states in the tetrahedral symmetry

Table 2. HF orbital energies and characters

Symmetry	Character[a]		Orbital energy (eV)
Occupied orbitals			
1e	Tc(4d)+O(2p)	:B	-12.92
1t2	Tc(4d)+O(2p)	:B	-12.84
1a1	Tc(4d)+O(2p)	:B	-8.66
2t2	O(2p)	:L	-8.60
1t1	O(2p)	:L	-7.77
Unoccupied orbitals			
2e	Tc(4d)-O(2p)	:A	4.62
2a1	Tc(5s)	:M	5.65
3t2	Tc(5p)	:M	5.70
4t2	Tc(4d)-O(2p)	:A	7.35

[a] (+) and (-) denote bonding and antibonding combinations, respectively. B, A, L, and M mean bonding, antibonding, ligand and metal orbitals, respectively

Table 3. Total energy and the valence electron population for the ground state of TcO_4^-

Method	Energy	Tc				O		
	(Hartree)	5s	5p	4d	charge	2s	2p	charge
HF	-4500.66022	0.032	0.310	4.755	+1.800	1.968	4.737	-0.700
SAC	-4501.15316	0.035	0.361	5.013	+1.487	1.967	4.660	-0.622
Δ^a	-0.49294	+0.003	+0.051	+0.258	-0.313	-0.001	-0.077	+0.078

[a]The difference between HF and SAC values

Table 4. Occupation numbers of the HF orbitals and the SAC natural orbitals for the ground state of TcO_4^-

Orbital	HF	SAC	Difference	(per MO)
Occupied orbitals				
1e	4.0	3.9542	-0.0458	-0.0229
$1t_2$	6.0	5.9240	-0.0760	-0.0253
$1a_1$	2.0	1.9688	-0.0312	-0.0312
$2t_2$	6.0	5.9029	-0.0971	-0.0324
$1t_1$	6.0	5.8961	-0.1039	-0.0346
Unoccupied orbitals				
2e	0.0	0.1237	+0.1237	+0.0619
$2a_1$	0.0	0.0494	+0.0494	+0.0494
$3t_2$	0.0	0.1078	+0.1078	+0.0359
$4t_2$	0.0	0.0252	+0.0252	+0.0084

Table 5. Ground and excited states of TcO_4^-

State	Main configuration (C≥0.3)	nature[a]	Excitation energy (eV)		Oscillator strength		Net charge	
			exptl.	SAC-CI	exptl.	SAC-CI	Tc	O
XA_1	1.00(HF)			0.00			+1.486	-0.622
$1T_1$	0.96($1t_1 \rightarrow 2e$)	L→A		3.83	forbidden		+1.283	-0.571
$1T_2$	0.77($1t_1 \rightarrow 2e$)	L→A	4.27	4.28	middle	0.0171	+1.293	-0.573
	0.57($2t_2 \rightarrow 2e$)	L→A						
$2T_1$	0.95($2t_2 \rightarrow 2e$)	L→A		4.61	forbidden		+1.319	-0.580
$1E$	0.96($1a_1 \rightarrow 2e$)	B→A		4.98	forbidden		+1.305	-0.576
$2T_2$	0.71($2t_2 \rightarrow 2e$)	L→A	5.00	5.29	strong	0.0415	+1.315	-0.579
$2E$	0.67($1t_1 \rightarrow 4t_2$)	L→A		6.08	forbidden		+1.268	-0.567
$3T_2$	0.55($1t_1 \rightarrow 4t_2$)	L→A	6.59	6.20	weak	0.0025	+1.259	-0.564
$3T_1$	0.57($1t_1 \rightarrow 4t_2$)	L→A		6.42	forbidden		+1.227	-0.557
$1A_2$	0.48($1t_1 \rightarrow 4t_2$)	L→A		6.54	forbidden		+1.237	-0.559
$4T_1$	0.85($1t_1 \rightarrow 2a_1$)	L→M		6.95	forbidden		+0.657	-0.414
$1A_1$	0.48($2t_2 \rightarrow 4t_2$)	L→A		7.03	forbidden		+1.274	-0.569
$5T_1$	0.56($2t_2 \rightarrow 4t_2$)	L→A		7.10	forbidden		+1.213	-0.553
$3E$	0.66($2t_2 \rightarrow 4t_2$)	L→A		7.19	forbidden		+1.249	-0.562
$4T_2$	0.39($2t_2 \rightarrow 4t_2$)	L→A		7.45	weak	0.0000	+1.042	-0.510
	0.37($1a_1 \rightarrow 4t_2$)	B→A						
	0.34($2t_2 \rightarrow 2a1$)	L→M						
	0.32($1t_1 \rightarrow 3t_2$)	L→M						
$5T_2$	0.58($2t_2 \rightarrow 2a_1$)	L→M		7.56	weak	0.0046	+0.858	-0.465
	0.42($1a_1 \rightarrow 4t_2$)	B→A						
$2A_1$	0.85($1a_1 \rightarrow 2a_1$)	B→M		8.18	forbidden		+0.608	-0.402
$6T_2$	0.67($2t_2 \rightarrow 2a_1$)	L→M		8.19	strong	0.0339	+0.623	-0.406

[a] B, A, L and M denote bonding, antibonding, ligand and metal orbitals, respectively

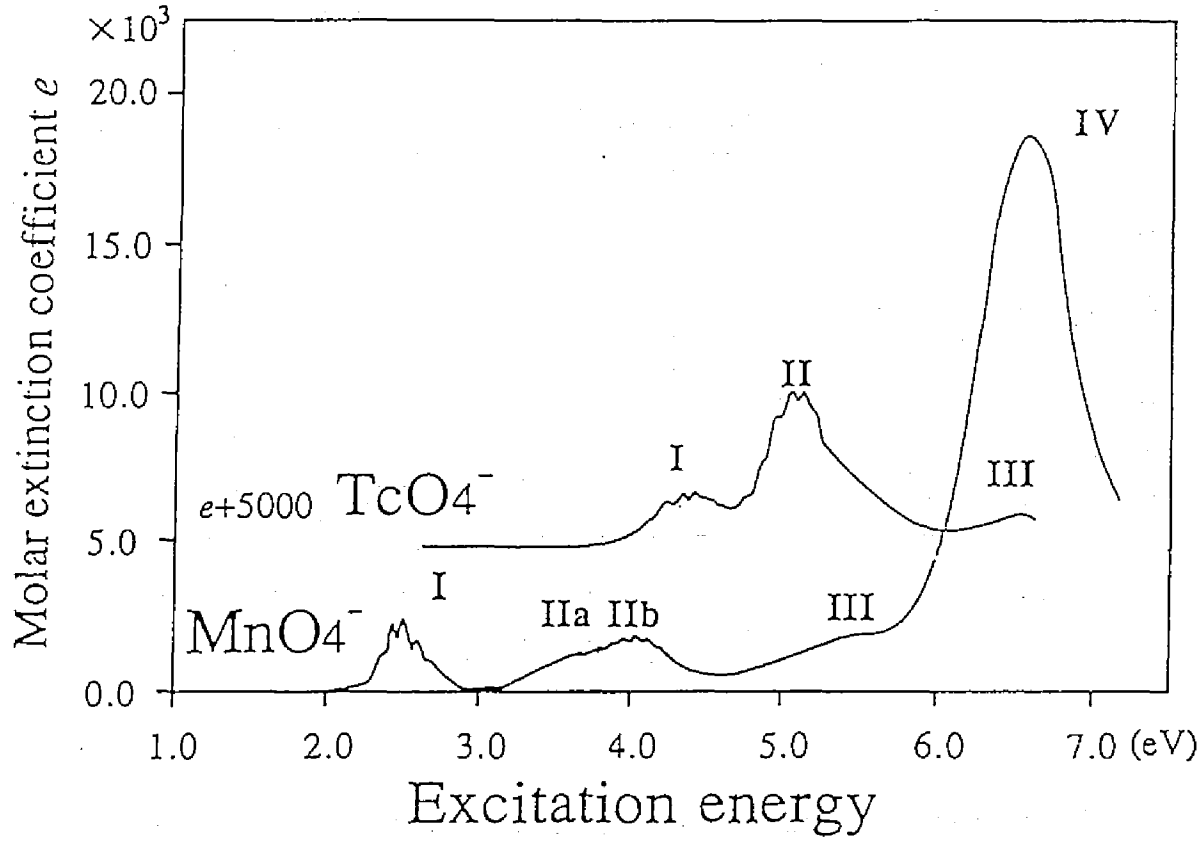

Fig. 1. Electronic absorption spectra of TcO_4^- and MnO_4^- in the vapor phase, see ref. 14

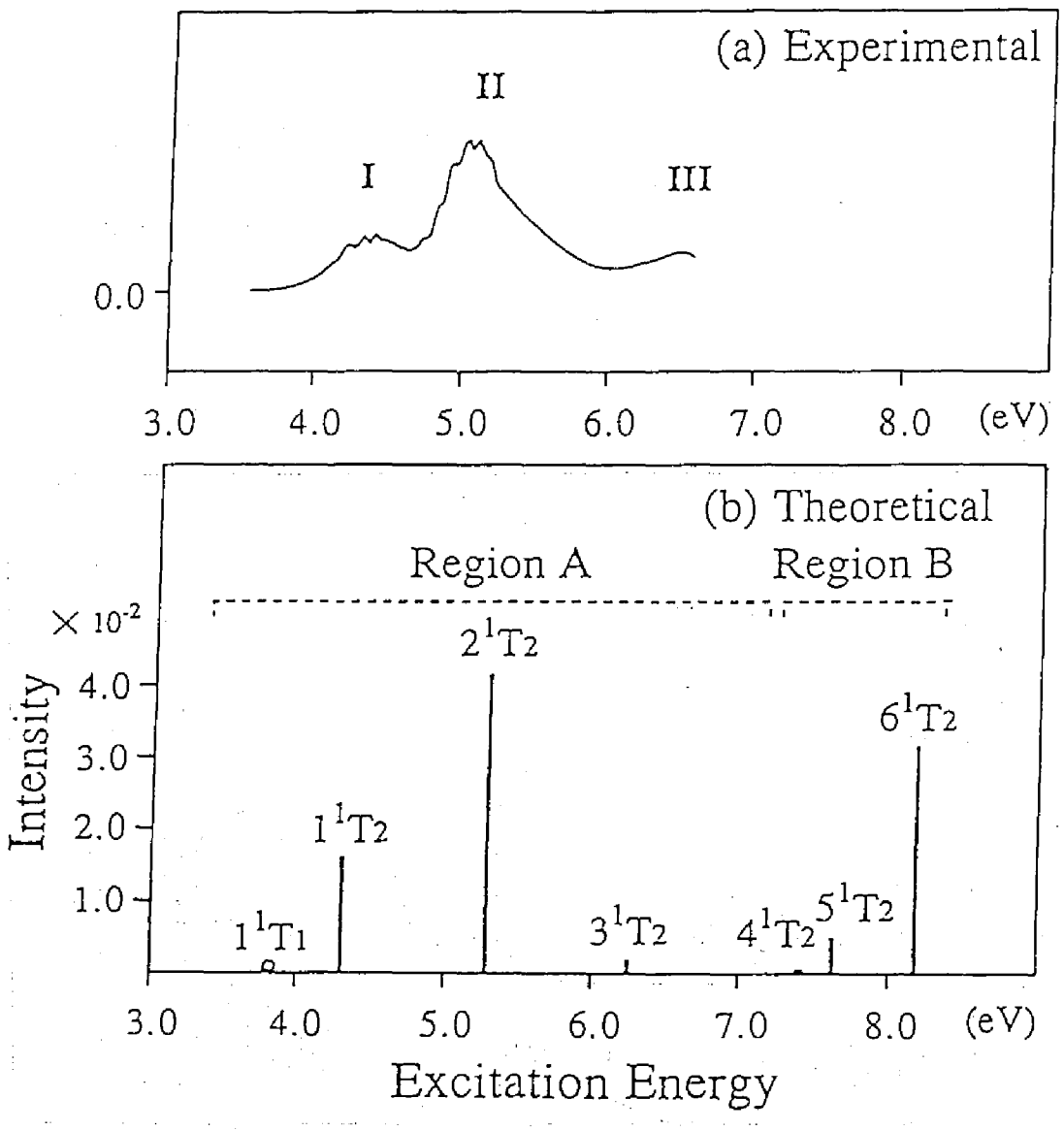

Fig. 2. (a) Experimental and (b) theoretical spectra of TcO_4^-. Experimental spectrum is due to Mullen et al., see ref. 14. The optically forbidden state is indicated by an open circle

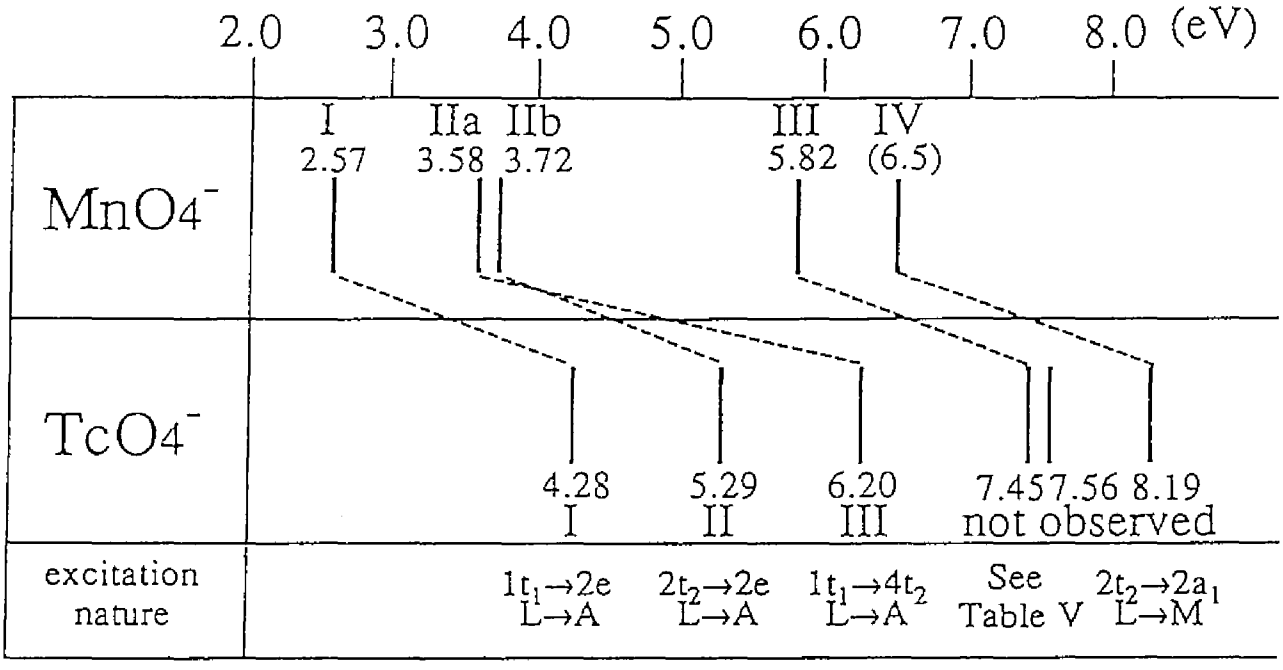

Fig. 3. Comparison of the calculated excitation energies for optically allowed $^1T_2$ states of MnO_4^- and TcO_4^-. For MnO_4^-, see ref. 7

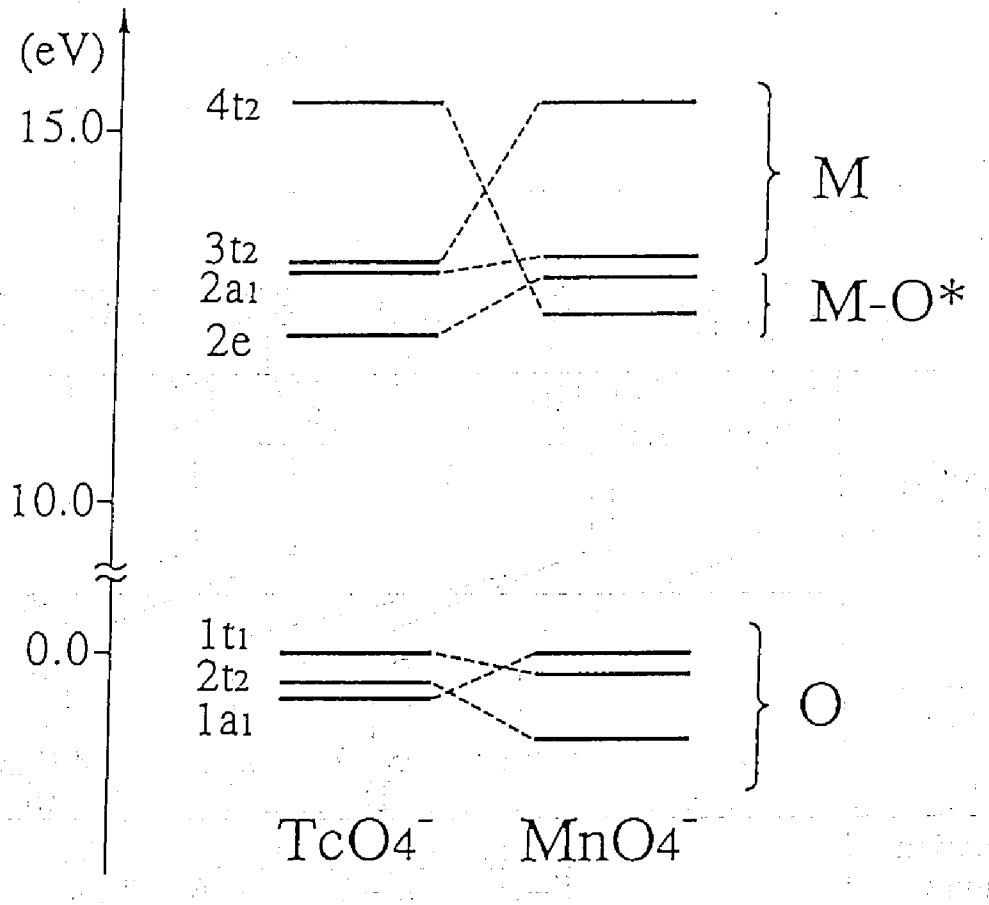

Fig. 4. Orbital energy levels of TcO_4^- and MnO_4^- with their HOMO's as the reference level. The MOs having the same nature are connected by the dotted line

List of publications

Part I

Chapter 1.

Excited and ionized states of free base porphin studied by the symmetry adapted cluster-configuration interaction (SAC-CI) method
H. Nakatsuji, J. Hasegawa, and M. Hada
J. Chem. Phys. 104 (1996) 2321

Chapter 2.

Ground and excited states of Mg porphin studied by the SAC/SAC-CI method
J. Hasegawa, M. Hada, M. Nonoguchi, and H. Nakatsuji
Chem. Phys. Letters 250 (1996) 159

Chapter 3.

Ground and excited states of oxyheme: SAC/SAC-CI study
H. Nakatsuji, J. Hasegawa, H. Ueda, and M. Hada
Chem. Phys. Letters 250 (1996) 379

Chapter 4.

Theoretical study of the excited states of chlorin, bacteriochlorin, pheophytin *a*, and chlorophyll *a* by the SAC/SAC-CI method
J. Hasegawa, Y. Ozeki, K. Ohkawa, M. Hada, and H. Nakatsuji
J. Phys. Chem. B in press.

Part II

Chapter 5.

Theoretical study of the excited states of the photosynthetic reaction center: SAC-CI study
J. Hasegawa, K. Ohkawa, and H. Nakatsuji
To be submitted

Chapter 6.

Theoretical study of the electron transfer reactions in the photosynthetic reaction center
J. Hasegawa and H. Nakatsuji
To be submitted

Part III

Chapter 7.

Theoretical study on the ionized states of ethylene by the SAC-CI (general-*R*) method
J. Hasegawa, M. Ehara, and H. Nakatsuji
Chem. Phys. submitted

Chapter 8

Theoretical study on the electronic spectrum of TcO_4^-
J. Hasegawa, K. Toyota, M. Hada, H. Nakai, and H. Nakatsuji
Theoret. Chim. Acta. 92 (1995) 351

Other publications

SAC-CI study of the excited states of free base tetrazaporphin
K. Toyota, J. Hasegawa, and H. Nakatsuji
Chem. Phys. Letters 250 (1996) 437

Ground and excited states of carboxyheme: SAC/SAC-CI study
H. Nakatsuji, Y. Tokita, J. Hasegawa, and M. Hada
Chem. Phys. Letters 256 (1996) 220.

SAC-CI study of the excited and ionized states of Free Base Porphin : effect of polarization and Rydberg functions
Y. Tokita, J. Hasegawa, and H. Nakatsuji
J. Phys. Chem. A in press.

Excited states of Free Base Phthalocyanine studied by the SAC-CI method
K. Toyota, J. Hasegawa, and H. Nakatsuji
J. Phys. Chem. A 101 (1996) 446.

Outer Valence Ionization Energies of Thiazyl Halides: A SAC-CI Study
P. Tomasello, J. Hasegawa, and H. Nakatsuji
To be submitted

Molecular trench: Highly complementary binding sites for tartaric acid dialkyl ester
Y. Kuroda, Y. Kato, M. Ito, J. Hasegawa, and H. Ogoshi
J. Am. Chem. Soc. 116 (1994) 10338

Chiral amino acid recognition by a porphyrin-based artificial receptor
Y. Kuroda, Y. Kato, T. Higashioji, J. Hasegawa, S. Kawanami, M. Takahashi, N. Shiraishi, K. Tanabe, H. Ogoshi
J. Am. Chem. Soc. 117 (1995) 10950